Winter Climate Response to Continental Snow Anomalies

by

Gavin Gong

M.S. Civil and Environmental Engineering
Massachusetts Institute of Technology, 1994

B.E. Civil Engineering
The Cooper Union for the Advancement of Science and Art, 1991

Submitted to the Department of Civil and Environmental Engineering
in partial fulfillment of the requirements for the degree of

Doctor of Philosophy
in Hydrology

at the

MASSACHUSETTS INSTITUTE OF TECHNOLOGY

June 2003

Author . . . . . .
Department of Civil and Environmental Engineering
May 9, 2003

Certified by . . . . . .
Dara Entekhabi
Professor of Civil and Environmental Engineering
Thesis Supervisor

Accepted by . . . . . .
Oral Buyukozturk
Chairman, Departmental Committee on Graduate Studies

Winter Climate Response to Continental Snow Anomalies

by
Gavin Gong

Submitted to the Department of Civil and Environmental Engineering
on May 9, 2002 in partial fulfillment of the
requirements for the degree of
Doctor of Philosophy in Hydrology

ABSTRACT

Climate variability has emerged in recent decades as an important field of geoscience research. A thorough understanding of the patterns and causes of climate variability is required to predict and prepare for upcoming climatic shifts, and also to accurately distill anthropogenic climate change signals from naturally occurring variations. In the extratropical Northern Hemisphere, regional climate patterns are strongly related to a hemispheric-scale mode of variability known as the Arctic Oscillation (AO). A major challenge for current climate variability studies is to predict the phase and magnitude of the AO, as it is a fundamental, internal mode of the atmosphere, but can nevertheless be triggered through a myriad of external perturbations.

In this thesis the influence of one hypothesized external perturbation, continental-scale land surface snow anomalies, is investigated. Satellite observations of historical autumn-winter snow cover are used to develop model boundary conditions for a series of snow-forced numerical General Circulation Model (GCM) experiments. Realistic snow forcing over Siberia is found to exert a modulating influence on the winter season AO mode, which is consistent with observations. This winter climate response occurs via an atmospheric teleconnection pathway involving established stationary wave – mean flow interaction processes throughout the troposphere and stratosphere. The pathway is enabled by the specific and unique geographic and orographic conditions that exist in Siberia, and their role in the development of planetary waves.

This model-simulated pathway provides a physical explanation for how regional land surface snow anomalies can influence hemispheric-scale winter climate. The results of this study may potentially lead to improved seasonal predictions of winter climate, based on remotely-sensed Siberian snow conditions during the preceding autumn. The results also contribute to the field of land surface – atmosphere coupling by demonstrating interactions that occur outside of the warm season, and on broad continental and hemispheric scales.

Thesis Supervisor: Dara Entekhabi
Title: Professor of Civil and Environmental Engineering

Acknowledgements

This work has been supported by National Science Foundation Grants ATM-9902433 and ATM-0127667. Additional support has been provided through the Martin Family Society of Fellows for Sustainability.

I owe a tremendous debt of gratitude to my advisor, Dara Entekhabi, on many levels; for encouraging my return to the Parsons Lab and enthusiastically resuming our academic relationship, for permitting me to pursue my research independently while always providing support when needed, for giving me ample opportunity to develop my teaching skills, and for being a friend as well as a mentor. I am also indebted to Judah Cohen, for being the driving force behind this research project, for providing continual guidance and support, and for many interesting and informative conversations while traveling together. Thanks also to the rest of my committee, Rafael Bras, Elfatih Eltahir and David Robinson, for exemplifying such high academic standards for me to aspire to. Special thanks to Dennis McLaughlin for unwittingly initiating my return to academia after a five-year leave of absence.

It has been my privilege to be part of the Parsons Lab community on two separate occasions, and I am grateful to all of the students, faculty and staff for fostering a friendly and supportive learning environment. I am especially grateful to Sheila Frankel and Vicky Murphy for remembering me and welcoming me back so warmly, and for their invaluable assistance with all things administrative and bureaucratic.

I would like to thank my parents, Gregory and Sanne Gong, for supporting my decision to go back to school, even though they may not have fully understood my rationale. Heartfelt thanks to Uncle Peter and Aunt Helen for their constant enthusiasm, encouragement and advice as I follow my various academic and professional pursuits. Thanks also to Gar-Yee and Yun for allowing me to witness and partake in their transition from youth to adult, which provided an oft-needed and highly entertaining diversion from my work.

This thesis is dedicated to my late uncle, Dr. Thomas Moy, who valued academic achievement, and in particular the honor and prestige associated with this degree, more so than anybody else I know.

During the course of this work, my wife Michelle has wholeheartedly shared in my successes, and empathetically eased my worries. This truly would not have been possible without her love, patience and reassurance. Despite her constant assertions to the contrary, I in fact love her more. Finally, my son Zachary has been a constant source of joy during this work. Regardless of how my research was progressing, he has been there at the end of each day to greet me with a warm smile and a loud “dada!”, immediately turning the bad days into good ones, and the good days into great ones.

Contents

List of Figures

List of Tables

Chapter 1

Introduction

1.1 Motivation

Over the entire course of human history, civilizations have developed under an implicit assumption that the climate in which they exist is relatively stable. Henry David Thoreau describes four necessities of life for humankind: food, shelter, clothing and fuel. The ways in which these necessities are procured depend upon the prevailing climatic characteristics of a given region. For example, the amounts and seasonal patterns of precipitation affect the type of agriculture that is sustainable in that region. Also, the type of shelter constructed is dependent upon expected climatic events such as floods, storms, and frosts. As the population continues to grow and global economies emerge, the assumption of a relatively stable climate in one part of the world has the potential to impact the entire world.

Recent scientific study of the Earth's climatic history has established that in actuality, the climate does not reside in this assumed steady state, but rather varies with recognizable periodicities ranging from years to millions of years (Keller, 1999). In addition, abrupt variations in climate can be attributed to instantaneous naturally occurring factors such as volcanic eruptions. Since so much of society's well-being and stability depends on climate, we are vulnerable to these naturally occurring shifts in climatic features. The collapse of several well-established civilizations in the past has been attributed to sustained climatic variations (Weiss et al., 1993). Therefore, a thorough understanding of naturally occurring climate variability is needed to provide society with a sound basis for adapting to potential changes. Furthermore, development of the ability to predict upcoming climatic shifts based on known forcings can not only mitigate negative impacts of anticipated changes, but also provides the opportunity to capitalize on any positive impacts (NRC, 1998).

The recent predictions of human-induced climate change are also affected by natural climate variability. Observations of global warming and associated climatic trends over the past twenty years may be caused by anthropogenic factors such as increased greenhouse gas emissions, but may also be a consequence of the current phase in one or more decadal or longer scale climate periodicities. Thus an understanding of climate variability over multiple timescales is critical for the accurate distillation of anthropogenic climate change signals from naturally occurring variability (WCRP 1995).

Climate variability has received considerable scientific attention over recent decades, which has deepened our understanding of long-recognized regional climate phenomena such as the El Nino Southern Oscillation (ENSO) and the North Atlantic Oscillation (NAO). This thesis contributes to this important basic geoscience research field, as it is directed at an improved understanding of the causes of wintertime climate variability in the mid-latitude region of the Northern Hemisphere, at interannual timescales. Land surface – atmosphere interaction has also emerged as an important field of research, as exemplified by the large-scale climatic impacts of soil moisture, vegetation stress and deforestation. This thesis also contributes to research on the large-scale coupling between the land surface and the atmosphere, by investigating the specific role of land surface snow anomalies in hemispheric-scale winter climate variability.

Understanding climate variability in the extratropical Northern Hemisphere is of particular inherent value to society, since the majority of the world's population lives in this region, and hence is directly affected by climate shifts. The global society is likewise affected, since much of the agriculture that sustains the world population is grown in the extratropical Northern Hemisphere. Crop planting and irrigation strategies could be optimized based on predicted climate in upcoming years. Wintertime climate variability is of particular importance, as an enormous amount of fossil fuel is consumed (fuel being another one of Thoreau's necessities of life) to provide heat for the vast populace located in this sector of the world. Reliable long-range climate forecasts would enable improved management of energy supplies, tremendously influencing the global economy and providing an opportunity to conserve our finite natural resources. These are but a few examples of how skillful climate forecasts can be of value to society (NRC 1999). Accurate climate predictions require a sound grasp of natural climate variability. Thus an improved understanding of the causes of wintertime extratropical Northern Hemisphere climate variability is not only of fundamental scientific interest, but would also be of practical value and have direct engineering applications.

1.2 Northern Hemisphere Climate Variability

The dominant pattern of extratropical Northern Hemisphere climate variability is characterized by simultaneous and opposite-signed oscillations of atmospheric mass between high and mid-latitudes. The oscillations are most prevalent in the winter season, and occur over a wide range of timescales, from intraseasonal to interdecadal. This pattern of climate variability is commonly referred to hemispherically as the Arctic Oscillation (AO; Thompson and Wallace, 1998) or the Northern Annular Mode (NAM; Thompson and Wallace, 2001), and regionally as the North Atlantic Oscillation (NAO; Wallace and Gutzler, 1981). The NAO in particular has been shown to exert a strong influence on climate in western Europe and eastern North America, via latitudinal shifts in the wintertime North Atlantic storm track and associated variations in temperature, precipitation and cyclonic activity (Hurrell, 1995; Serreze et al., 1997). Climatic conditions have a considerable societal impact in the populous regions bordering either side of the North Atlantic. This has prompted research efforts to better understand the mechanisms which drive this overall pattern of variability (hereafter referred to as the

AO). A major goal of these efforts is to predict the phase and magnitude of the AO mode on seasonal timescales, in order to better anticipate wintertime climatic conditions over the mid-latitude Northern Hemisphere.

Figure 1-1a shows a common expression of the winter AO mode, consisting of the leading empirical orthogonal function (EOF1) for the Northern Hemisphere winter (DJF) sea level pressure (SLP) field, computed using NCEP/NCAR reanalysis data (Kalnay et al. 1996) from 1971-1997. As described in Appendix A, the EOF diagnostic captures the dominant spatial patterns of temporal variability within a gridded data set. As indicated in Figure 1-1a, a negative signed anomaly center occurs over polar regions concurrently with two positive signed anomalies at mid-latitudes, centered about the North Atlantic and North Pacific basins. This dipole pattern explains 37% of the total variability in the SLP dataset, and the North Atlantic is generally more responsive than the North Pacific. Figure 1-1b shows the associated EOF1 principal components time series over the 27 year winter dataset, typically referred to as the winter AO index. Years with strongly positive values (positive AO years, e.g., 1988) follow the spatial pattern shown in Figure 1-1a, while years with strongly negative values (negative AO years, e.g., 1976) follow the exact opposite pattern, i.e., positive (negative) anomalies at high (mid) latitudes.

A substantial amount of research has been performed in an attempt to determine the influences on atmospheric circulation which may be responsible for the AO mode. The ocean boundary has received considerable attention as a potential driving force, and a number of studies have detected significant relationships between observed interannual SST variations and the NAO in particular (e.g., Latif et al., 2000; Rodwell et al., 1999; Robertson et al., 2000; Dong et al., 2000; Hoerling et al., 2001). However, different studies have linked climate in the North Atlantic sector atmosphere with SSTs in various regions, including the North Atlantic, South Atlantic and equatorial Pacific. Seager et al. (2000) found that North Atlantic SSTs do not force, but rather respond to, changes in atmospheric circulation. Unlike the El Niño-Southern Oscillation (ENSO), in which SST anomalies in the equatorial eastern Pacific are clearly associated with climate variations in the tropics and even the extratropics, a definitive relationship has yet to be established between SSTs and climate variability in the North Atlantic Sector.

Another set of studies links the surface and upper-level features of the AO mode of variability to planetary scale tropospheric-stratospheric wave interactions (e.g., Baldwin and Dunkerton, 1999; Christiansen, 2000; Kodera and Kuroda, 2000; Perlwitz et al., 2000). These studies portray the equivalent barotropic nature of the AO mode, extending from the surface to the middle stratosphere. However, different studies have found signals to originate in both the troposphere and stratosphere, and both upward and downward wave propagations have been detected. Furthermore, no clear causal mechanisms have been linked to the signal origins. Anthropogenic climate change factors and episodic events such as volcanic eruptions have been suggested (Kodera and Yamazaki, 1994; Graf et al., 1994; Shindell et al., 1999), but have yet to prove conclusive.

Land-surface characteristics also have the potential to affect Northern Hemisphere climate variability, since the largest land masses on Earth reside in the mid-latitudes of the Northern Hemisphere. Despite this potential, possible linkages between interannual snow anomalies and the AO pattern of variability have received relatively little attention.

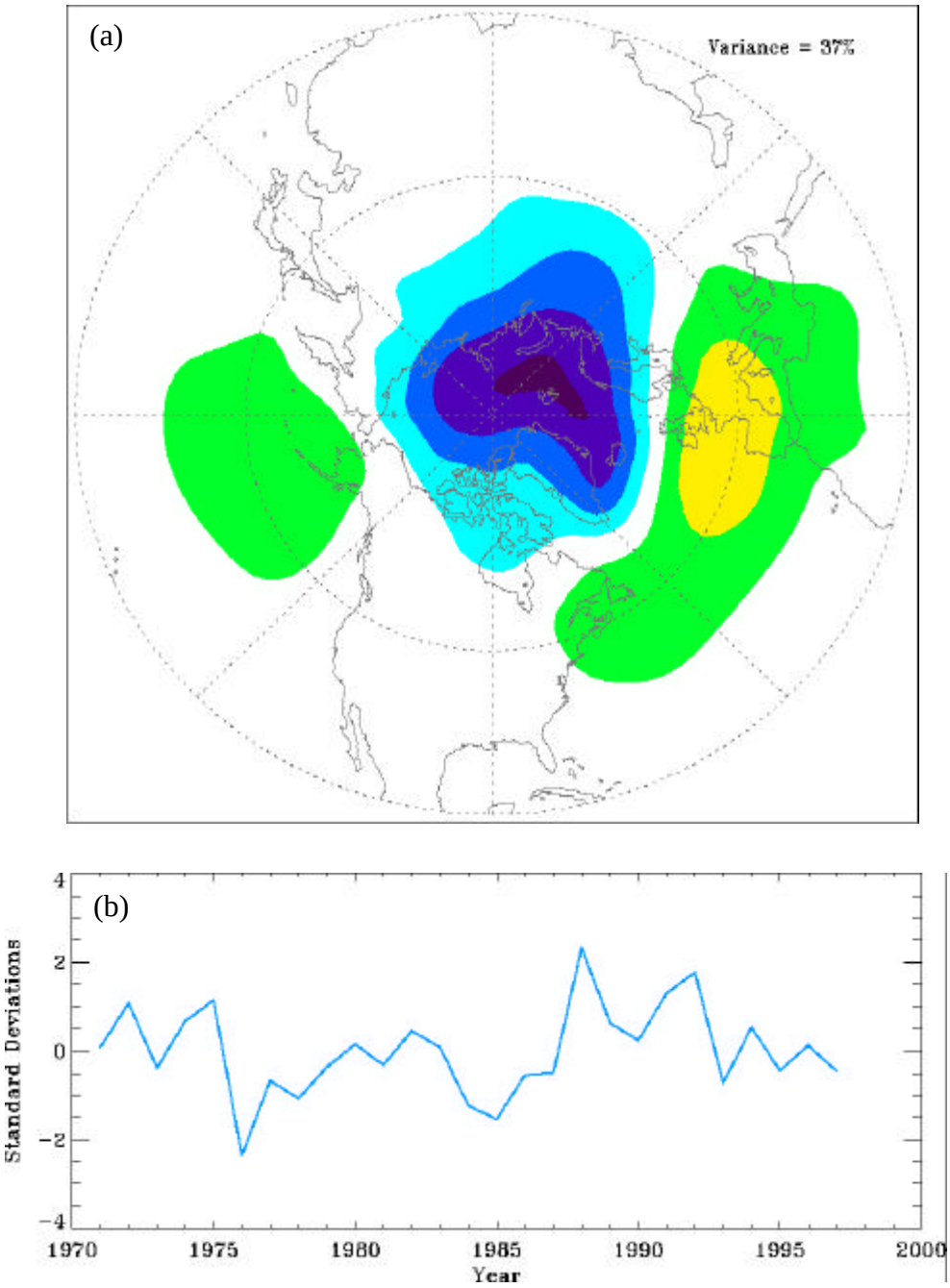

Figure 1-1: The AO mode of variability, depicted using empirical orthogonal function analysis of the Northern Hemisphere (north of the equator) winter (DJF) sea level pressure (SLP) field, computed from 1971-1997 NCEP/NCAR reanalysis data (Kalnay et al. 1996). a) The leading spatial pattern of winter variability (EOF1), which accounts for 37% of the total SLP field variability. Contour values are arbitrary, and represent relative magnitudes within the spatial EOF1 pattern. Dashed line denotes negative contour value. b) The EOF1 principal components interannual winter time series.

The literature relating snow and Northern Hemisphere climate will be reviewed in Section 1.3.

Many of these studies have attempted to establish that interannual variations in a particular external mechanism serves as the principal driving force behind the AO mode of variability. Although SSTs, and both upper-level atmospheric and land surface conditions have demonstrated significant statistical relationships with the AO, no single feature has emerged as the dominant characteristic which precedes, governs, and enables the prediction of winter climate in the extratropical Northern Hemisphere. Hence, recent studies have suggested that the AO is not an externally forced mode at all, but rather a fundamental internal mode of the atmospheric system (Robertson, 2001; Baldwin, 2001). Feldstein (2000, 2002) uses daily unfiltered data to demonstrate that the AO fluctuates primarily on intraseasonal timescales arising from processes internal to the atmosphere, and that on interseasonal timescales variations in the AO may be considered simply "climate noise".

A related question which therefore arises is, if the AO is in fact not driven by external forcings, then can it still be modulated by boundary conditions on an interseasonal timescale at a level greater than internal noise? A consensus is building within the scientific community that the AO is indeed a fundamental and internal mode of variability in the Northern Hemisphere, but one which may be modulated by various external forcings (Baldwin, 2001; Feldstein, 2002). This idea is supported by modeling studies with climatological surface (land and ocean) boundary conditions, which nonetheless exhibit the AO mode of variability (Robertson, 2001). Understanding the role played by external forcings, such as anomalies in sea surface temperatures (SSTs), land surface conditions and the stratosphere, will improve our overall understanding of Northern Hemisphere climate variability. Improved understanding of climate variability is critical to improving climate predictability on seasonal or longer timescales. In this thesis the role of land surface snow conditions in modulating the winter AO signal is investigated.

1.3 Climate Modulation by Land Surface Snow

The impact of snow on local weather and climate has been extensively studied and is well understood. An inverse relationship generally exists between snow cover and surface air temperature, caused by a change in the surface energy balance due to the presence of snow (Dewey, 1977; Namias, 1985; Cohen and Rind, 1991; Leathers and Robinson, 1993). The primary mechanism involved is decreased solar radiation due to a higher albedo, but other responsible surface thermodynamic mechanisms include increased thermal emissivity, decreased thermal conductivity, and increased latent heat via snowmelt (McFadden and Ragotzkie, 1967; Wagner, 1973; Cohen 1994; Walland and Simmons, 1996).

The impact of snow on atmospheric dynamics and remote climate has also been studied. Cohen (1994) provides a review of studies in which a climatic response is detected in subsequent seasons and remote regions relative to the snow anomaly. Anomalously high snow cover has been correlated with a delayed springtime surface air

temperature rise, reduced 500 hPa geopotential height, a weakened Indian summer monsoon, weakened cyclogenesis in eastern North America, and increased spring and summer soil moisture. Most of these studies focus on snow in the late winter season and its impact on subsequent spring and summer climate in regions adjacent to the snow anomaly. Perhaps the most widely studied climatic response is that of the Indian summer monsoon. Numerous observational and modeling studies have consistently reported an inverse relationship between Eurasian winter snow cover and subsequent Indian summer monsoon rainfall (Hahn and Shukla, 1976; Barnett et al., 1989; Douville and Royer, 1996; Bamzai and Shukla, 1999).

The extent and characteristics of land surface snow suggest the potential to influence climate on a much broader scale than has traditionally been investigated. Large, contiguous land masses comprise roughly half of the total surface area north of 30ºN, as indicated in Figure 1-2. During the autumn-winter season, these extratropical land masses are characterized by extensive snow cover. In addition, snow cover and snow mass exhibits considerable variability in both time and space, especially during the autumn season (Gutzler and Rosen, 1992; Robinson et al., 1993).

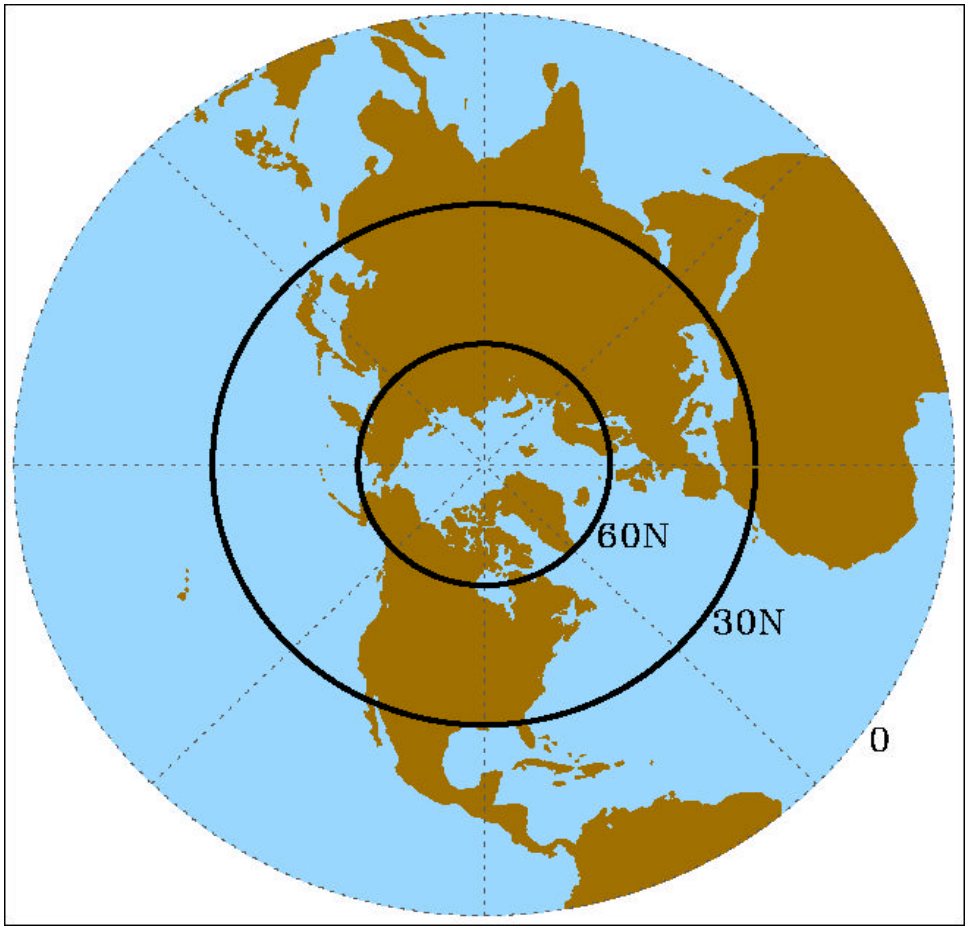

Figure 1-2: Land and water surfaces over the Northern Hemisphere. North of 30ºN, land surfaces comprise roughly 50% of the total surface area.

The breadth of the snow-covered land surface suggests that snow anomalies may influence climate not just on a regional scale, but possibly on a continental or even hemispheric scale. Watanabe and Nitta (1999) investigated the decadal-scale negative to positive AO climate shift that occurred in winter 1989, and suggested that anomalously low Eurasian snow cover anomalies during the preceding autumn may have played a role comparable in magnitude to SST anomalies in amplifying the observed climatic shift. Clark and Serreze (2000) associated snow cover variations in east Asia with winter atmospheric circulation anomalies over the North Pacific. Cohen and Entekhabi (1999) reported a significant interannual correlation of 0.71 between satellite-derived Eurasian autumn snow cover area and the winter AO mode, represented by the first empirical orthogonal function of the observed winter 500 hPa Northern Hemisphere geopotential height field. Cohen and Entekhabi (2001) used a similar approach to establish a significant statistical relationship between interannual winter Eurasian snow cover variations and the winter AO mode. Cohen et al. (2001) performed interannual correlation analyses using gridpoint sea level pressure data, Eurasian autumn snow cover area, and a downward propagating AO index; they demonstrated that the winter AO may originate as an autumn sea level pressure anomaly over Siberia. Saito et al. (2001) perform an array of diagnostic and statistical analyses to demonstrate that the winter AO may be associated with autumn stationary wave activity flux anomalies over Eurasia.

These observational studies imply but do not conclusively prove a causal relationship between snow and the winter AO, due to competing physical processes and noise inherent in the observed data. Therefore numerical modeling studies are needed to complement the observational studies, by isolating the effect of snow anomalies on winter climate. Unfortunately, relevant modeling studies to date have generally been exploratory in nature. In an early study, Walsh and Ross (1988) perturbed North American and Eurasian snow cover separately for 30-day periods during the late-winter. In general they found the large-scale atmospheric circulation to be more sensitive to positive Eurasian snow cover perturbations, with colder air temperatures up to 500 hPa, higher pressure/heights in the Asian Arctic, and lower pressure/heights in the Aleutian region and western Europe. Walland and Simmonds (1997) performed idealized GCM experiments of the January climate response to changes in observed Northern Hemisphere snow cover. They found non-local geopotential height and cyclone activity responses over both the North Atlantic and North Pacific basins, and attributed them to local responses over the land surface snow anomalies being swept downstream. Watanabe and Nitta (1998) performed six month (Sep-Feb) GCM simulations with an artificial low snow perturbation applied to eastern Eurasia. The modeled climatic response resembled the observed winter 1989 climatic shift (i.e., extreme positive AO mode), and was similar to the climatic response of a related GCM simulation forced with observed 1988/1989 SSTs, although the magnitude of the snow-forced response was somewhat smaller. Cohen and Entekhabi (2001) performed a three month (Dec-Feb) GCM experiment with an idealized but representative high snow perturbation, which yielded a climatic response resembling a negative AO phase, consistent with observations. These modeling studies are all suggestive of a causal relationship between snow and winter climate, but the idealized conditions that were employed may have led to exaggerated, suppressed, or otherwise unrealistic results.

Another requirement for a complete understanding of the snow-winter climate relationship is a detailed explanation of the physical mechanisms involved, to show that the relationship is real and not a chance or model artifact. Previous studies have hypothesized various potential teleconnection pathways, such as an orographically-constrained poleward migration of the semi-permanent Siberian High pressure system (Cohen et al., 2001), or a vertical pathway involving upward propagating stationary wave activity and the stratospheric polar vortex (Saito et al., 2001; Cohen et al., 2002). However, they have not been conclusive in showing that these pathways occur.

The aforementioned studies utilize either statistical analyses of observed long-term datasets, or numerical simulations of atmospheric General Circulation Models (GCMs). Both types of analyses pose challenges to identifying and characterizing the snow – winter AO relationship. One difficulty with observational analyses is the interdependency of numerous parameters in the complex atmospheric system, which make it problematic to associate causality with any observed statistically significant relationship. GCM studies provide an experimental platform for isolating the climatic effect of a specified forcing. However, despite continual advances, GCMs still do not replicate the atmospheric system with adequate precision and accuracy, and simulation results can vary substantially between different models. In addition, GCM studies must either be of sufficiently long duration, or include a sufficient number of independent realizations, to distinguish the climatic response to a boundary forcing from intrinsic model climate variability. In the case of the GCM studies involving snow forcing described above, the exploratory nature of these investigations has generally limited them to short term integrations (one to six months), and five or fewer realizations.

1.4 Research Focus

The aim of this thesis is to investigate the extent to which winter climate in the extratropical Northern Hemisphere responds to continental-scale snow anomalies. Previous studies have focused primarily on snow anomalies in Eurasia, and specifically Siberia, since it is the largest contiguous land surface region in the world, and is characterized by extensive and variable snow conditions. Thus Siberia holds the greatest potential for modulating the AO mode. This research will continue to focus on Siberia, and will identify the unique features of this region which enable it influence hemispheric-scale climate.

A GCM modeling approach is adopted for this research, in order to explicitly isolate the climatic response to a Siberian snow forcing. This numerical modeling study complements the extensive observational analyses that have been performed regarding the snow-AO relationship (Cohen and Entekhabi 1999, 2001; Cohen et al. 2001; Saito et al. 2001). Since both types of analyses have drawbacks, consistent results for both data analysis and modeling studies are key to establishing the actuality of the snow-AO relationship.

The first objective is to develop and implement an effective GCM simulation framework for establishing an explicit relationship between Siberian snow and winter climate. This framework improves upon the limitations associated with previous

exploratory model studies. The issue of realistic forcings will be addressed by modeling the climatic response to observation-based snow forcings over Siberia during the autumn-winter season, using a historical dataset of weekly visible-satellite snow cover provided by NOAA. Using snow forcings based on observed data will facilitate a meaningful comparison between model results and observed AO mode variability. Another improvement over previous modeling studies is the use of a large-ensemble modeling approach, in which each snow-forced experiment consists of twenty independent realizations using the same boundary condition. This large ensemble approach is necessary to distinguish snow-related changes from the naturally-occurring interannual variability associated with the AO mode.

A second objective is to develop and validate a conceptual model which explains the physical processes by which observed anomalies in autumn Siberian snow lead to observed fluctuations in winter extratropical Northern Hemisphere climate. This physically-based conceptual model will include land surface forcings, atmospheric dynamics, cause-effect linkages, and any feedback loops which may exist. In other words, a seasonal teleconnection pathway between Siberian snow and the winter AO mode will be identified, that describes precisely how interannual variations in the former produce corresponding interannual variations in the latter. Hypothesized pathways from previous studies will be fully evaluated, and a causal relationship will be established.

A final objective is to refine our understanding of the causal relationship between Siberian snow and the winter AO, by studying various land surface features that act to constrain the teleconnection pathway. The land surface features that will be investigated are orographic barriers, geographic location and surface thermodynamics related to snow cover and snow depth. Such an analysis will enable us to understand the specific physical and dynamical reasons why regional snow anomalies in Siberia can influence hemispheric-scale winter climate, and improve our overall understanding of Northern Hemisphere climate variability. Improved understanding of climate variability is critical to the ultimate goal of improving climate predictability on seasonal or longer timescales.

Thus the goal of this thesis is to fully identify and characterize a causal relationship between Siberian snow anomalies and the winter AO mode, on interannual timescales. This research will lead to an improved understanding of the causes of wintertime climate variability, and will also serve as a demonstration of large-scale land surface – atmosphere interaction during the cold season. Chapter 2 describes the GCM that is used and the modeling approach that is employed. Chapter 3 presents the results of a preliminary set of experiments to evaluate the climate response to model-generated interannual snow variations. The main GCM experiments are presented in Chapters 4-6. Chapter 4 presents the climate response to realistic, observation-based snow forcings over Siberia, and fully characterizes the atmospheric teleconnection pathway that occurs. Chapter 5 evaluates orographic constraints on this pathway in the form of mountains in southern and eastern Siberia. Chapter 6 evaluates geographic constraints by comparing the climate response to snow forcing in Siberia and North America. Chapter 7 briefly presents the results of additional experiments investigating the effect of specific snow forcing characteristics, i.e., snow cover vs. snow depth. Finally, conclusions and avenues for future research are presented in Chapter 8.

Chapter 2

Methods

2.1 ECHAM3 GCM

2.1.1 Model Description

Numerical simulations are conducted using the ECHAM3 GCM, developed by the Max-Planck Institute for Meteorology in Hamburg, Germany. ECHAM3 has evolved from the spectral operational weather forecast model used at the European Center for Medium-Range Weather Forecasts (ECMWF), incorporating physical parameterizations and revised numerical methods appropriate for climate simulations (Roeckner et al. 1992). In general, ECHAM3 simulates observed climate features with considerable skill (Kaurola, 1997), and the model performs well in comparison to other GCMs within the guidelines of the Atmospheric Model Intercomparison Project (AMIP; Gates et al., 1998). In particular, a spherical harmonics formulation is used by ECHAM3 to represent dynamical fields, which facilitates a more accurate simulation of high-latitude, winter climatology and variability as expressed by the AO mode. In contrast, GCMs which use a cartesian system for model dynamics require numerical filters to prevent instabilities at the poles, which damp out wave propagations in mid and high latitudes. Validation of the ECHAM3 model for parameters relevant to this study is presented in the following section.

All model integrations are performed with the spherical harmonic series triangularly truncated at wave number 42 (T42), which corresponds to a cartesian resolution of roughly 2.8° latitude by 2.8° longitude, as depicted in Figure 2-1. This resolution is adequate for the study of hemispheric-scale atmospheric patterns, while allowing numerous large ensemble experiments to be conducted in a computationally affordable manner. Vertical discretization consists of a second order finite difference scheme applied to a 19 layer hybrid sigma-pressure coordinate system, with the uppermost layer centered at 10 hPa. Note however that the stratosphere is poorly resolved in ECHAM3, with only four layers centered above 100 hPa, and only seven layer above 200 hPa. Monthly climatological sea surface temperature (SST) and sea ice values are prescribed throughout the model domain for the ocean boundary, derived from the COLA/CAC dataset developed for the Atmospheric Model Intercomparison Project (Gates, 1992).

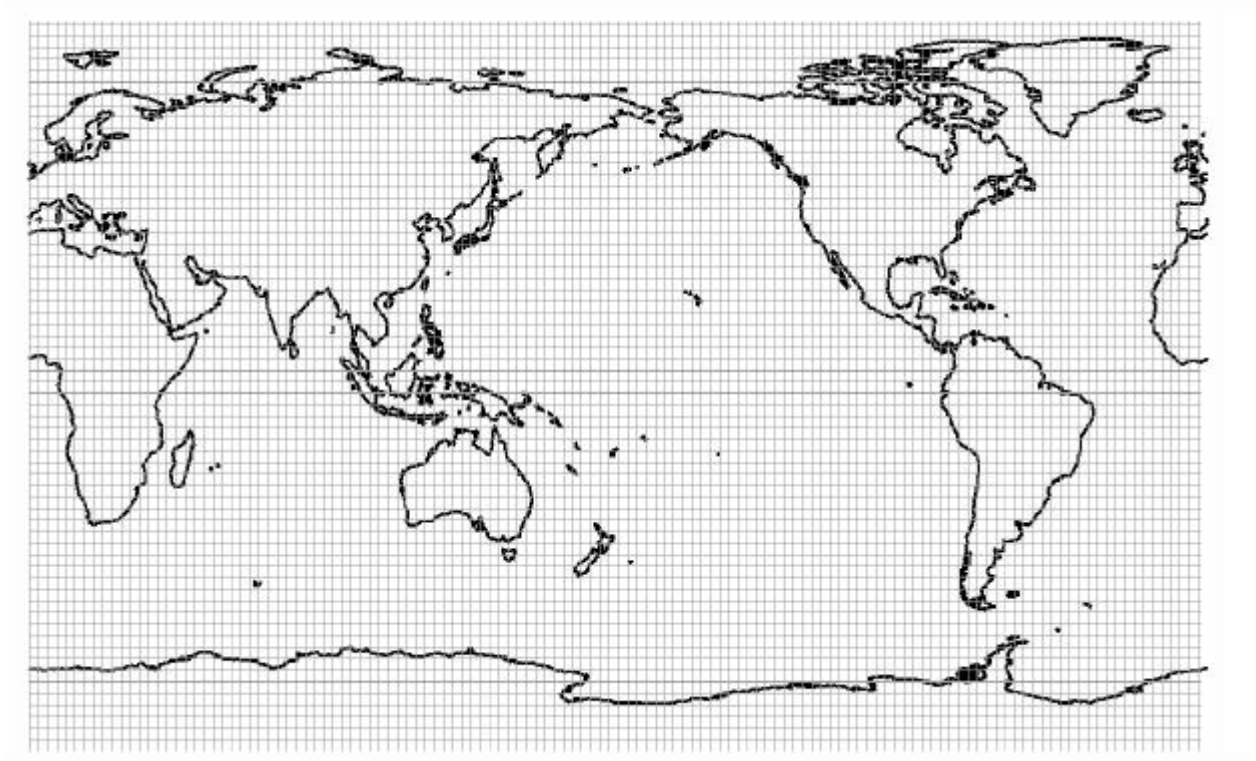

Figure 2-1: Cartesian gridcell resolution (2.8125° latitude by 2.8125° longitude; T42 spherical truncation) for all ECHAM3 GCM experiments.

The more recent model version ECHAM4 (Roeckner et al. 1996) has also been considered for use. The primary difference in the two model versions involves improved parameterizations for radiation, convection and water vapor transport. Relevant land surface parameterizations such as snow are unchanged. The land surface energy and water budgets are improved slightly in ECHAM4, due primarily to the improved representation of radiation. However, because snow properties such as albedo and thermal conductivity are unchanged, the relative impact of snow cover anomalies is expected to be similar between the two model versions. In addition, the availability of ECHAM4 is more restricted, therefore ECHAM3 is used.

ECHAM3's land surface parameterization is derived from the Simple Biosphere model (Sellers et al., 1986). Snow is parameterized in a straightforward manner (DKRZ 1994). Snow depth is maintained at each gridcell as an internal state variable S, in the form of snow water equivalent (SWE). A distinct snowpack layer resides above the surface soil layers, and evolves according to a budget equation:

$$\frac{\partial}{\partial t} S = \frac{J_S + P_S - M_S}{r_w} \tag{2.1}$$

where J_S = evaporation rate over the snowpack, P_S = snowfall rate over the snowpack, M_S = snowmelt rate over the snowpack, and r_w = density of water. For snow depths greater than 0.025 m SWE, snowpack temperature T_S evolves via a separate heat conduction equation for the snowpack:

$$\frac{\partial}{\partial t} T_S = \frac{F}{r_S C_S S} \tag{2.2}$$

where F = sum of radiative and turbulent fluxes at the surface, r_S = snow density, and C_S = heat capacity of snow. For snow depths less than 0.025 m SWE, T_S is not updated, and the basic surface heat conduction equation is solved irrespective of the snowpack. Surface albedo a_{surf} is related to the snow depth via:

$$a_{surf} = a_b + (a_S - a_b)\frac{S}{S + S^*} \tag{2.3}$$

where a_b = surface background albedo, a_S = snow albedo, and S^* = 0.01 m SWE. Finally, the snow-covered gridcell fraction C_S is parameterized as:

$$C_S = \min(1, \frac{S}{S_c}) \tag{2.4}$$

where S_c = 0.015 m SWE.

2.1.2 Snow and AO Mode Validation

ECHAM3's simulation of snow cover and snow mass compares reasonably well with observations and with other GCMs (Foster et al., 1996; Frei and Robinson, 1998). Figure 2-2a shows the average October snow depth over Eurasia simulated by a twenty year control simulation of the GCM, designated as CTRL, using monthly climatological sea surface temperature boundary conditions. Model SWE depth is multiplied by r_w / r_s to convert to snow depth, where r_w = 1000 kg/m^3 is used for water density and a typical value of r_s = 300 kg/m^3 is used for snow density (DKRZ, 1994; Foster et al., 1996). For comparison, the U.S. Air Force Environmental Technical Applications Center (USAF/ETAC) monthly observed global snow depth climatology (Foster and Davy, 1988) for October is shown in Figure 2-2b. The model appears to replicate the general snow depth features reasonably well, i.e., the location of the southern boundary, and separate maxima in northern and eastern Siberia. Snow depths are fairly consistently underestimated throughout Eurasia; this discrepancy has been noted previously in the literature, and attributed in part to deficiencies in the observed data (Foster et al., 1996). Note that snow variability is considerable in October, which presents a challenge to achieving accuracy in both model simulations and observations.

Figure 2-2c shows plots of monthly average snow covered area over Eurasia during the autumn-winter season, for the CTRL simulation, the USAF/ETAC snow depth climatology, and NOAA visible satellite snow cover observations (Robinson et al., 1993). All three sources indicate very sparse snow cover in September, a steady increase during autumn and early winter, and peak values in January and February. Once again the CTRL run appears to underestimate the USAF/ETAC observations. At the same time, the CTRL run also slightly overestimates the NOAA observations. This contradiction between the USAF/ETAC and NOAA datasets highlights the shortcomings of snow observations, especially given the general scarcity of data in Siberia and the variable nature of snow in autumn. Overall, the CTRL simulation does a credible job of reproducing the basic observed snow features over Eurasia, and thus serves as a valid platform for conducting snow perturbation experiments.

The leading AO mode of variability over the 20 realizations of the model-simulated Northern Hemisphere winter (DJF average) is evaluated using empirical orthogonal function analysis. This measure captures the dominant spatial patterns of temporal variability within a gridded data set. Figure 2-3a shows the leading empirical orthogonal function (EOF1) for the Northern Hemisphere (north of the equator) sea level pressure (SLP) field, for the CTRL simulation. For comparison, Figure 2-3b shows the corresponding EOF1 obtained from 27 years (1971-1997) of NCEP/NCAR reanalysis data (repeated from Fig. 1-1a). The model replicates the characteristic dipole pattern between high and mid-latitudes associated with the hemispheric AO mode. It explains 39% of the total variance in the modeled SLP field, which is comparable to the 37% explained using the reanalysis data. However, the modeled Pacific anomaly is stronger than the Atlantic anomaly, whereas observations generally indicate a stronger anomaly in the Atlantic. The corresponding EOF1 for the 500-hPa geopotential height field (not shown) is likewise comparable to observations.

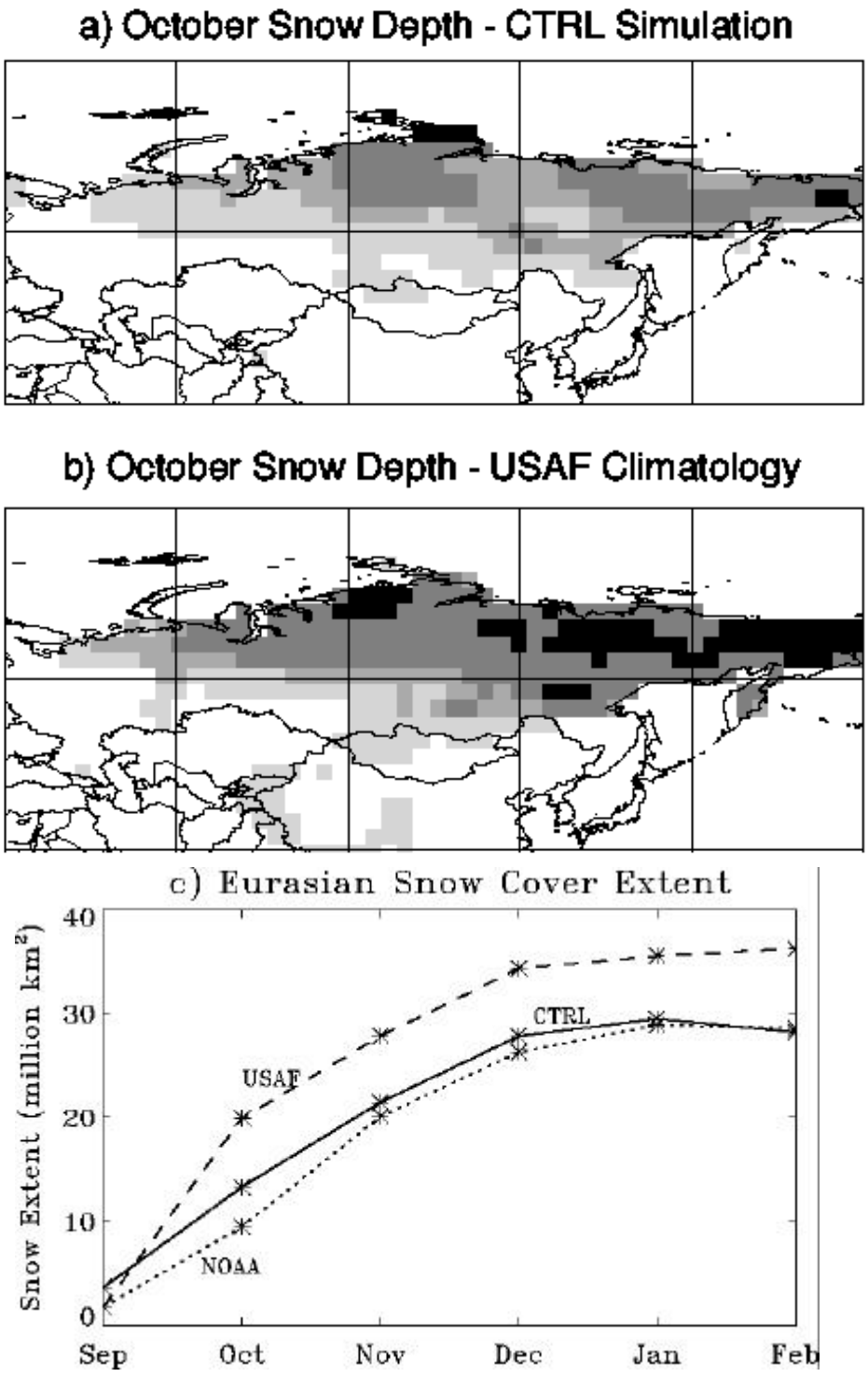

Figure 2-2: a) Average October snow depth over Eurasia for the CTRL simulation. Shading represents 1-5 cm (lightest), 5-10 cm, 10-20 cm, and 20+ cm (darkest). b) Same as a), except for USAF/ETAC observed climatology dataset. c) Monthly average snow cover extent over Eurasia during September-February, for CTRL simulation, USAF/ETAC observations, and NOAA visible satellite observations.

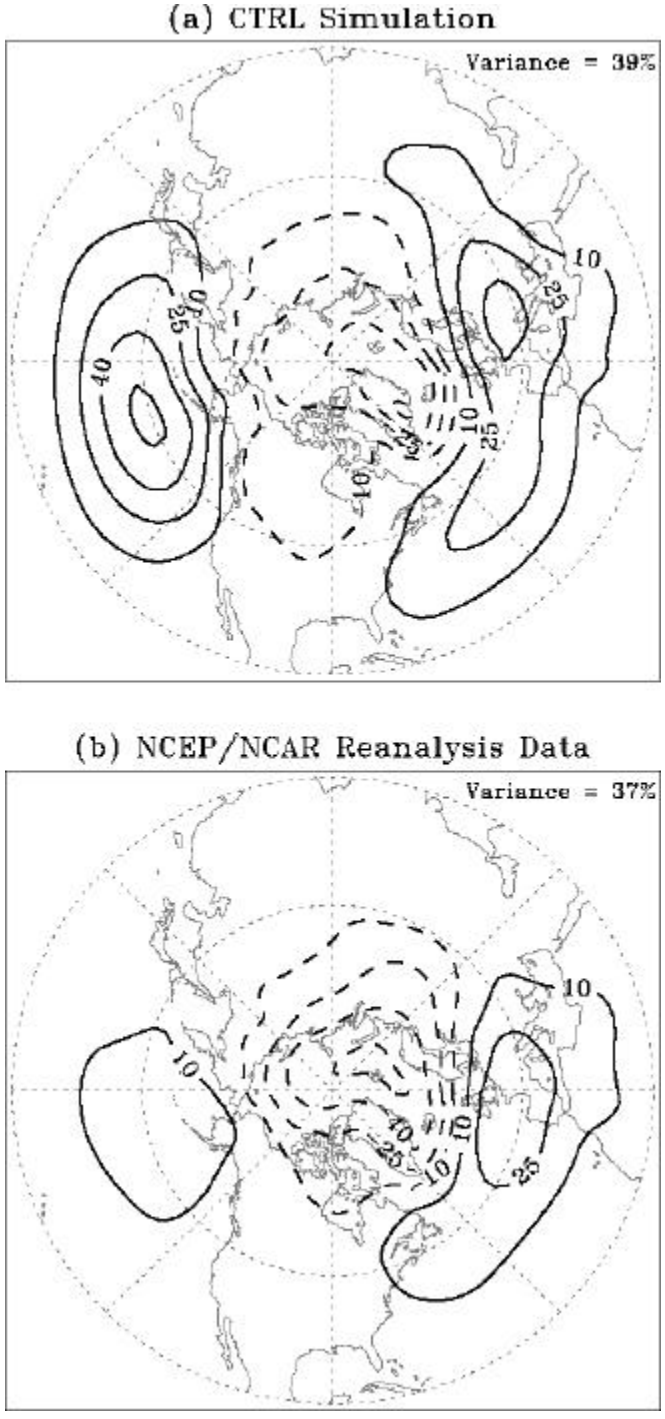

Figure 2-3: The AO mode of variability, depicted using empirical orthogonal function analysis of the Northern Hemisphere (north of the equator) winter (DJF) sea level pressure (SLP) field. a) The leading spatial pattern of winter variability (EOF1) for the twenty year CTRL simulation. b) Same as a), except for 27 years of NCEP/NCAR reanalysis data. Contour values are arbitrary, and represent relative magnitudes within the spatial EOF1 pattern. Dashed line denotes negative contour value.

2.2 Experimental Design

Each GCM experiment consists of 20 independent integrations of autumn-winter climate, under a specified land surface boundary condition forcing. The model integration period runs from September through February, to capture the season of greatest snow variability (autumn) and the subsequent (winter) climate response when the AO mode is strongest. The spring and summer seasons are not simulated, based on the assumption that there is no year-to-year memory in snow cover/snow depth. This assumption is reasonable since the CTRL simulation, the USAF/ETAC snow depth climatology, and the NOAA snow cover dataset all consistently indicate that Northern Hemisphere snow cover virtually disappears each summer, with the exception of glacial regions such as the Greenland ice sheet.

A large (twenty member) ensemble is simulated for each experiment. Recent literature on ensemble GCM integrations suggests that earlier studies consisting of six or fewer realizations may be insufficient to distinguish externally forced impacts from internal model variability, especially during the winter when extratropical variability is high. For example, Mehta et al. (2000) use sixteen realizations of a 44-year GCM simulation to illustrate that with increasing ensemble size, the average correlation between modeled and observed NAO indices increases, and the range of correlations over all ensemble set permutations decreases. As described in Appendix B, gridpoint sea level pressure statistics for our twenty-member ensemble experiments similarly exhibit a decreasing range of possible values over all permutations with increasing ensemble size, with considerably larger variability for ensemble sizes less than ten. Furthermore, the AO is known to exhibit variability at a wide range of timescales, from intraseasonal to interannual or even longer. A large ensemble is needed to fully capture the interannual variability associated with the AO, so that snow-forced differences in the AO mode in excess of the naturally occurring variability can be effectively realized.

A set of 20 independent September 1 initial conditions is used to start the six-month model integrations for each experiment, obtained from the 20-year CTRL simulation. Initiating the numerical experiments with September 1 conditions from 20 different years instead of 20 consecutive days within a single year ensures that the 20 model integrations are reasonably independent.

A total of twelve GCM experiments are performed in this thesis. A high snow forcing is applied in five of the experiments, and a corresponding low snow forcing is applied in five others. Two other experiments involve control conditions (freely-varying snow) and climatological snow conditions. All twelve experiments are summarized in Table 2-1, with respect to the all relevant boundary conditions, including the snow forcing region, specific snow forcing characteristics, orography and surface albedo.

All experiments involve the specification of SST and snow cover/snow depth boundary conditions in the model. Whereas SSTs represent true passive boundary conditions for this atmospheric GCM, snow is treated by the model as an active internal state variable, since snow accumulation, snowmelt, and a five layer land surface scheme are included in the model's land surface parameterization. Thus prescribing snow depth as an external boundary condition in the GCM experiments may potentially disrupt the energetics of the land surface. To minimize any surface imbalances, snow depth is

Experiment	Snow Forcing Region	Snow Cover Forcing	Snow Depth Forcing	Other Boundary Conditions
FREE (CTRL)	-	--	--	--
FIX	Global	GCM Climatology	GCM Climatology	--
SIB High Snow	Siberia	Sep76 – Feb77 Observations	Shifted Climatology	--
SIB Low Snow	Siberia	Sep88 – Feb89 Observations	Shifted Climatology	--
ORO High Snow	Siberia	Sep76 – Feb77 Observations	Shifted Climatology	Siberian Mountains Removed
ORO Low Snow	Siberia	Sep88 – Feb89 Observations	Shifted Climatology	Siberian Mountains Removed
NA High Snow	North America	Sep96 – Feb97 Observations	Shifted Climatology	--
NA Low Snow	North America	Sep87 – Feb88 Observations	Shifted Climatology	--
ALB High Snow	Siberia	Sep76 – Feb77 Observations	--	--
ALB Low Snow	Siberia	Sep88 – Feb89 Observations	--	--
INS High Snow	Siberia	Sep76 – Feb77 Observations	Shifted Climatology	Background (snow-free) Surface Albedo
INS Low Snow	Siberia	Sep88 – Feb89 Observations	Shifted Climatology	Background (snow-free) Surface Albedo

Table 2-1: Summary if all GCM experiments

specified at each timestep prior to updating the surface moisture and energy fluxes, so that the prescribed snow is subject to melting and evaporation. The resulting surface energy balances for all experiments are evaluated in Appendix C, to confirm that the energy balance terms are not unduly disrupted by the snow specification.

Chapter 3

Climate Response to Model Generated Snow Variability

3.1 Description of Experiments

This research is based on the idea that interannual variations in land surface snow can exert a modulating influence on interannual variability of the winter AO mode. As a preliminary exploration of this hypothesis, a pair of large-ensemble atmospheric GCM experiments is conducted to investigate the degree to which wintertime extratropical Northern Hemisphere climate variability is influenced by interannual variability in surface snow conditions.

The first experiment is designated as FIX. It consists of prescribed monthly climatological SSTs and sea ice throughout the global model domain, derived from the COLA/CAC dataset developed for the Atmospheric Model Intercomparison Project (Gates, 1992). Climatological snow depth values are also prescribed, on a weekly basis throughout the global model domain. The "fixed" snow depth climatology applied in this experiment is derived by averaging the weekly model-generated snow depth over the 20-year CTRL simulation. This experiment therefore includes no interannual variations in either the land surface snow or the SST boundary condition.

The second experiment is designated as FREE. Monthly climatological SSTs and sea ice are once again prescribed. Snow depth is not prescribed, but left unaltered as an internally varying, i.e. "free", land surface state variable. This experiment therefore includes intraseasonal and interannual variations in the land surface snow depth boundary condition as generated by the model, but no interannual variations in the SST boundary condition. Note that this experiment essentially consists of the September-February months from the CTRL simulation. To demonstrate the extent of these interannual snow variations, Figure 3-1 shows the Northern Hemisphere snow depth field for two different realizations of the FREE experiment, which generate relatively extensive (Fig. 3-1a) and limited (Fig. 3-1b) snow. The figures represent mid-October conditions, when

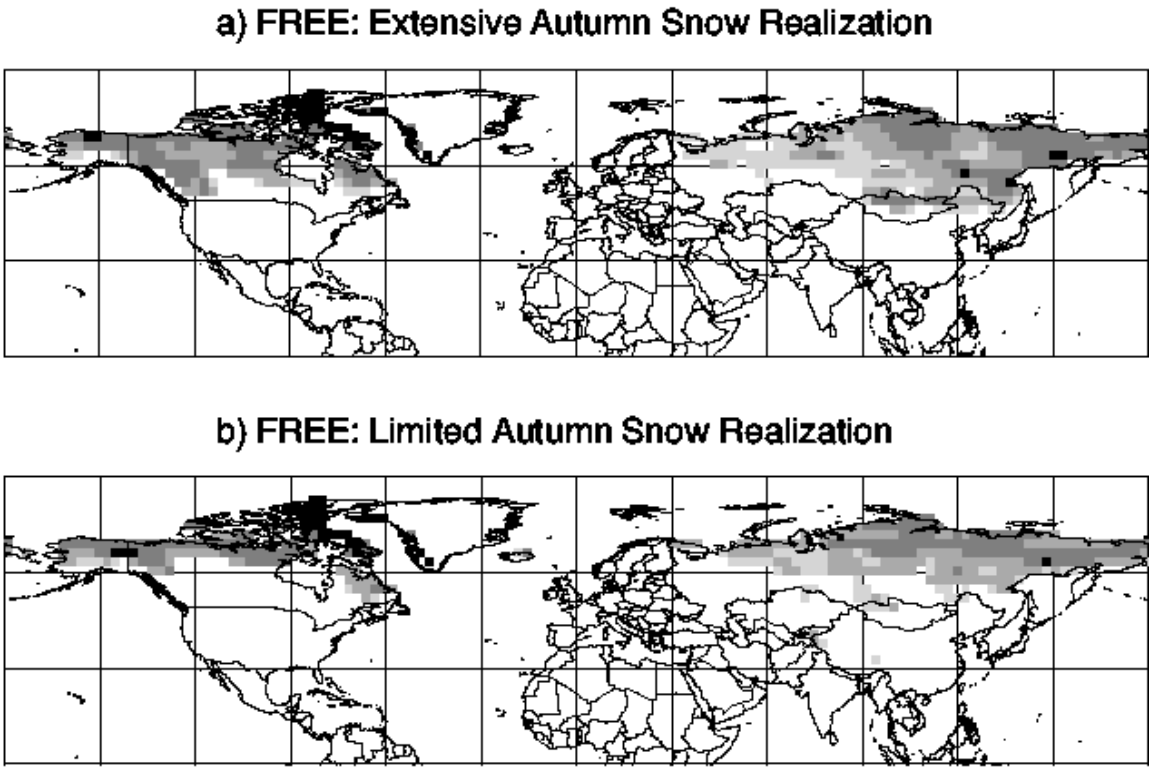

Figure 3-1: Mid-October Northern Hemisphere snow depth fields for the FREE experiment: a) realization with extensive autumn snow; b) realization with limited autumn snow. Shading represents 0.1-1 cm (lightest), 1-5 cm, 5-25 cm, and 25+ cm (darkest).

interannual variations in snow depth are expected to be substantial. The most notable differences occur over southern Siberia and southern Canada.

One experiment (FIX) uses the same prescribed climatological snow depths for all realizations while the other (FREE) retains the freely varying model snow depths generated by each realization. However both experiments have identical ensemble mean snow depths throughout the six-month integration period. Thus the sole difference between the two experiments is the inclusion of interannual snow variability in FREE but not in FIX. Also note that the snow variability contained in FREE is generated internally by the GCM, and that GCMs generally underestimate the observed snow variability. The climate response to more realistic, observation-based snow forcings will be discussed in subsequent chapters.

3.2 Modeled AO as an Internal Mode of Variability

As in Chapters 1 and 2, the leading AO mode of variability over the 20 realizations of the model simulated Northern Hemisphere winter (DJF average) is evaluated using empirical orthogonal function analysis. Figure 3-2 shows the leading empirical orthogonal function (EOF1) for the Northern Hemisphere (north of the equator) sea level pressure (SLP) field, for the FIX experiment. The characteristic dipole pattern between high and mid-latitudes associated with the hemispheric AO mode is produced and explains 43% of the total variance in the SLP field, which is comparable to that obtained from NCEP/NCAR reanalysis data (Fig. 1-1a). However, in Figure 3-2 the Pacific anomaly is stronger than the Atlantic anomaly, whereas observations generally indicate a stronger anomaly in the Atlantic. The corresponding EOF1 for the 500-hPa geopotential height field (not shown) is likewise comparable to observations.

Figure 3-2 indicates that even in the absence of interannual variations for both the snow depth and SST boundary forcings, the model climate still exhibits the classic AO pattern of variability at the surface. Since interannual external forcings are not included in the FIX experiment, the resulting AO mode arises solely from intraseasonal fluctuations, i.e., internal climate noise (Feldstein, 2002). This result agrees with recent studies (described in Chapter 1) which assert that the principal mechanisms which drive this dominant mode of climate variability likely do not reside in the surface boundary conditions, but rather are internal to the atmospheric system. This internal mode is also observed in other GCMs forced with seasonally-varying climatological SSTs (Robertson, 2001), and in coupled atmospheric-ocean models (Fyfe et al., 1999; Stone et al., 2001).

Although surface conditions do not appear to govern the AO, they may nevertheless be influential enough to modulate this pattern of climate variability in some respect. Both SSTs and snow have been shown to influence other features of the climate system, such as ENSO related climate variability and summer monsoon activity. Also, previous studies have revealed statistically significant relationships between the AO and both SSTs and snow cover. Even if the AO is a fundamental internal atmospheric mode, it can potentially be varied by surface boundary conditions, such that the total interannual variability in the observed AO mode is not comprised entirely of internal climate noise. In the next section, one such forcing, interannual snow depth variations, will be studied in detail.

3.3 Effect of Interannual Snow Variations

3.3.1 Mean Climate State

Before evaluating the effect of interannual snow depth variations on the characteristics of the modeled AO mode, the impact of prescribing climatological snow depth values on the mean climatic state of the model will be briefly addressed. Figure 3-3 shows the ensemble mean difference (FREE-FIX) in surface albedo, surface temperature, and sea level pressure (SLP), for the autumn (SON) and winter (DJF) seasons. Neither albedo (Fig. 3-3a,d) nor temperature (Fig. 3-3d,e) exhibits any coherent difference over land

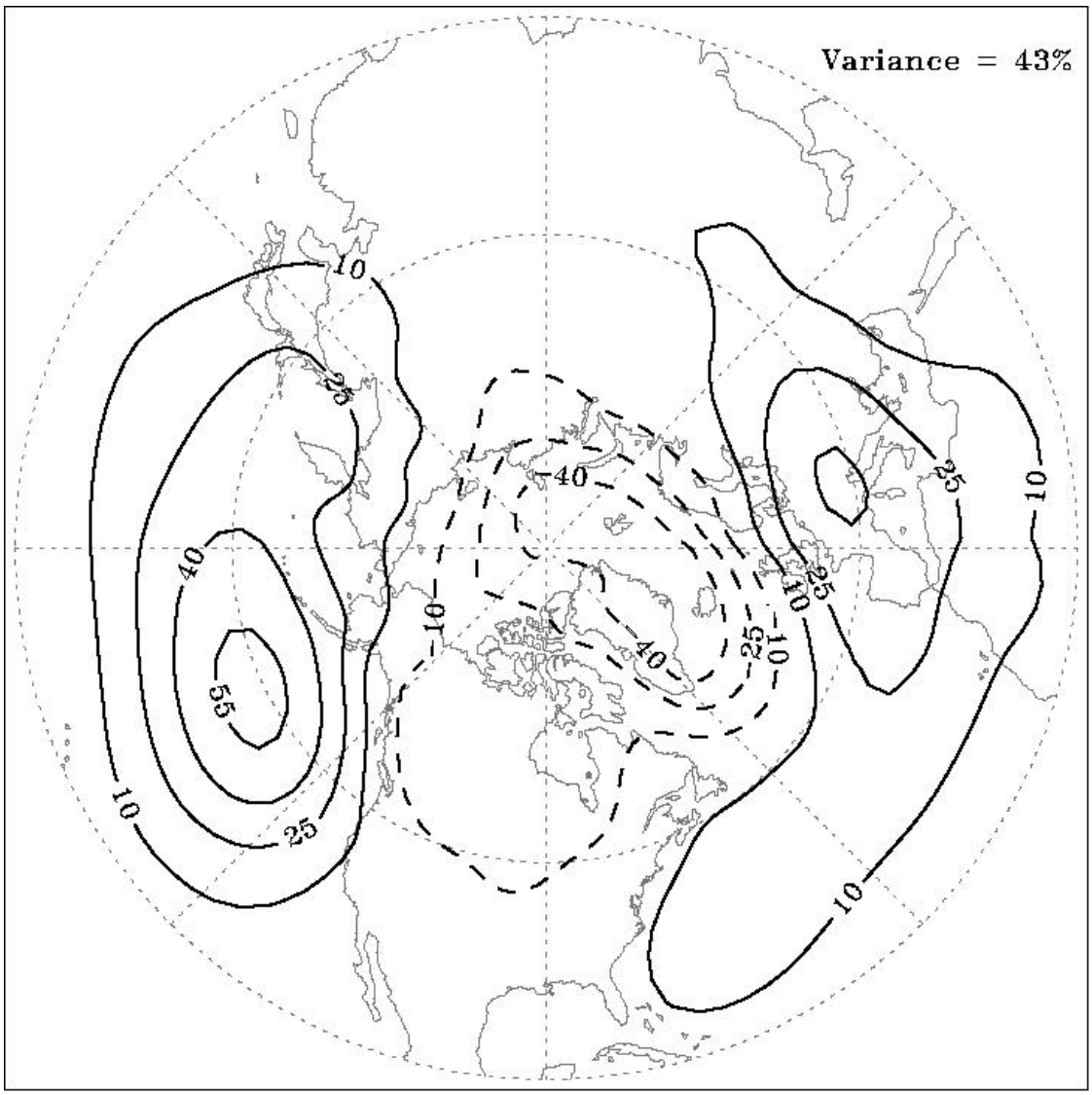

Figure 3-2: Leading empirical orthogonal function (EOF1) of Northern Hemisphere (north of the equator) DJF average SLP field, computed from the 20 realizations of the FIX experiment (prescribed monthly climatological SSTs and prescribed weekly climatological snow depth), including the percent of total variance in SLP explained by the EOF1 mode. Contour values are arbitrary, and represent relative magnitudes within the spatial EOF1 pattern. Dashed line denotes negative contour value.

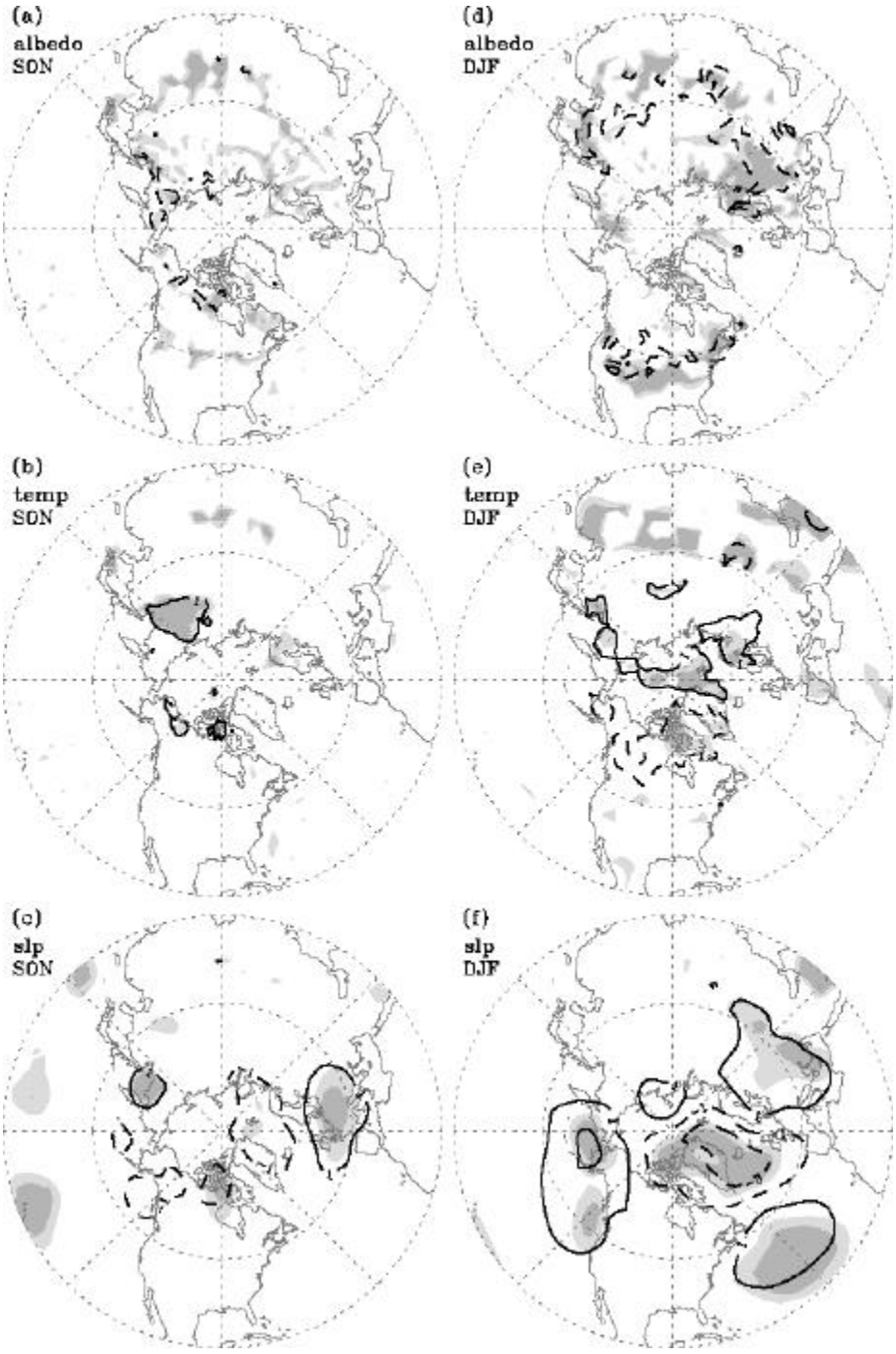

Figure 3-3: Ensemble mean surface climatology response to interannual snow variability (FREE-FIX), over the extratropical Northern Hemisphere, for autumn (a-c) and winter (d-f) seasons. Surface albedo (a,d) contours drawn at ± 0.02, 0.1, 0.25. Surface temperature (b,e) contours drawn at ± 1, 3, 5 °C. Sea level pressure (c,f) contours drawn at ± 1, 3, 5 hPa. Dashed line denotes negative contour value. Light (dark) shading indicates 90% (95%) statistical significance.

surface regions, indicating a negligible ensemble mean local thermodynamic response to interannual snow variability. Winter SLP (Fig. 3-3f) does exhibit some regions of significant difference between FREE and FIX. These differences are somewhat reminiscent of the AO mode, although the spatial patterns are not well organized. Winter tropospheric geopotential height and zonal wind fields (not shown) exhibit a similarly weak and disjointed response. This slight shift in mean climatic state might suggest that winter climate responds nonlinearly to the positive vs. negative snow anomalies contained in FREE, relative to FIX. On the other hand, it may simply be a random consequence of naturally-occurring internal atmospheric variability. Overall, the mean climate is not notably affected by the use of prescribed snow depth climatology in FIX.

3.3.2 AO/NAO Characteristics

Figure 3-4 presents the leading empirical orthogonal function (EOF1) of the Northern Hemisphere (north of the Equator) SLP field, for the FREE experiment (repeated from Fig. 2-3a). As for the FIX experiment in Figure 3-2, the major AO characteristics (i.e., spatial pattern and percentage of total variance explained) are produced, although the Pacific anomaly is once again stronger than the Atlantic anomaly. In addition, the principal components for the two EOF1 patterns have statistically identical standard deviations (87.6 hPa for FIX, 85.7 hPa for FREE), indicating that the interannual snow variations in FREE do not result in increased hemispheric climate variability. These similarities are further demonstration that the AO is a fundamental internal mode of the atmosphere. However, a close comparison of FIX vs. FREE indicates that the inclusion of interannual snow variations results in subtle but notable changes to the AO pattern. These changes are revealed in Figure 3-5, which presents the difference between the EOF1 fields shown in Figures 3-2 and 3-4. Interannual snow variations result in relatively stronger climate variability over Siberia, a broad land surface region subject to considerable snow and snow variations. Climate variability is also relatively stronger over Greenland, Iceland, the North Atlantic and western Europe, regions far removed from major interannual snow variations, but typically associated with the NAO. It should be noted that the contour intervals in Figure 3-5 are less than in Figures 3-2 and 3-4. Thus interannual snow variations enhance the AO mode of variability (albeit slightly) only over specific regions which complement recent observational studies associating snow cover over Eurasia with North Atlantic climate (Cohen and Entekhabi 1999; Cohen et al., 2001; Saito et al., 2001).

The principal components time series for the EOF1 patterns shown in Figures 3-2 and 3-4 also exhibit a very low and statistically insignificant correlation (0.18) between the FIX and FREE experiments. Similarly, a regional NAO Index is computed, by differencing winter SLP values between the Arctic and North Atlantic centers of action indicated by the EOF1 modes. As for the EOF1 principal components, this NAO index over all 20 realizations is poorly correlated (0.12) between FIX and FREE. This lack of correlation may be associated with the introduction of interannual snow variations in FREE, under the presumption that a significant correlation would result if the snow anomalies had a negligible effect on climate variability. On the other hand, the poor

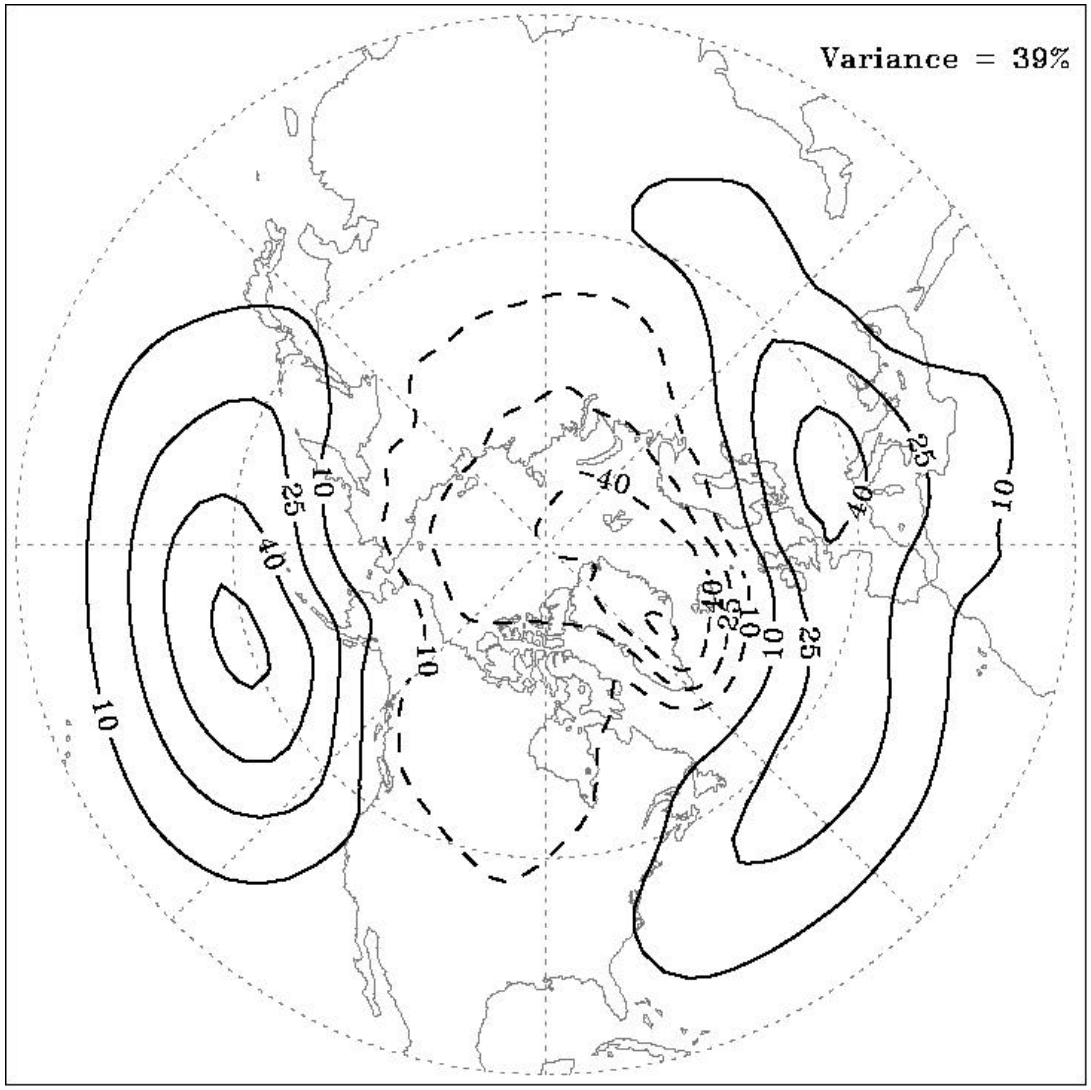

Figure 3-4: Leading empirical orthogonal function (EOF1) of Northern Hemisphere (north of the equator) DJF average SLP field, computed from the 20 realizations of the FREE experiment (prescribed monthly climatological SSTs and internally varying model snow depth), including the percent of total variance in SLP explained by the EOF1 mode. Contour values are arbitrary, and represent relative magnitudes within the spatial EOF1 pattern. Dashed line denotes negative contour value.

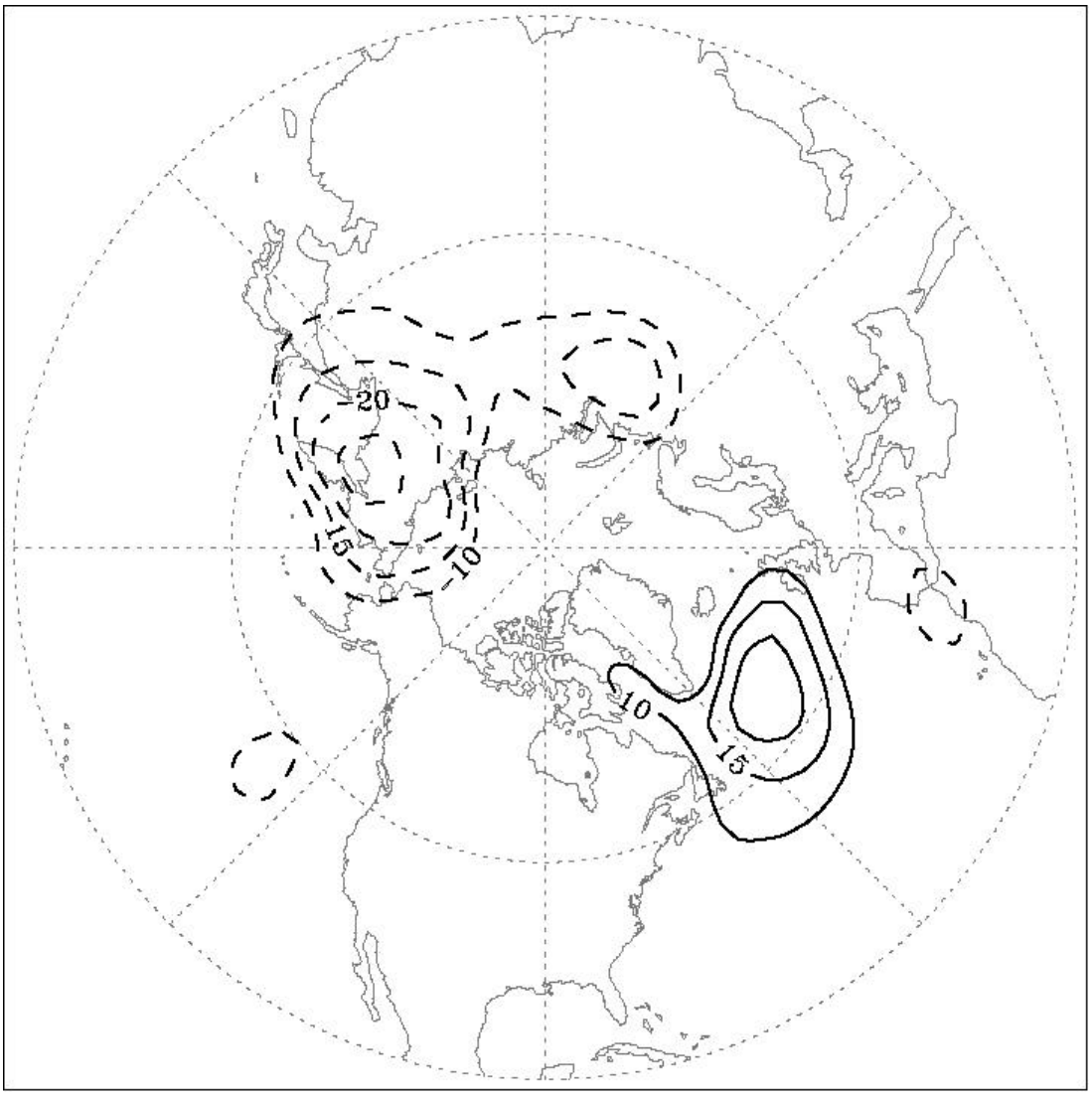

Figure 3-5: Difference in leading empirical orthogonal function (EOF1) of Northern Hemisphere (north of the equator) DJF average SLP field, between the FREE and FIX experiments. Contour values are arbitrary, and represent relative magnitudes within the spatial EOF1 difference pattern. Dashed line denotes negative contour value.

climate index correlation between the realizations of the two experiments may simply be attributed to chaos in the system.

In an attempt to confirm this reasoning, the Antarctic Oscillation (AAO) Index is evaluated, which describes a pattern of high to mid-latitude Southern Hemisphere climate variability analogous to the NAO Index in the Northern Hemisphere (Gong and Wang, 1999). The winter AAO Index is much more highly correlated (0.52, which is statistically significant at 95%) between the FIX and FREE experiments than is the winter NAO Index (0.12). Due to the very limited occurrence of land surface snow in the modeled Southern Hemisphere, interannual snow variations are not expected to have a substantial impact on Southern Hemisphere climate variability. Therefore the significant correlation in the southern index suggests that the lack of correlation in the northern index may be due in part to the considerable snow variations in the Northern Hemisphere and associated climate modulations. It must be noted that this exploratory evaluation of the AAO Index not a precise test of the predictability of the AO and AAO, nor of the implications of the poor correlations found for the AO indices. Nevertheless, this comparison between Northern and Southern Hemisphere fields yields results that are notable and which may provide insight into the role of the differences between the experiments, i.e. the results maintain the possibility that interannual snow variations are a modulator of winter Northern Hemisphere climate.

3.3.3 Vertical Extent of the AO/NAO

An important facet of the AO as derived from observed data is its vertical extent, characterized by highly correlated dominant modes of variability extending from the surface into the stratosphere (Thompson and Wallace, 1998). This feature is evaluated for both the FIX and FREE experiments by correlating the winter (DJF) EOF1 principal components between SLP and geopotential height at various atmospheric pressure levels, as shown in Figure 3-6. For FREE, the surface signal is well correlated with the troposphere, and reasonably well correlated throughout most of the stratosphere. Statistically significant correlations at 95% extend to a height of 20 hPa, which is consistent with observations. This result implies that with the inclusion of interannual snow variations, the resulting AO mode of variability occurs throughout the atmosphere. For FIX however, even though the correlation with the troposphere is again very strong, the correlation with the stratosphere is notably weaker, and no longer statistically significant. This result is strongly suggestive that without interannual snow variations, the dominant modes of variability in the troposphere and stratosphere may be essentially uncoupled. Thus interannual snow variations at the land surface boundary are necessary to maintain the full vertical extent of the AO mode of variability. Hypothesized dynamical mechanisms for generating this connectivity include the vertical propagation of Rossby waves, excited by surface diabatic heating changes over snow anomalies (Saito et al., 2001, Cohen et al., 2002).

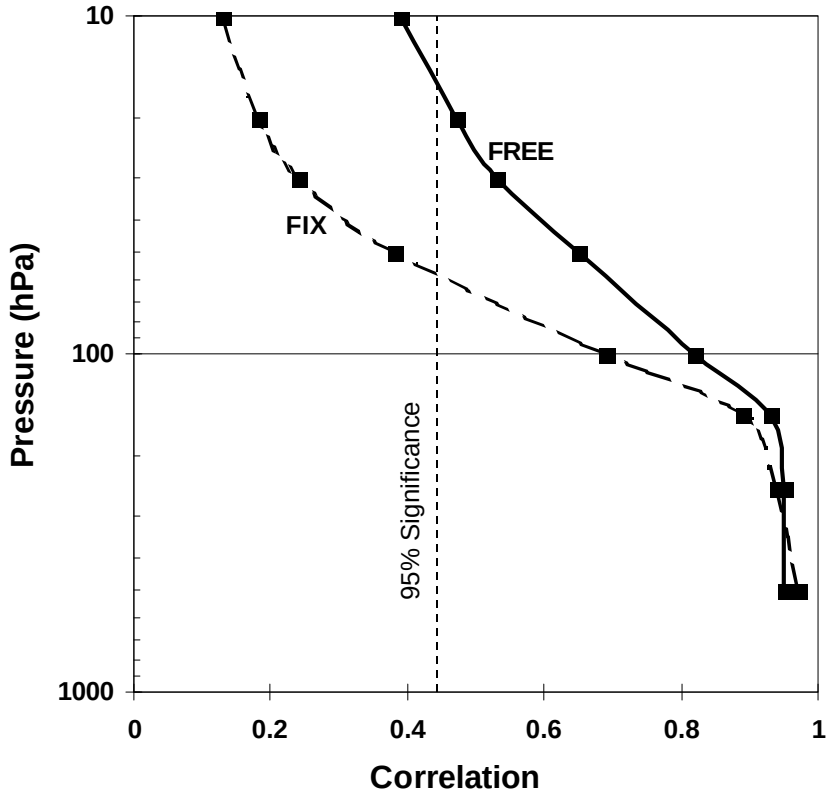

Figure 3-6: Northern Hemisphere DJF average EOF1 principal components correlation between SLP and geopotential height at various pressure levels throughout the troposphere and stratosphere, for the FREE (solid line) and FIX (dashed line) experiments.

3.3.4 Origins of the AO/NAO

In Cohen et al. (2001), 27 years of NCEP/NCAR reanalysis data (Kalnay et al., 1996) are used to correlate a winter climate index describing the AO mode of variability to 45-day average gridded values of surface parameters (e.g., SLP). A temporal sequence of correlation fields from October through January demonstrates the role of the Siberian High in Northern Hemisphere climate variability. In this section, a similar analysis is conducted using GCM output from both the FREE and FIX experiments, intended as a numerical modeling counterpart to the observational analysis of Cohen et al. (2001).

Figure 3-7 presents the correlation between the EOF1 principal components for winter (DJF) Northern Hemisphere 50-hPa geopotential height, and a series of gridded 45-day average SLP fields spanning the September-February GCM integration period, for FREE. For reference, regions of 90% and 95% statistical significance as determined by t-tests are indicated by light and dark shading, respectively. It should be noted that such

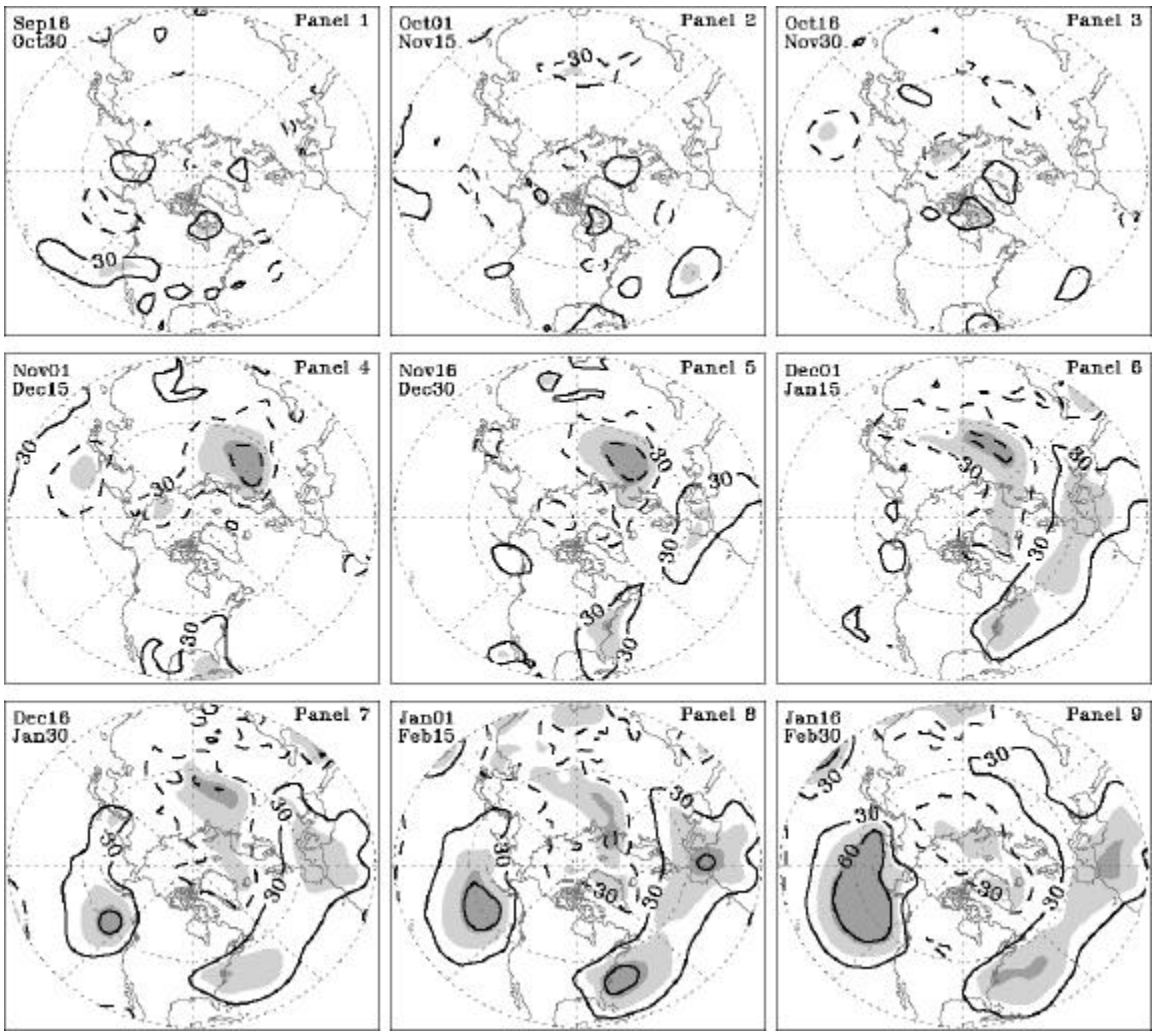

Figure 3-7: Percent correlation between EOF1 principal components for DJF average Northern Hemisphere 50-hPa geopotential height field and a series of 45-day average gridpoint SLP, for the FREE experiment. Contours drawn at +/- 30, 60, 80 percent correlation. Solid (dashed) lines denote positive (negative) correlation. Light (dark) shading represents absolute correlations in excess of 44 (56) percent, representing 95% (99%) statistical significance.

traditional measures of statistical significance have come under recent scrutiny (Nicholls, 2000); therefore the focus should be on the overall spatial patterns of correlation, and not just on regions of statistical significance. Figure 3-7 indicates a region of negative correlation which emerges in western Siberia in late autumn (panel 4), and expands northward with the onset of winter into the Arctic and high-latitude North Atlantic. Concurrent with this expanding region of negative correlation during winter is the emergence of a region of positive correlation in the mid-latitude North Atlantic and western Europe (panel 6), and another positive correlation region in the North Pacific (panel 7). The ultimate late winter correlation field (panels 8 and 9) resembles the AO pattern of variability.

Figure 3-7 indicates that with the inclusion of interannual snow variations, the winter AO signal originates in the autumn as a SLP anomaly over Siberia, which subsequently appears to migrate over the Arctic and into the North Atlantic during the course of the autumn-winter season. In response, the winter Icelandic and Aleutian Low pressure cells are apparently forced to migrate southward, contributing to the dipole SLP anomaly pattern characteristic of the AO. Figure 3-7 is analogous to Figure 2 (based on 27 years of NCEP/NCAR reanalysis data) of Cohen et al. (2001), which similarly portrays an apparent surface teleconnection pathway originating as an autumn SLP anomaly over Siberia, and migrating over the Arctic to contribute to the winter AO/NAO pattern. Note that Siberia is a broad high to mid-latitude land surface region, whose dominant autumn-winter land surface feature is snow cover. In addition, interannual snow cover variability over Siberia is most likely to occur in autumn, as opposed to winter when snow cover is fully established. Thus the origin of the AO pattern is coincident with the region and season of greatest interannual snow variability in the FREE experiment, which demonstrates how autumn snow conditions in Siberia may modulate winter climate throughout the extratropical Northern Hemisphere. This apparent surface pressure teleconnection pathway implies that even though the AO mode in FREE is generated from intraseasonal fluctuations in the atmosphere (i.e., internal climate noise), it is not isolated from interseasonal variations in surface boundary conditions.

Figure 3-7 also provides further evidence that snow variations modulate climate patterns throughout the atmosphere, since the surface SLP teleconnection pathway for the AO signal is observed using EOF1 principal components at 50 hPa, i.e., an upper level climate index. Figure 3-8 is identical to Figure 3-7, except that the gridpoint SLP fields are instead correlated to EOF1 principal components for winter (DJF) SLP, the traditional surface level AO climate index. Figure 3-8 indicates an obvious AO winter correlation pattern (panels 7-9), since the climate index used is derived from SLP values, so that winter gridpoint SLP values are essentially correlated to themselves. However, the autumn Siberian SLP anomaly and subsequent Arctic migration (panels 4-6) is not as prevalent using the surface index in Figure 3-8 as with the upper level index in Figure 3-7. Consistent with the statistically significant correlation of EOF1 principal components throughout the troposphere and stratosphere in the FREE experiment (Fig. 3-6), this result suggests that a vertical teleconnection pathway may also exist.

Both Figures 3-7 and 3-8 correlate gridpoint SLP values to winter (DJF average) EOF1 climate indices. However, this results in a temporal overlap between the winter

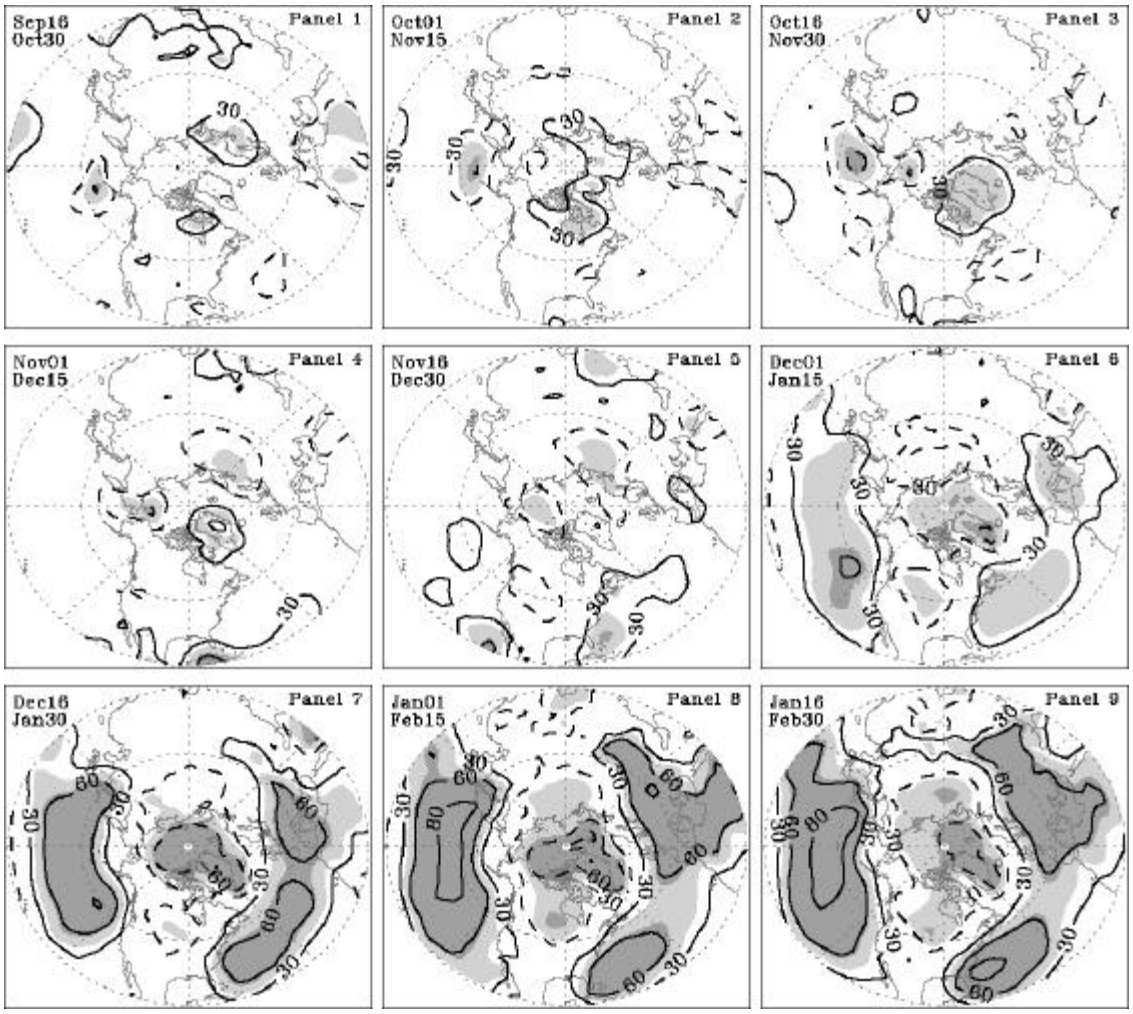

Figure 3-8: Percent correlation between EOF1 principal components for DJF average Northern Hemisphere SLP field and a series of 45-day average gridpoint SLP, for the FREE experiment. Contours drawn at +/- 30, 60, 80 percent correlation. Solid (dashed) lines denote positive (negative) correlation. Light (dark) shading represents absolute correlations in excess of 44 (56) percent, representing 95% (99%) statistical significance.

index and the 45-day average periods beginning with panel 4 of the figures. The Siberian SLP anomaly associated above with the AO signal first emerges during an overlapping period (panel 4), which raises the possibility that the observed Siberian SLP anomaly is an artificial result of the overlapping periods. Therefore the correlation sequences shown in Figures 3-7 and 3-8 were reevaluated using EOF1 principal components averaged over January-February only, so that overlaps do not occur until panel 6. This two month period was sufficiently long to exhibit 50-hPa geopotential height and SLP EOF1 patterns equivalent to those for the DJF average. The resulting correlations sequences (not shown) are very similar to, and thereby validate, Figures 3-7 and 3-8; a negative SLP anomaly again appears over Siberia in autumn, and migrates over the Arctic to produce the winter AO pattern.

Figure 3-9 shows the gridpoint SLP correlation sequence to winter 50-hPa geopotential height EOF1 principal components, computed for the FIX experiment. In contrast to the FREE experiment (Fig. 3-7), an autumn SLP anomaly over Siberia fails to materialize without interannual snow variability. Furthermore, the winter AO pattern also does not materialize, since for the FIX the stratospheric EOF1 mode was found to be uncoupled from the surface AO signal (see Fig. 3-6). Comparison of Figure 3-9 (FIX, upper level index) with Figure 3-7 (FREE, upper level index) clearly demonstrates the manner in which snow variations modulate the interannual variability of the AO. Exclusion of snow variations (FIX) results in an internal AO mode driven purely by intraseasonal fluctuations (i.e., climate noise), which is limited to the lower atmosphere, and unrelated to autumn conditions over Siberia. Inclusion of interannual snow variations (FREE) results in a modulated AO mode influenced by varying surface boundary conditions, coupled to the stratosphere, and which originates as an autumn SLP pressure anomaly over Siberia.

3.4 Discussion

The aim of this set of preliminary experiments is to evaluate the extent to which interannual variations in the land surface snow boundary condition can trigger, excite or otherwise modulate the fundamental internal AO mode of variability. Experiments conducted with and without interannual snow variability are compared to evaluate changes in Northern Hemisphere climate characteristics. Even though interannual snow variations do not drive the AO, results indicate that they are influential enough to alter regional and temporal aspects of the overall AO from the pattern that arises purely from intraseasonal climate noise, in several ways:

The AO mode of variability over the North Atlantic sector is apparently enhanced by interannual snow variations, as indicated by relatively stronger winter SLP EOF1 anomalies over Greenland, Iceland, the North Atlantic and western Europe.

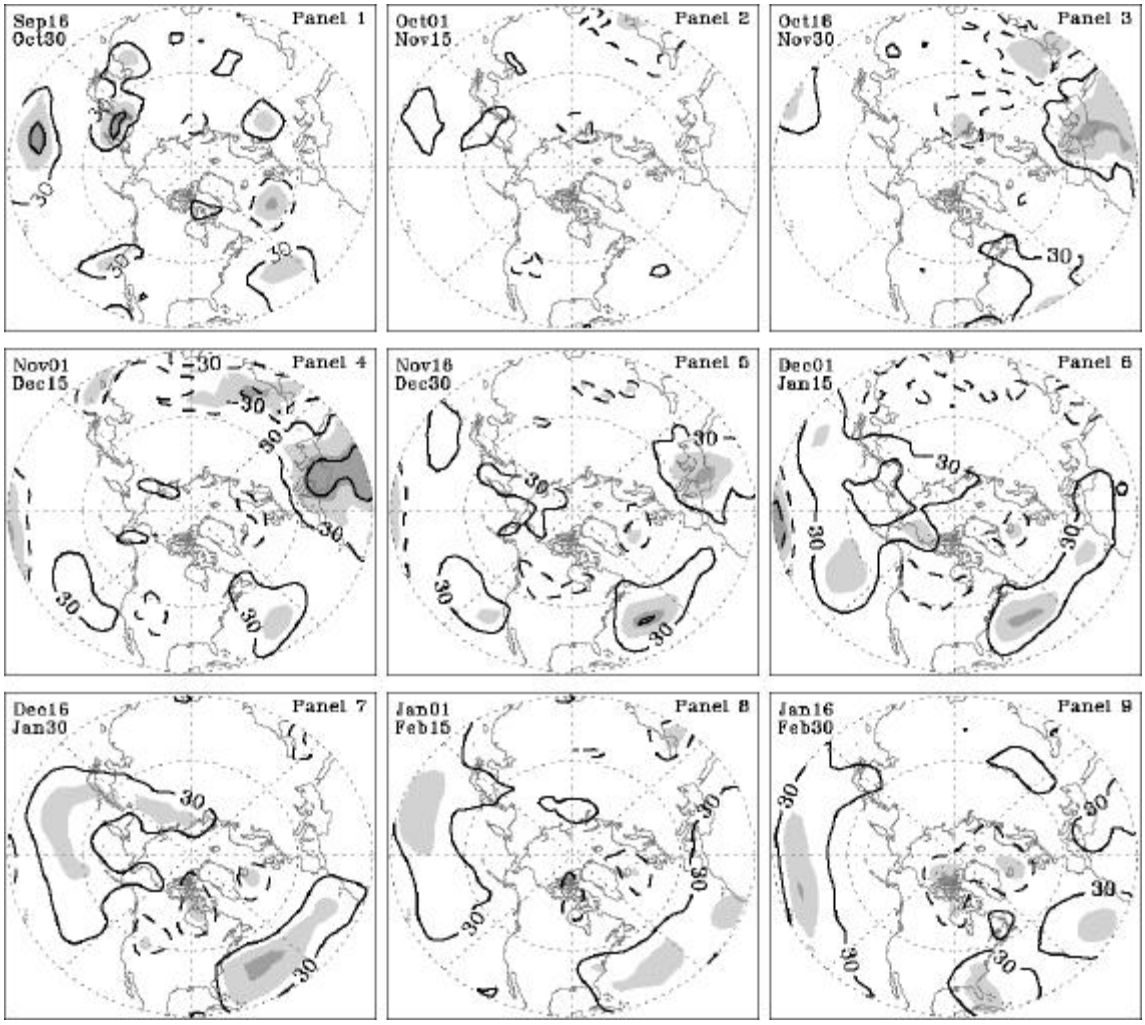

Figure 3-9: Percent correlation between EOF1 principal components for DJF average Northern Hemisphere 50-hPa geopotential height field and a series of 45-day average gridpoint SLP, for the FIX experiment. Contours drawn at +/- 30, 60, 80 percent correlation. Solid (dashed) lines denote positive (negative) correlation. Light (dark) shading represents absolute correlations in excess of 44 (56) percent, representing 95% (99%) statistical significance.

As evidenced by significant correlation of the EOF1 principal components between atmospheric levels, the AO mode of variability extends into the stratosphere only when snow variations are included, otherwise the simulated AO pattern is limited to the troposphere.

With the inclusion of interannual snow variations, the interannual winter AO signal is found to originate in autumn over Siberia, a season and region of maximum snow cover variability. Without interannual snow variations, the interannual winter AO signal may be unrelated to autumn conditions over Siberia.

These modeling results are consistent with previous observational studies in which a causal relationship between Eurasian snow cover and winter extratropical Northern Hemisphere climate variability has been hypothesized and investigated. The required inclusion of interannual snow variability to reproduce the full vertical extent of the AO mode is suggestive of a vertical teleconnection pathway, as discussed in Saito et al. (2001). The autumn SLP anomaly over Siberia which evolves into the winter AO pattern echoes the surface teleconnection pattern described in Cohen at al. (2001). This agreement between observational analyses and numerical modeling experiments is critical to building a more complete case regarding the ability of interannual snow variations to at least modulate, if not drive, mid-latitude Northern Hemisphere climate variability during the winter season. The results of this study and its predecessors consistently suggest that anomalous values of the interannual winter AO index may be preceded by anomalous autumn snow conditions in Siberia.

Despite the apparent ability of interannual snow variations to modulate the AO pattern of variability, and the identification of Siberia as a possible source region for this modulation, winter climate indices such as the SLP EOF1 principal components and NAO Index are not directly correlated with autumn snow cover area over Siberia during the FREE experiment (not shown). This appears to contradict previous observation-based analyses which do exhibit a statistically significant correlation between autumn Eurasian snow cover and winter climate indices (Cohen and Entekhabi, 1999; Saito et al., 2001). Potential reasons for this discrepancy include: 1) although snow variations modulate the modeled AO, they are not the principal forcing mechanism (as indicated in Chapter 1), so a direct correlation is not necessarily expected; and 2) internal snow cover and snow depth variability within the ECHAM3 model is notably less than that observed, so the magnitude of the snow forcing in the FREE experiment may be insufficient to yield a direct relationship with the AO pattern. For example, mid-October snow covered area over Siberia (defined as 1.6×10^7 km^2 of land surface area within 45N – 90N and 45E – 135E) ranges from roughly 8.5x106 km2 to 1.3×10^7 km^2 over the 20 realizations of the FREE experiment. In contrast, 20 years (1972-1992) of visible satellite observations (Robinson et al,, 1993) range from 3.0×10^6 km^2 to 1.5×10^7 km^2, a spread nearly three times as large as for FREE.

Note that the results presented in Figures 3-7 and 3-8 indicate a clear correlation between autumn SLP anomalies over Siberia and winter climate indices, which implies that the connection between Siberian snow and the overlying SLP is lacking in the FREE experiment, and suggests that snow forcing in FREE may be insufficient. The following

chapters describe additional GCM experiments in which weekly snow cover and snow depth is prescribed based on observations during extreme high and low autumn snow cover years, and the ensemble mean response to these snow perturbations is evaluated. These experiments will build upon the results presented here by analyzing the effect of snow anomalies that are larger than those contained in FREE, yet still realistic. Also, the hypothesized surface and vertical teleconnection pathways, e.g., the expansion and migration of semi-permanent surface sea level pressure cells, and the vertical propagation of stationary waves, will be investigated in greater detail.

Chapter 4

Climate Response to Observed Siberian Snow Conditions

4.1 Description of Experiments

One of the research goals presented in Chapter 1 is to conduct a focused GCM modeling study to complement the extensive observational analyses that have been performed regarding the snow-AO relationship. Figure 4-1 shows one of the key elements of this observed relationship, namely an interannual time series correlation of 0.56 between the winter AO index (repeated from Fig. 1-1b) and NOAA visible satellite observations of snow cover over Eurasia during the preceding autumn (Robinson et al. 1993; Robinson 2000). This figure is an updated version of Figure 1b from Cohen and Entekhabi (1999). Note that the sign of the AO index is reversed in Figure 4-1, indicating a negative correlation between autumn Eurasian snow and the winter AO index. Although the correlation is statistically significant, the relatively modest magnitude of 0.56 suggests that snow is but one of a number of factors which can influence the AO.

In this chapter, the winter climatic response to a realistic Siberian snow forcing is evaluated. As stated in Chapter 1, this research focuses on autumn snow anomalies over Siberia as a modulating factor for the subsequent winter AO mode. This region exhibits the greatest variability in autumn snow extent between extensive and limited snow years, and thus holds the greatest potential for modulating winter climate. Therefore, snow forcing is only prescribed over Siberia, specifically land surface gridcells within 36.5N to 90.0N, and 67.5E to 140.5E, as indicated in Figure 4-2. Gridcells outside of this Siberia region are left unaltered, i.e. snow is generated and maintained internally by the model. By limiting the snow forcing to a specific targeted region, the climatic response arising from this region can be isolated.

Two snow-forced experiments are performed, in which gridcell snow water equivalent (SWE) depth values are prescribed at each model timestep, derived from NOAA visible satellite observations of weekly snow cover. One experiment simulates high snow conditions, and is based on observations from September 1976 through February 1977, which represents the year with the highest recorded autumn snow cover

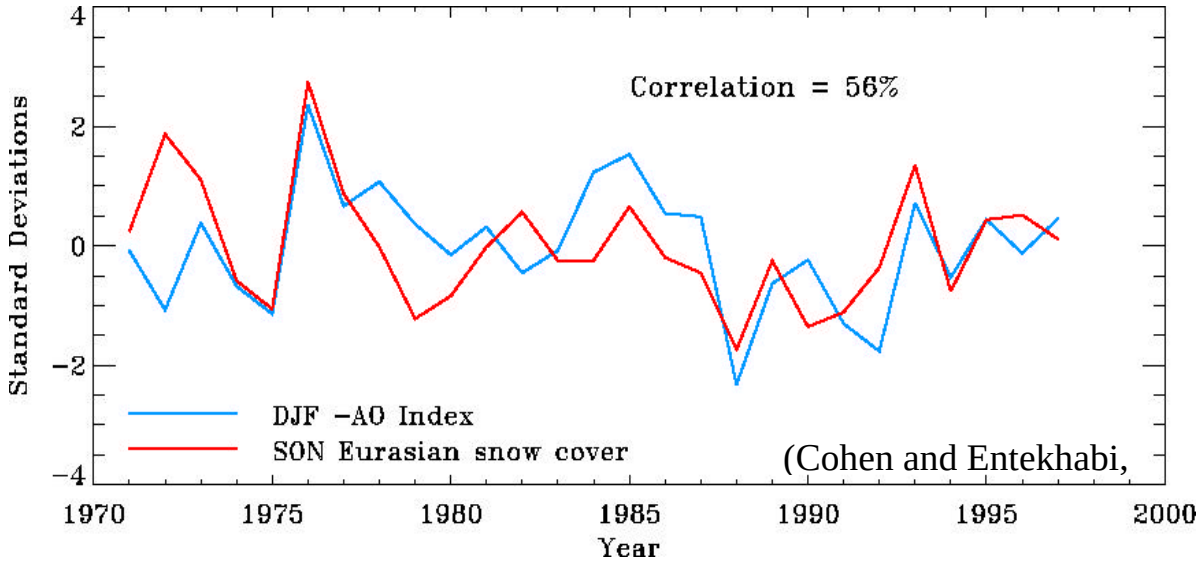

Figure 4-1: Negative winter AO index (solid line) correlated with NOAA visible satellite observations of snow cover over Eurasia during the preceding autumn (dashed line). Correlation of 0.56 is statistically significant at the 99% level.

over Eurasia (see Fig. 4-1). Similarly, the other experiment simulates low snow conditions, and is based on observations from September 1988 through February 1989, which represents the year with the lowest recorded autumn snow cover over Eurasia. These two periods also represent the highest and lowest autumn snow extents over the Siberia forcing region specified in Figure 4-2. The next section describes the specification of observed snow conditions in greater detail. The prescribed snow is then subject to melting and evaporation at each timestep, to minimize disruption of the surface energy balance (see Appendix C).

Ensemble mean differences between the two experiments are computed as (high snow experiment) – (low snow experiment); this explicit climatic response to a realistic, observation-based positive snow forcing over Siberia is designated as SIB. Statistical significance of the mean difference between these two twenty-member ensembles is determined using the t-test. Based on previous studies, it is expected that a positive snow

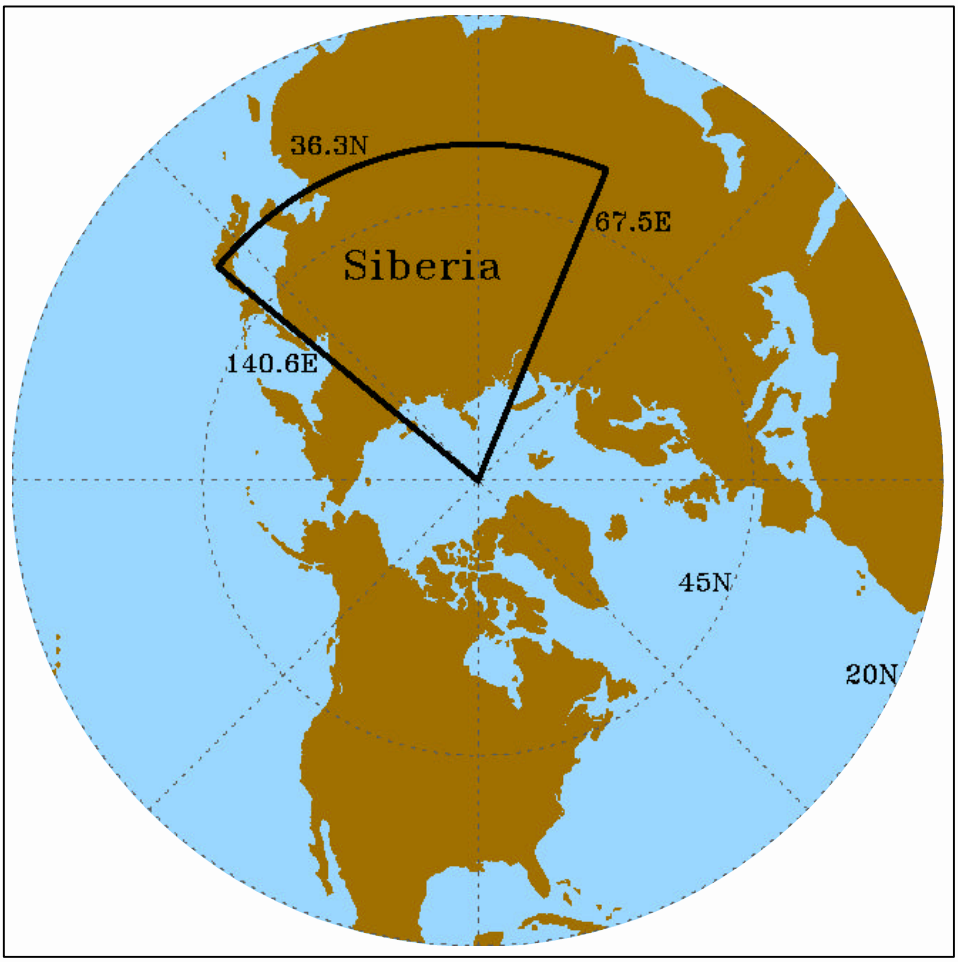

Figure 4-2: Siberia snow forcing region applied for the SIB high snow and low snow experiments. Snow outside of this region is maintained by the model as an internal state variable.

forcing over Siberia will yield a winter climatic response consistent with a negative AO mode. A comprehensive set of diagnostic parameters is evaluated and presented in the following sections to confirm or refute this hypothesis, and to identify the teleconnection pathways that occur.

4.2 Specification of Observed Snow Conditions

4.2.1 Snow Cover Forcing

At every timestep during the model integration period, Siberian gridcells are specified as snow or no-snow according to each experiment's respective time period from the NOAA visible satellite weekly dataset. Figure 4-3 shows the satellite-observed snow extent over

Asia during a week in mid-October, for both the high snow experiment (1976) and the low snow experiment (1988). Also shown is the Siberia forcing region used in both experiments. In 1976 the snow line has reached Mongolia and northern China, whereas for the same period in 1988 only the extreme northeast fringe of Siberia has snow cover. This large contrast in October represents a considerable snow cover forcing between the two experiments, and highlights the potential for autumn snow anomalies to influence climate.

Figure 4-3 illustrates extreme mid-October snow cover conditions based on observations, which can be compared to the model's internally generated extreme mid-October snow cover conditions, as depicted in Figure 3-1. Note that the maximum (minimum) observed snow cover over Asia is notably more extensive (limited) than what is simulated by the model. This comparison exemplifies the underestimation of snow

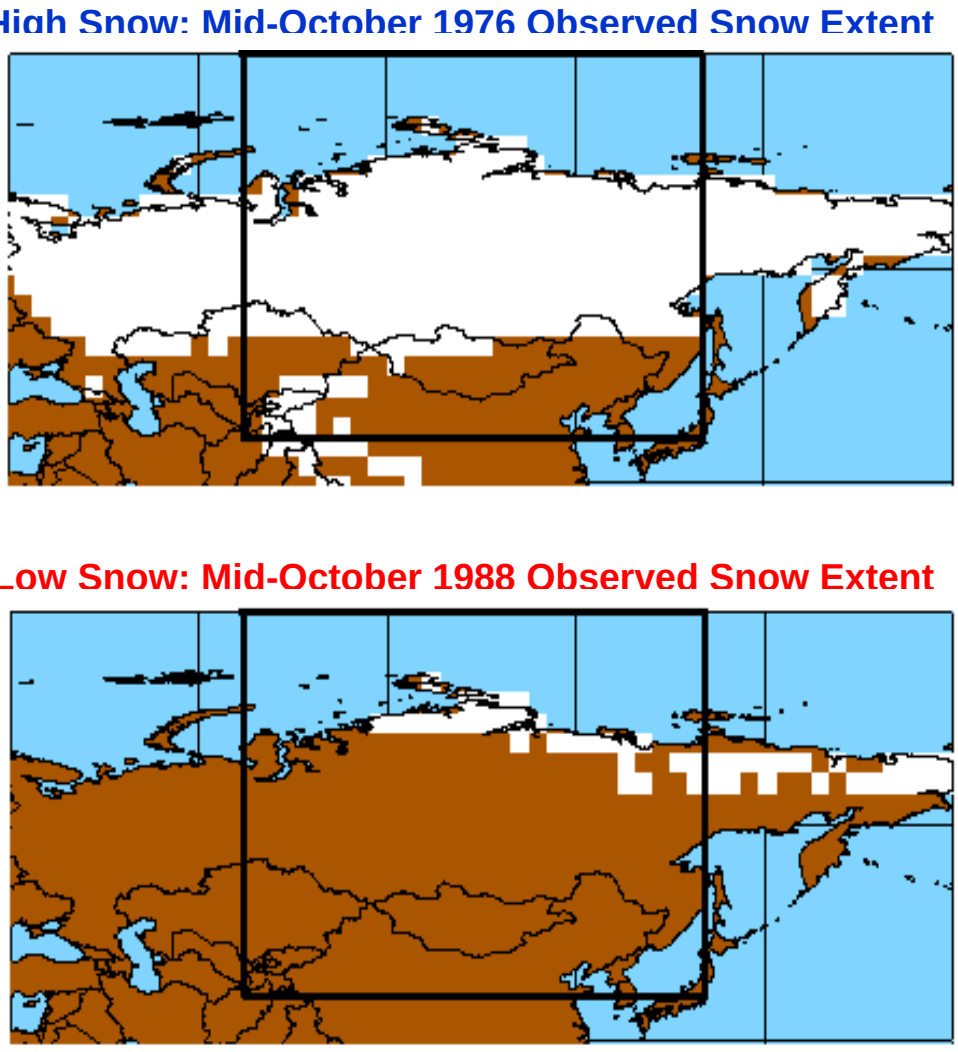

Figure 4-3: NOAA visible satellite observations of snow extent over Asia during a week in mid-October. a) October 1976, used for the high snow experiment. b) October 1988, used for the low snow experiment. Also shown is the Siberia forcing region used in both SIB experiments.

cover variability that is typical for most GCMs, and demonstrates the value of using observation-based snow forcings in the SIB experiments.

Figure 4-4 shows the weekly timeseries of total snow cover extent over the Siberia forcing region for both experiments, throughout the model integration period. Snow cover variations over Siberia begin in late September, and continue steadily into December. The largest differences occur in October, when the snow cover extent can vary by roughly a factor of five. Thus the Siberian snow cover forcing applied in SIB is not only substantial, but also persistent over a three month period from early autumn to early winter. In contrast, during mid-late winter the snow cover forcing is minimal since all of Siberia is essentially covered with snow for both experiments.

4.2.2 Snow Depth Forcing

The NOAA visible satellite observations provide snow cover forcing conditions, but do not provide any information regarding snow depth. Prescribing realistic weekly snow depths presents a challenge, since reliable and comprehensive historical snow depth data are not readily available. Yet their inclusion in the model boundary conditions is desirable, since snow depths can vary considerably over Siberia (see Fig. 2-2), and some of the mechanisms known to affect local climate (e.g., thermal emissivity and thermal

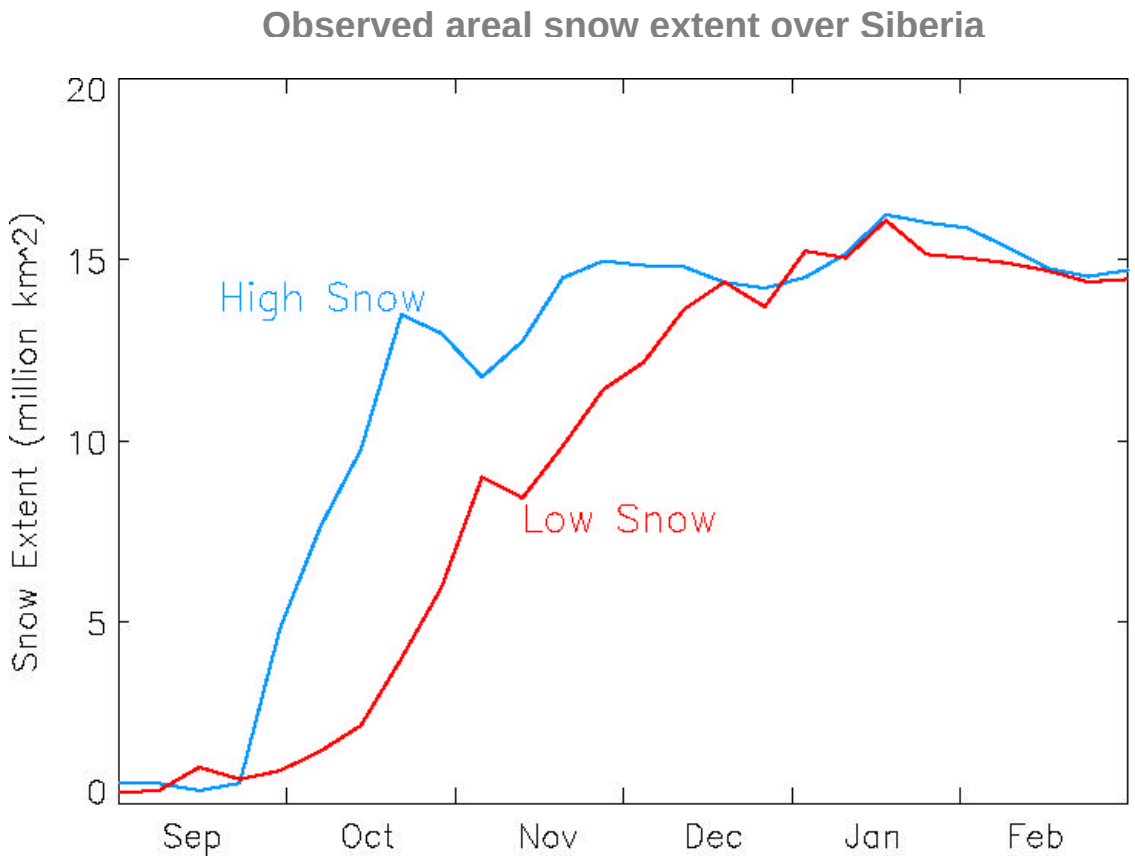

Figure 4-4: Weekly timeseries of satellite-observed total areal snow extent over the Siberia snow forcing region, for the SIB high snow and low snow experiments.

conductivity) vary with snow depth. A 25-year dataset (1966-1990) of thrice-monthly observed snow depths at roughly 1300 stations in the Former Soviet Union (FSU) is available (NSIDC), but coverage is too sparse over much of the modeled Siberia forcing region to be used as the basis for spatial interpolation and gridpoint snow depth input.

Therefore, an approximate method is developed for prescribing Siberian SWE depths associated with the observed snow cover used in the two SIB experiments. This method is based on the simplifying assumption that an earlier snow cover results in a uniformly deeper snow depth. At every Siberian gridcell, the date of initial snow occurrence (i.e., the snow arrival date) is determined for the CTRL simulation, and also from the snow cover forcings applied for the high snow and low snow experiments. Next, the weekly SWE timeseries is assembled for the CTRL simulation. A corresponding SWE timeseries for the high snow (low snow) experiment is then obtained by shifting the CTRL timeseries backward (forward) in time. The magnitude of the shift is determined by the difference in snow arrival date between the high snow (low snow) experiment and CTRL, and the shifted timeseries is applied as the snow depth forcing for that gridcell. This procedure is repeated for each gridcell in the Siberia forcing region. As a result, the high snow experiment consistently exhibits not only broader snow cover but also deeper snow depths than the low snow experiment, throughout the model integration period and the Siberia forcing domain.

This temporal translation of the weekly CTRL SWE timeseries can be expressed as:

$$S_{HS}(t) = S_{CT}(t + [t^*_{CT} - t^*_{HS}]) \tag{4.1}$$

$$S_{LS}(t) = S_{CT}(t - [t^*_{LS} - t^*_{CT}]) \tag{4.2}$$

where S_{HS} = SWE depth for the high snow experiment, S_{LS} = SWE depth for the low snow experiment, S_{CT} = SWE depth for CTRL, t = time during model integration period, t^*_{CT} = snow arrival date for the high snow experiment, t^*_{LS} = snow arrival date for the low snow experiment, and t^*_{CT} = snow arrival date for CTRL. The observation-based snow cover forcings for the two SIB experiments represent extreme early and late autumn snow cover, so that generally $t^*_{HS} < t^*_{CT} < t^*_{LS}$, and hence $S_{LS} < S_{CT} < S_{HS}$ at all t. Also, the magnitude of the SWE variation is directly proportional to the magnitude of the difference in initial snow dates.

The snow specification datasets were checked and adjusted as needed to ensure that the high snow (low snow) forcing always exhibits more (less) extensive snow cover, earlier (later) initial snow occurrence, and larger (smaller) SWE values over Siberia, relative to the CTRL run, thereby representing a positive (negative) snow perturbation. Furthermore, a minimum SWE value of 4.0 cm was applied to the high snow forcing experiment, in order to maximize the surface thermodynamic contrast between the two experiments. 4.0 cm SWE exceeds the critical thresholds for maximum snow impact on the surface energy balance in the ECHAM3 GCM land surface parameterization described in Chapter 2.

This procedure is illustrated graphically for a gridcell in central Siberia in Figure 4-5, which shows the snow depth timeseries for the CTRL simulation, and the shifted

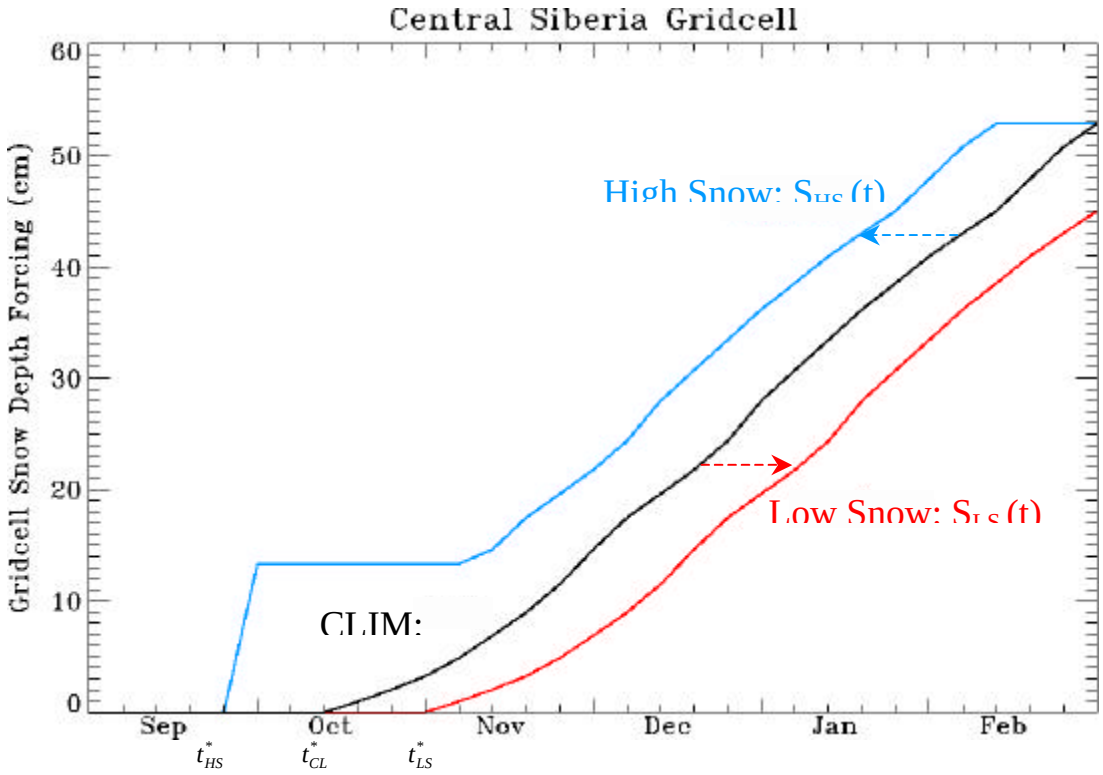

Figure 4-5: Snow depth forcing timeseries applied at a gridcell in central Siberia, for the SIB high snow (dashed line) and low snow (dotted line) experiments. Also shown are the snow arrival dates obtained from the snow cover forcings and the snow depth timeseries for the CTRL simulation (solid line), from which the SIB snow depth forcings are derived.

timeseries for both SIB experiments. SWE values used by the model are converted to snow depth using a snow density of 300 kg/m^3 (see Chapter 2). A consistent snow depth forcing is applied throughout the model integration period, as indicated by the difference between the high snow and low snow experiments at any given time. The magnitude of this snow depth forcing is proportional to the magnitude of the snow cover forcing at this gridcell, as represented by the difference in snow arrival dates for the two experiments. Note that since the timeseries for the high snow experiment is shifted backwards in time, no data from the CTRL simulation is available at the end of the simulation period. Therefore the latest snow depth value from the CTRL simulation is simply repeated until the end of the simulation, as indicated in Figure 4-5.

The resulting Siberian snow boundary conditions are compared to FSU station observation, bearing in mind the sparse coverage over much of the modeled Siberia forcing region. Figure 4-6 shows a weekly timeseries of the average snow depth over Siberia for the high snow and low snow experiments. Also shown are the observed areal average values interpolated from the FSU station data, for each of the 25 years of historical observations. Note that some regions within the defined Siberia region, such as extreme northern Siberia, Mongolia and northern China, contain little or no observations

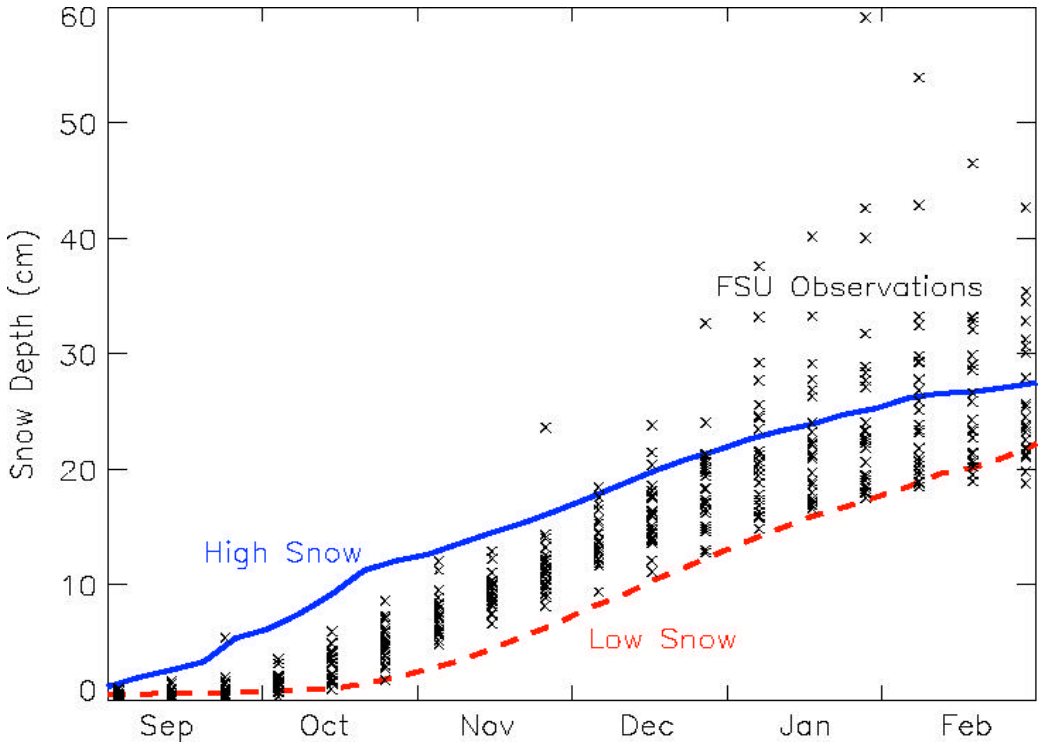

Figure 4-6: Timeseries of average snow depth over Siberia for the high snow (solid line) and low snow (dashed line) experiments, and for the Former Soviet Union (FSU) 25-year observed point-station snow depth dataset. Each column of crosses represents 25 annual values for each thrice-monthly measurement period.

and thus may be subject to extrapolation errors. For example, the exceedingly large observed winter values in Figure 4-6 are due to the erroneous extrapolation of snow depth point measurements into Mongolia and northern China.

The high snow and low snow experiments appear to envelop the observed range of average Siberian snow depth reasonably well. Thus the snow cover and snow depth conditions prescribed by the two SIB experiments represent realistic cases of positive and negative Siberian snow anomalies, so that the climatic differences that result from the GCM experiments will be reflective of realistic Siberian snow forcings. Note that although the difference in winter snow cover extent is minimal between the two experiments (Fig. 4-4), the difference in winter snow depth (Fig. 4-6) is considerable, due to the inclusion of snow depth forcings. This provides a potential mechanism by which winter snow anomalies may also modulate winter climate, or at least maintain the modulations initiated by the autumn anomalies.

4.3 Seasonal Mean Climatic Response

The first necessary test is to evaluate the three-month seasonal mean climatic response over the Northern Hemisphere, in sequential order of known snow cover impact on the

atmosphere (i.e., from local thermodynamic to regional and hemispheric dynamical). Figure 4-7 shows the autumn (SON) and winter (DJF) response for surface albedo, surface temperature and sea level pressure (SLP). The autumn season (Fig. 4-7a,b,c) exhibits the expected local response to positive snow forcing over Siberia, i.e., higher surface albedo, lower surface temperature, and higher SLP.

During the winter (Fig. 4-7d,e,f), a notable surface albedo response occurs over Siberia, despite the minimal snow cover forcing indicated in Figure 4-4. This is due to the prescribed snow depth forcing (Fig. 4-6), and the fact that surface albedo is directly related to SWE depth in the model snow parameterization (Chapter 2). The response occurs mainly over southern Siberia (around 45N), since the surface albedo parameterization is more sensitive to the lower SWE depths that generally reside at lower latitudes. Also important is the fact that solar radiation is more intense over southern Siberia, so that the stronger albedo anomaly translates into a stronger temperature anomaly. Thus the winter surface temperature and SLP fields also indicate a corresponding local response to snow forcing in southern Siberia.

The winter surface temperature response (Fig. 4-7e) is not limited to southern Siberia, but rather encompass a broad region extending north and west into the Arctic, northern Europe, and even North America. Other surface thermodynamic mechanisms, e.g., increased thermal emissivity and decreased thermal conductivity, may be responsible for the local temperature response in northern Siberia, but they do not explain the remote response outside of the Siberia forcing region. Winter SLP (Fig. 4-7f) exhibits a very broad, hemispheric scale response, with a large positive anomaly at high latitudes, and large negative anomalies at low latitudes, centered in the North Atlantic and North Pacific basins. The temperature and SLP patterns are reminiscent of a negative AO mode, and suggest that a positive Siberian snow forcing results in a negative winter AO response. This represents the translation of the local thermodynamic response to a local snow perturbation into a hemispheric dynamical effect.

Figure 4-7f qualitatively demonstrates that realistic interannual Siberian snow forcings can modulate the hemispheric winter AO mode. Next, this modulation is evaluated quantitatively by developing an unstandardized AO index metric, and assessing the difference in this metric between the high snow and low snow experiments. The commonly used surface AO index derived from the first empirical orthogonal function (EOF1) of the Northern Hemisphere SLP field (Thompson and Wallace, 1998) is a normalized measure, and thus not applicable to assessing changes due to external forcings. A simple AO index is computed here, by subtracting the average SLP north of 61.5N from the average SLP within the zonal band from 28N to 50N. These two regions were selected to capture the centers of action in the SLP EOF1 field, and the resulting winter AO index for each experiment is highly correlated ($r = +0.97$ for SNO76; $r = +0.90$ for SNO88) with its respective EOF1-based index.

The resulting ensemble mean winter AO index with high snow forcing is roughly 5 hPa less than for low snow forcing, which is statistically significant at 99%. This exercise was repeated using 500 hPa and 50 hPa geopotential heights, and the resulting AO indices exhibited a snow-forced decrease at 99% and 97% significance, respectively. Thus a positive Siberian snow forcing results in a quantifiable and significant decrease in the winter AO mode throughout the atmosphere.

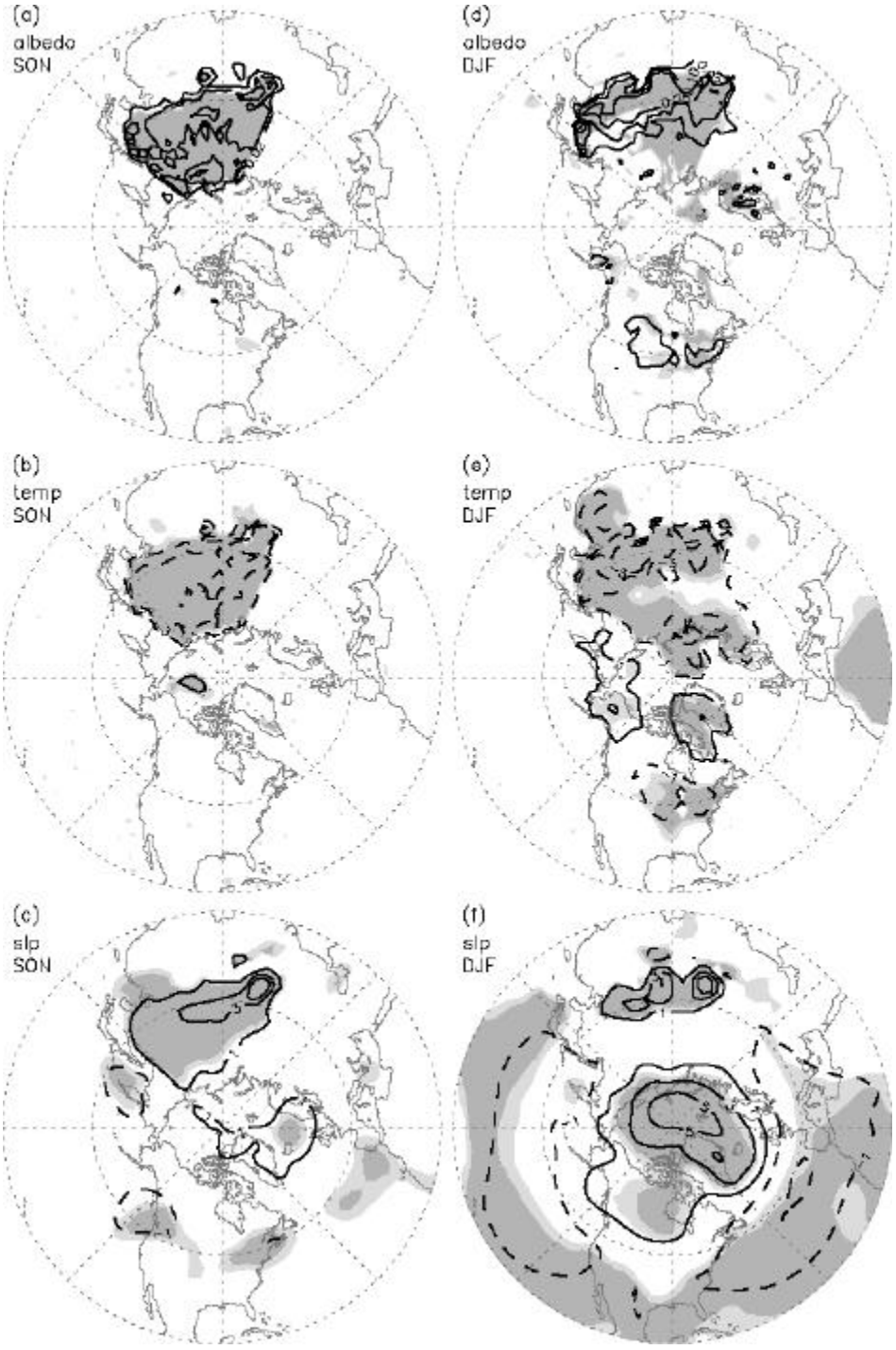

Figure 4-7: Surface climatic response to positive Siberian snow forcing, over the extratropical Northern Hemisphere, for autumn (a-c) and winter (d-f) seasons. Surface albedo (a,d) contours drawn at ± 0.02, 0.1, 0.25. Surface temperature (b,e) contours drawn at ± 1, 3, 5 °C. Dashed line denotes negative contour value. Sea level pressure (c,f) contours drawn at ± 1, 3, 5 hPa. Light (dark) shading indicates 90% (95%) statistical significance.

The model simulated negative winter AO response to positive Siberian snow anomalies concurs with observational analyses by Cohen and Entekhabi (1999), Cohen et al. (2001) and Saito et al. (2001). Since realistic, observation-based snow forcings are applied in this model study, it is worthwhile to directly compare the modeled winter SLP response in Figure 4-7f against the observed response using NCEP reanalysis data (Kalnay et al., 1996) presented in Figure 3b of Cohen and Entekhabi (1999). The spatial gridpoint correlation coefficient between the two figures is +0.87, which indicates that the modeled spatial response pattern is similar to the observed pattern. However, the spatial standard deviation over gridpoints north of 20N in Figure 4-7f is 2.45 hPa, compared to a value of 8.1 hPa for Cohen and Entekhabi (1999) Figure 3b. Thus the snow-forced winter AO response pattern is statistically significant and resembles the observed response pattern, but the magnitude of the modeled response is only about 30% that of the observed response.

One potential explanation for the relatively damped model response is that the ECHAM3 GCM does a poor job of simulating or resolving certain atmospheric features which link Siberian snow anomalies to the winter AO response. Teleconnection pathways will be evaluated in detail in the following section. Another potential explanation is that other atmospheric processes are occurring in nature which act in concert with the positive Siberian snow anomaly, and that these processes are neglected when isolating the climatic response to snow. That the modeled response is weaker but consistent with the observed response supports the notion that snow anomalies serve as an amplifier of the pre-existing winter AO signal.

4.4 Surface Sea Level Migration Pathway

One hypothesized teleconnection pathway involves the poleward expansion of the semi-permanent Siberian High pressure system. Cohen et al. (2001) shows that the Siberian High is bordered to the south and east by some of the tallest mountains in the world. They suggest that a positive snow anomaly over Siberia intensifies and expands the Siberian High, but that the expansion is constrained to the south and east by these orographic barriers. Therefore expansion is forced northward and westward, over the North Pole and into the North Atlantic. Consequently, the Icelandic Low pressure system is forced equatorward, and these displacements result in the high and mid-latitude anomalies characteristic of the NAO. To a lesser extent, the Aleutian Low is also displaced equatorward in the North Pacific, resulting in hemispheric anomalies characteristic of the AO.

This hypothesis is investigated using 42-day moving average SLP values over the Northern Hemisphere, to identify any lateral surface migration of snow-forced SLP anomalies that occurs. Figure 4-8 shows the temporal evolution of SLP differences (high snow – low snow) along a surface transect, beginning in southern Siberia at 90E longitude and 20N latitude, extending northward to the North Pole, then continuing southward through the North Atlantic to 337.5E longitude and 20N latitude. A large positive anomaly occurs over Siberia throughout the simulation period, consistent with Figures 4-7c and 4-7f. Also indicated are polar and mid-latitude dipole anomalies over

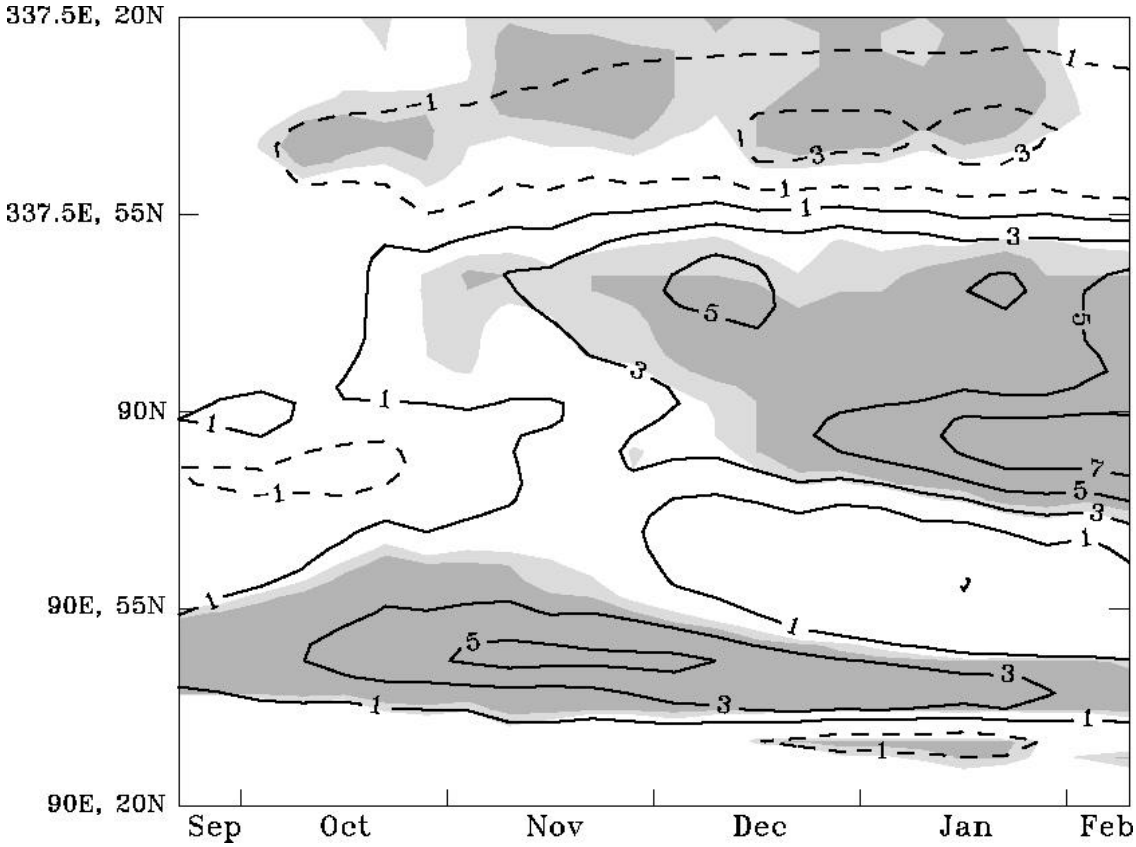

Figure 4-8: Weekly evolution (horizontal axis) of 42-day averaged sea level pressure response to positive Siberian snow forcing, along a surface transect (vertical axis) running north through Siberia (90E) then south through the North Atlantic (337.5E). Contours drawn at ± 1, 3, 5, 7 hPa. Dashed line denotes negative contour value. Light (dark) shading indicates 90% (95%) statistical significance.

the North Atlantic during winter months, again consistent with Figure 4-7f. Note that this dipole anomaly pattern over the North Atlantic begins in late October, and continues through the late autumn and winter. The Siberian and Arctic positive anomalies are connected over extreme northern Siberia in November, perhaps suggesting a migration from Siberia northwards into the Arctic. However, this connection is rather weak, and the dipole anomaly over the North Atlantic begins prior to, and independently of, this northward migration. Thus the snow-forced expansion and migration of the Siberian High over the North Pole and into the North Atlantic is not clearly indicated by the SIB experiments, as portrayed in Figure 4-8.

Northern Hemisphere fields of SLP and SLP difference similarly fail to demonstrate a clear polar migration pathway. Figure 4-9a shows the Northern Hemisphere gridpoint SLP response to positive snow forcing, averaged over a 42-day period centered in late October. The positive anomaly regions over Siberia and the Arctic are clearly evident, but they appear unrelated. Figure 4-9b shows selected SLP field contours over the same

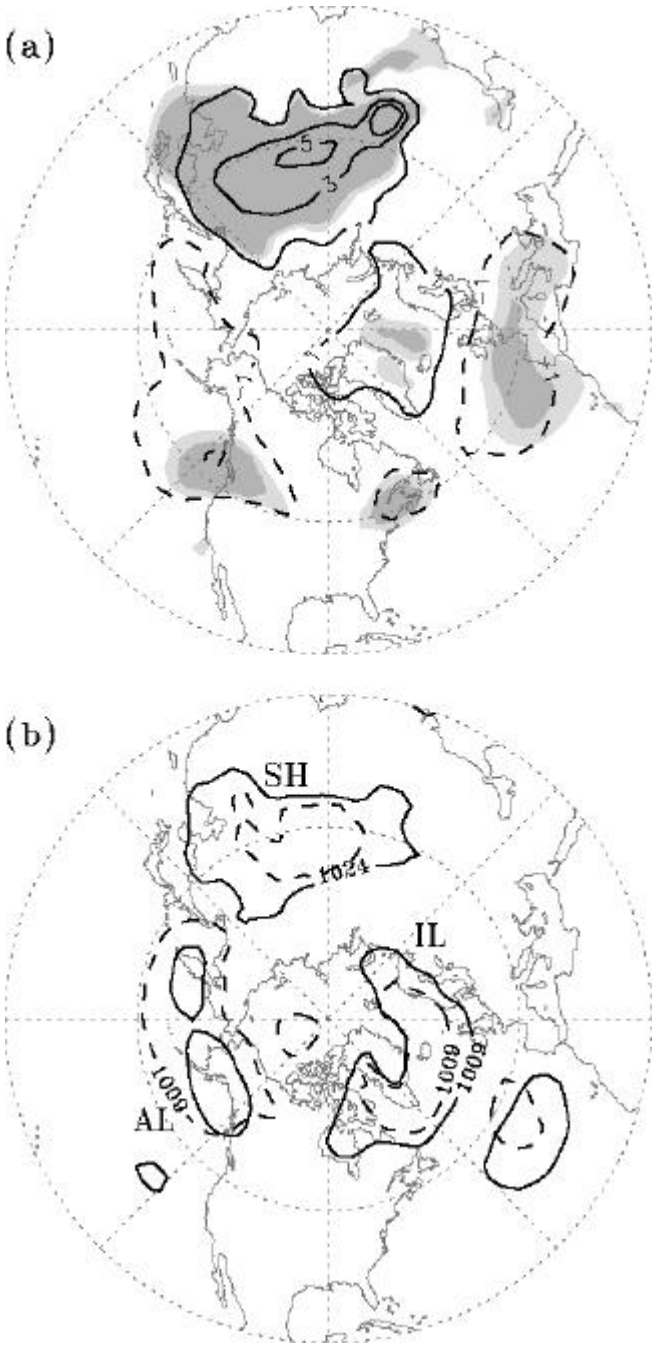

Figure 4-9: a) Sea level pressure response to positive Siberian snow forcing, over the extratropical Northern Hemisphere, for a 42-day period centered in late October. Contours drawn at ± 1, 3, 5 hPa. Dashed line denotes negative contour value. Light (dark) shading indicates 90% (95%) statistical significance. b) Sea level pressure field contours representing the Siberian High (SH: 1024 hPa), the Icelandic Low (IL: 1009 hPa) and the Aleutian Low (AL: 1009 hPa), for a 42-day period centered in late October. Solid line represents the high snow experiment, and dashed line represents the low snow experiment.

period for each experiment, with the 1024 hPa contour representing the Siberian High and the 1009 hPa contour representing the Icelandic Low and Aleutian Low. The high snow experiment (solid line) clearly exhibits a more expansive Siberian High than low snow experiment (dashed line), however the system remains centered around 45N, and has not migrated northward. The Icelandic Low is somewhat more expansive under high snow conditions, but the Aleutian Low is somewhat less expansive, and neither low pressure system has migrated southward.

The ensemble mean, 42-day moving averages presented in Figures 4-8 and 4-9 are designed to identify slowly evolving migration patterns for the semi-permanent SLP systems. Other metrics have also been evaluated, such as weekly averages and individual realizations, to identify more transient snow-forced polar excursions of Siberian SLP anomalies. Several alternative surface transects have also been considered. However, none of these analyses clearly indicate a poleward migration of the Siberian High into the North Atlantic. Thus the SIB experiments do not support the polar SLP surface migration teleconnection pathway hypothesized in Cohen et al. (2001).

4.5 Vertical Wave Propagation Pathway

Another hypothesized teleconnection pathway between the Siberian snow forcing and the hemispheric climate response involves the upward propagation of snow-forced stationary wave activity from the (local) surface to the stratosphere. Saito et al. (2001) and Cohen et al. (2002) describe some general features of this vertical pathway, as they relate to recent literature on the stratospheric forcing of the AO. In this section the manifestation of this dynamical pathway in the snow-forced GCM experiments is systematically evaluated, drawing on established wave-mean flow interaction principles as well as recent stratospheric-tropospheric coupling literature.

4.5.1 Model Climatology for Relevant Dynamical Parameters

The analysis makes extensive use of the three-dimensional stationary wave activity flux (WAF) diagnostic (Plumb, 1985). Atmospheric dynamics is often characterized using wave phenomena, and an important attribute of waves is that energy can be transported great distances along them, relative to the actual fluid element displacement. The WAF describes the transmission of stationary wave energy throughout the atmospheric system. Stationary waves are typically forced by land surface orography, large-scale diabatic heating (e.g., land-ocean contrasts, continental-scale temperature anomalies), and interaction with transient waves. This diagnostic is similar to the classic two-dimensional (zonally averaged) Eliassen-Palm flux (Edmon et al., 1980), but allows for regional analyses by resolving the longitudinal component, at the expense of neglecting transient waves. Computation of the WAF diagnostic is described in Appendix D.

Figure 4-10 shows the WAF climatology over the extratropical Northern Hemisphere, produced by the CTRL simulation, for autumn and winter seasons and at 500 hPa and 150 hPa. The model's winter climatology (Fig. 4-10c,d) can be compared directly against observed fluxes presented in Figure 4 of Plumb (1985). At 500 hPa (Fig.

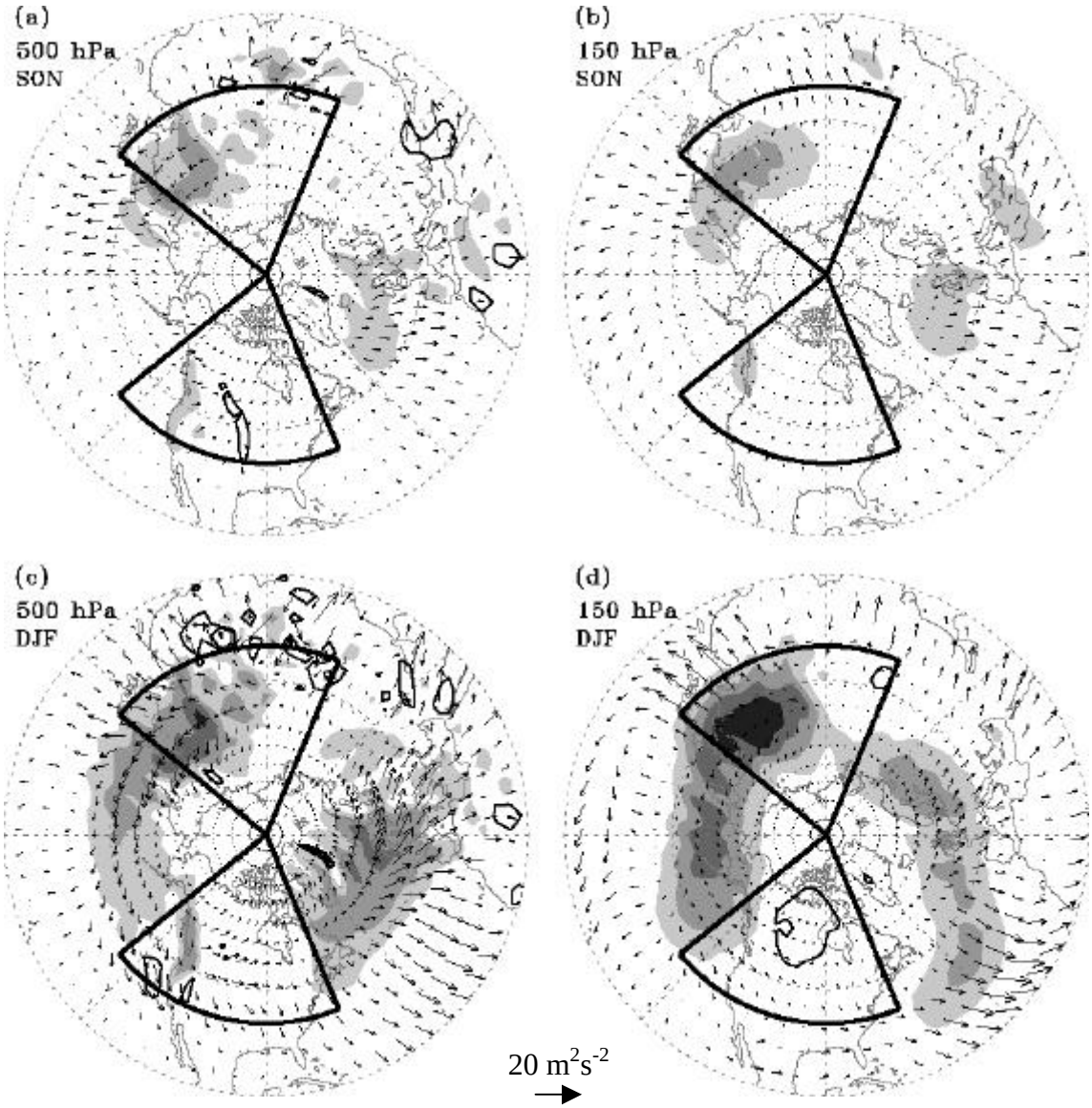

Figure 4-10: Three-dimensional wave activity flux (WAF) climatology over the extratropical Northern Hemisphere, for the CTRL simulation. The pattern and magnitude of the wave activity flux compares well with those calculated by Plumb (1985) based on observations. Two centers are evident, one located over Siberia and another over the North Atlantic. Vectors denote horizontal fluxes (scale indicated on figure), and filled (open) contours denote upward (downward) vertical fluxes. Also shown is the Siberia forcing region used in both SIB experiments. a) 500 hPa elevation, autumn. b) 150 hPa elevation, autumn. c) 500 hPa elevation, winter. d) 150 hPa elevation, winter. Contours for 500 hPa (a,c) drawn at ± .03, .07, .15, .25 m^2s^{-2}. Contours for 150 hPa (b,d) drawn at ± .01, .02, .03, .04 m^2s^{-2}.

4-10a,c), a large center of upward, eastward and predominantly equatorward wave activity is centered over Siberia and far-east Asia. A second major wave train with similar characteristics is also simulated over the North Atlantic, as well as a small region of activity in western North America. Upper level wave activity (150 hPa, Fig. 4-10b,d) also portrays the two major wave trains, propagating upward and equatorward, though the magnitude is considerably weaker than at lower elevations. These wave trains are apparent during both autumn (Fig. 4-10a,b) and winter (Fig. 4-10c,d), but the wave activity is much more pronounced during winter. Overall, the modeled wave activity compares favorably to observations, although the modeled wave propagation is somewhat more equatorward and less eastward than observations. Finally, note that the Siberia stationary wave train overlies the Siberia forcing region applied in the SIB experiments, as indicated in Figure 4-10. This areal co-location of the modeled snow forcing within a region of strong stationary wave activity is instrumental to the vertical propagation pathway that develops, as discussed below.

A second dynamical parameter involved in the vertical pathway is the Northern Hemisphere stratospheric polar vortex, which is characterized by a band of strong stratospheric westerly winds centered around 60N. The polar vortex is typically influenced by radiative forcings, latitudinal temperature gradients, and tropospheric planetary waves such as those described by the WAF (Holton 1972). Figure 4-11 shows the polar vortex simulated by the CTRL simulation, as represented by the zonal wind climatology over the Northern Hemisphere at 50 hPa elevation. An annular band of elevated zonal wind is clearly visible around 60N, which demonstrates that the vortex is a hemispheric-scale feature. As for the WAF, the polar vortex occurs during autumn (Fig. 4-11a) and winter (Fig. 4-11b), although it is notably stronger during winter.

4.5.2 Pathway Response to Positive Siberian Snow Forcing

Figure 4-12 shows the vertical WAF response to positive Siberian snow forcing during autumn (SON). Upward wave activity over Siberia increases in response to the local positive snow forcing and associated local negative temperature anomaly. Thermal forcings have been shown to amplify orographically forced stationary waves (Ringler and Cook, 1999), and observational studies have similarly associated vertical waves with snow (Saito et al., 2001) and temperature (Zhou et al., 2001). Note that the snow-forced local upward WAF anomaly is concentrated in south central and eastern Siberia, which is in the vicinity of one of the orographically-forced, climatological upward stationary wave trains identified in Plumb (1985) and shown in Figure 4-10. In other words, co-location of the snow forcing and the Siberia stationary wave train results in a strengthening of the upward component of this pre-existing wave train.

Figure 4-13 shows a sequential series of latitude-pressure profile plots, with the WAF response averaged over Siberia longitudes shown as vectors, and the zonal-mean zonal-wind response shown as contours. Each plot represents a 42-day average, centered around the time period shown on the plot. Beginning in early October (Fig. 4-13a), an upward surface WAF anomaly (indicative of the strengthened Siberia wave train) responds almost immediately to the snow-forced Siberian temperature anomaly. By early November (Fig. 4-13b) this upward WAF anomaly has propagated into the stratosphere

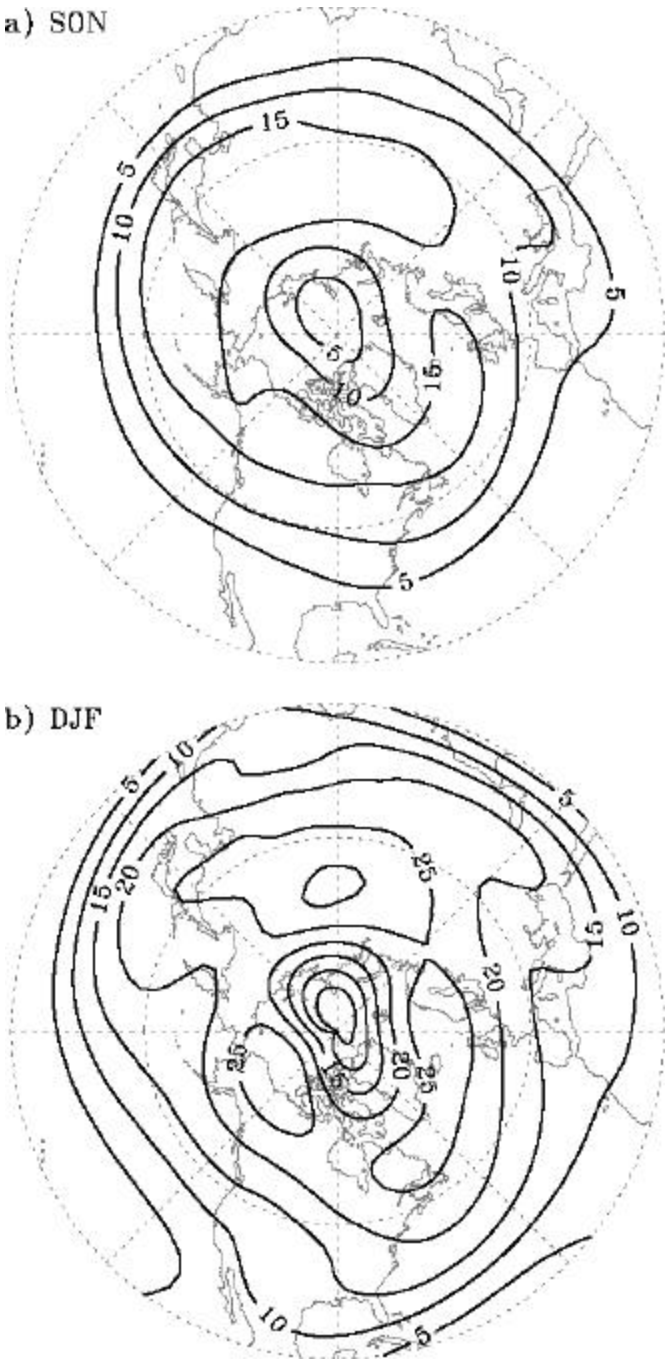

Figure 4-11: Stratospheric polar vortex for the CTRL simulation, as represented by zonal wind climatology at 50 hPa. Contours drawn at 5, 10, 15,20, 25, 30 ms^{-1}. a) autumn. b) winter.

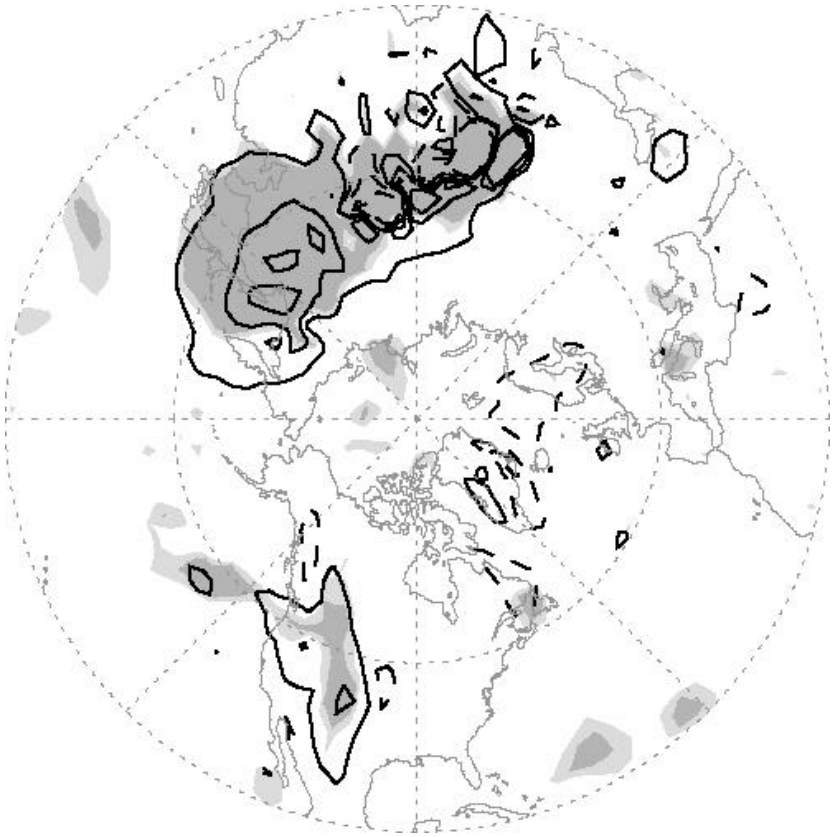

-12: Vertical wave activity flux response to positive Siberian snow forcing, at
e extratropical Northern Hemisphere, for autumn (SON).
Contours drawn at ± 0.01, 0.04, 0.08 m s⁻ . Dashed line denotes negative contour value. Light (dark) shading indicates 90% (95%) statistical significance.

-latitude troposphere
although magnitudes weaken considerably with elevation. The climatological stationary wave train over Siberia extends throughout the troposphere (Fig. 4 10), which provides a conduit for snow forced WAF anomalies

The increased wave activity in the stratosphere weakens the stratospheric polar
-13b by the emergence in early November of negative
-mean zonal wind anomalies around 60N. Corresponding positive

(1999) and Limpasuvan and Hartmann (2000) report similar vortex related zonal-anomalies forced by tropospheric vertical WAF anomalies. Zhou et al. (2001) asserts that
-generated wave anomalies than the

The weakened polar vortex causes subsequent upward tropospheric wave activity
-forced anomalie -occurring hemispheric fluxes) to
-wind anomalies at high latitudes. This is
-13b), concurrent with the onset of the weakened vortex

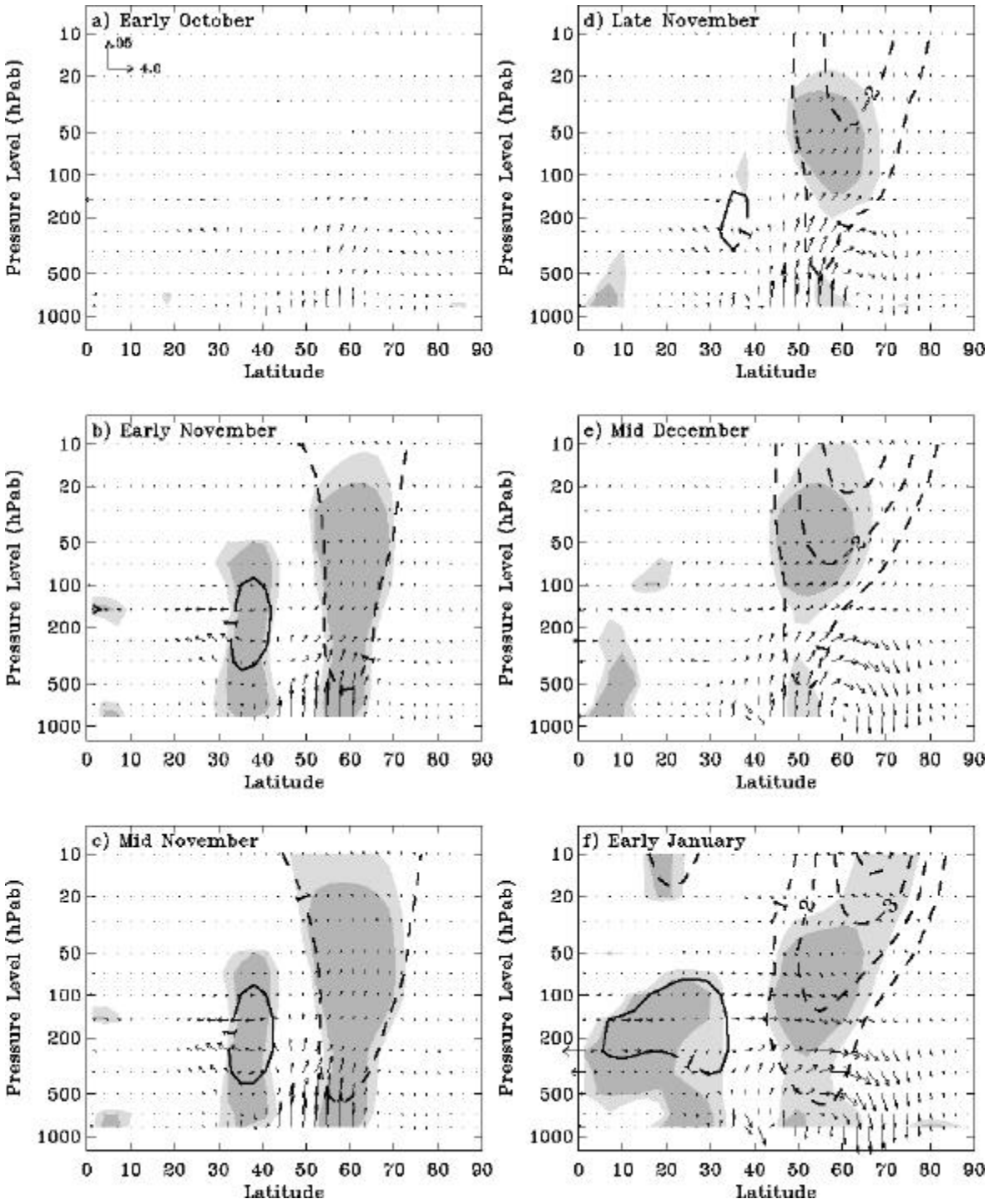

Figure 4-13: Latitude (0N-90N) vs. pressure (850hPa-10hPa) profiles of the response to positive Siberian snow forcing, for selected 42-day average periods from early October through early January. Vectors represent meridional and vertical wave activity flux response averaged over Siberia; scale in m^2s^{-2} is indicated in upper-left panel. Contours represent zonal-mean zonal wind response; contours drawn at ± 1, 2, 3, 4 ms^{-1}, and light (dark) shading indicates 90% (95%) statistical significance.

in these 42-day average plots. Limpasuvan and Hartmann (2000) and Zhou et al. (2002) report similar meridional wave refraction in the troposphere in response to polar vortex anomalies.

The poleward wave activity flux is associated with equatorward momentum flux (Zhou et al., 2001), which subsequently draws the stratospheric high-latitude zonal-wind and geopotential height anomalies associated with the weakened polar vortex down into the troposphere, and also generates opposite-signed mean-flow anomalies at mid-latitudes. This in turn causes additional poleward and even downward tropospheric wave refraction at lower elevations, and a positive feedback develops in which hemispheric-scale meridional wave activity, zonal wind and geopotential height anomalies all propagate downward from the stratosphere towards the surface, over the course of a few weeks. Figures 4-13b-d demonstrate this positive feedback during November, in the form of downward propagating poleward Siberian WAF anomalies and high-latitude negative zonal-mean zonal-wind anomalies.

The concurrent downward propagation of zonal-wind and meridional wave flux anomalies demonstrated here is consistent with a number of recent studies which describe stratospheric-tropospheric coupling on a sub-monthly timescale, and initiated by a stratospheric disturbance (Kuroda and Kodera, 1999; Kodera and Kuroda, 2000; Baldwin and Dunkerton, 1999; Zhou et al., 2002). These studies also suggest that upward propagating tropospheric waves may trigger the stratospheric disturbance. This study contributes to the discussion by showing that the upward propagating waves can in turn be caused by snow-forced upward WAF anomalies which originate at the surface and in a localized region, i.e. Siberia. The areal co-location in Siberia of the snow forcing and associated temperature (i.e., diabatic heating) anomaly, within a pre-existing stationary wave train, results in a strengthening of the upward component of this wave train, and initiates the vertical teleconnection pathway.

Once this pathway is initiated in late autumn, it continues into the winter, maintained by the poleward refraction of ambient vertical wave activity. The winter months presented in Figure 4-13e-f indicate gradually increasing meridional WAF anomalies and zonal-wind anomalies, even after the snow-forced upward WAF anomalies over Siberia have dissipated in early January. By mid-winter significant dipole zonal-mean zonal-wind (Fig. 4-13f) and geopotential height (not shown) anomalies have propagated down to the surface. This pattern is indicative of the negative winter AO mode presented in Figure 4-7f, and thereby completes the atmospheric teleconnection pathway linking Siberian snow anomalies to the winter AO mode via vertical stationary wave propagation and stratospheric-tropospheric coupling.

Additional analyses are now presented to portray specific features and thereby provide a more comprehensive description of the overall teleconnection. In Figure 4-13, the poleward wave refraction and downward mean flow propagation appears to occur more or less continuously from late autumn through winter. This is in part due to the 42-day averaging that is used, which masks short-term fluctuations in order to present a smoothed, generalized response pattern. Applying weekly averaging instead reveals that in fact the sub-monthly scale teleconnection pathway occurs in distinct pulses. Figure 4-14 shows plots that are similar to Figure 4-13, except that weekly averages are computed instead of 42-day averages. Figure 4-14a-c shows one pulse during a three week

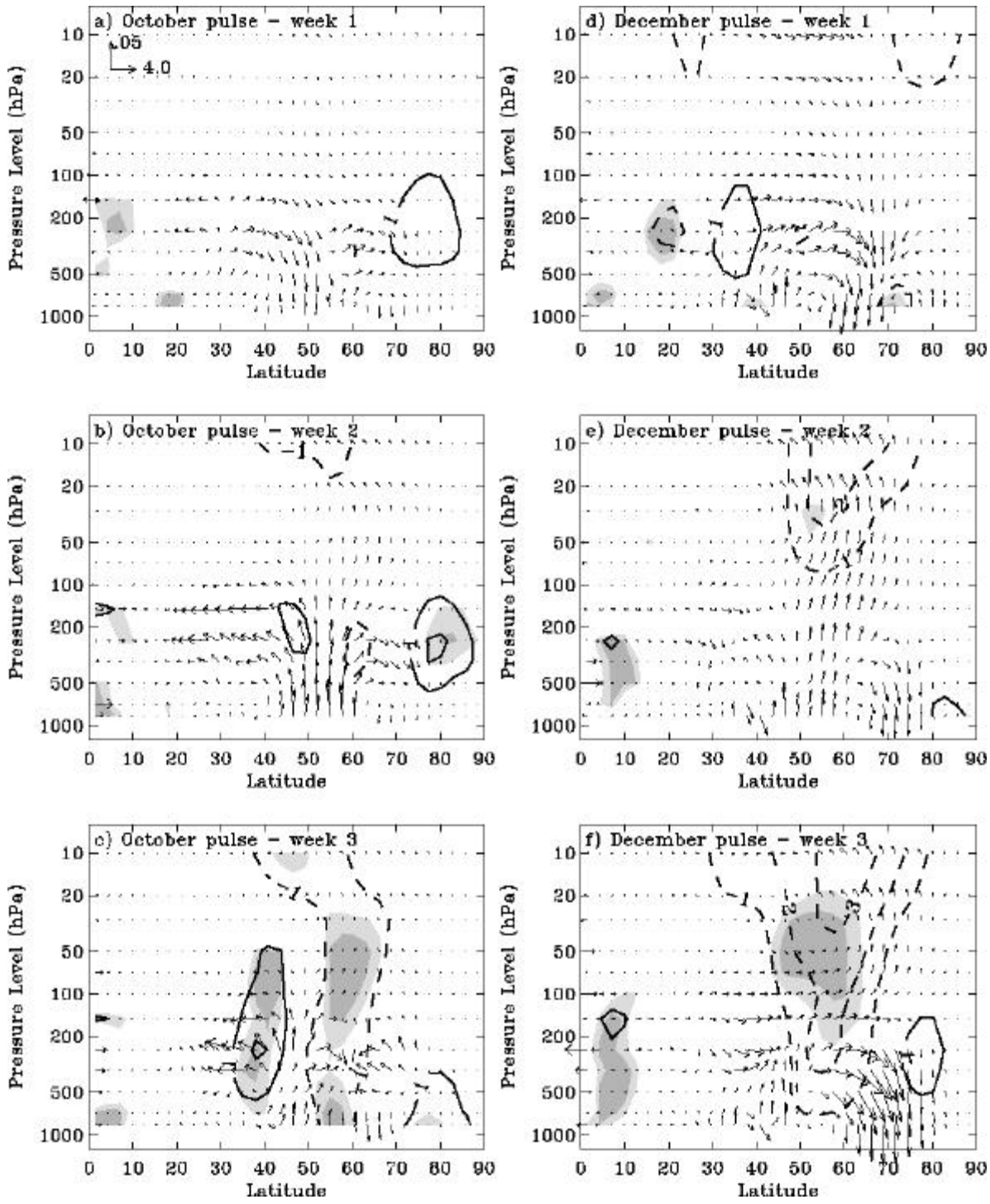

Figure 4-14: Same as for Figure 4-13, except for selected sequential one-week average periods in (a-c) October, and (d-f) December.

sequence in October, and Figure 4-14d-f shows a second pulse during a three week sequence in December. At the beginning of each sequence (Fig. 4-14a,d), no Siberian snow-forced upward WAF anomalies or zonal-mean zonal wind anomalies are apparent. The poleward and downward WAF anomalies in Figure 4-14d likely represent the latter stages of a preceding pulse. During the second week (Fig. 4-14b,e), a strong Siberian upward WAF anomaly originates at the surface and is maintained throughout the troposphere and well into the stratosphere, whereas the temporally smoothed plots in Figure 4-13 showed substantial weakening of the anomaly with elevation. Also, initial stratospheric zonal-wind anomalies associated with the weakened vortex begin to appear. The third week in each sequence (Fig. 4-14c,f) no longer exhibits a strong upward WAF anomaly, but does show clear downward propagating zonal-wind anomalies. The December pulse (Fig. 4-14f) exhibits a clear poleward and downward WAF propagation, while this response is less clear for the initial, early-season October pulse (Fig. F-14c).

Thus for each pulse, a rapid upward WAF anomaly is followed by downward propagating mean-flow anomalies, which dissipate after a few weeks, and another pulse begins soon after. The initial teleconnection pulse in mid-October is almost certainly caused by the initial October snow forcing anomaly (Fig. 4-4). Subsequent pulses may be due to other large anomaly periods in the observation-based snow boundary condition. Winter pulses may also be due to the increase in wave activity that naturally occurs in the winter months, which amplify the snow-forced WAF anomaly. The short timescale of the teleconnection pulses suggests that an AO type response may be noticeable as early as late October, following the initial October WAF anomaly pulse (Fig. 4-14a-c). Subsequent pulses gradually strengthen the AO signal, until it becomes apparent during the winter months in Figure 4-7 and Figure 4-13.

An important facet of this teleconnection pathway is the ability of a regional surface snow forcing over Siberia to generate a hemispheric-scale winter AO response. This occurs because the regional upward WAF anomaly over Siberia is strong enough (in climatology) to propagate to the stratosphere and weaken the polar vortex, which is a hemispheric phenomenon. This weakened vortex is then able to draw refracted stationary waves throughout the Northern Hemisphere, not just over Siberia. Figure 4-15 shows snow-forced horizontal WAF anomaly vectors in the upper troposphere (250 hPa) during winter (DJF). Poleward refraction can be seen throughout the Northern Hemisphere at mid to high latitudes. As a result, the downward propagation of mean-flow anomalies is hemispheric in scale, which yields the AO-type winter climatic response.

The downward propagating mean-flow anomalies suggest that the AO mode likewise propagates downward from the stratosphere to the surface. In Section 4.3, an unstandardized winter (DJF) AO index metric was developed in order to evaluate its response to Siberian snow forcing. Figure 4-16 presents the difference (high snow – low snow) in this index, computed and normalized over twelve different atmospheric levels from the 1000 hPa to 10 hPa, on a 42-day moving average basis over the September-February model integration period. A negative AO index anomaly first appears in the late autumn stratosphere, indicative of a weakened polar vortex. A rapid but weak downward propagation to the surface occurs during November, consistent with the sub-monthly timescale of the vertical teleconnection pathway. Stronger and more significant AO index anomalies remain in the stratosphere until late December, before propagating

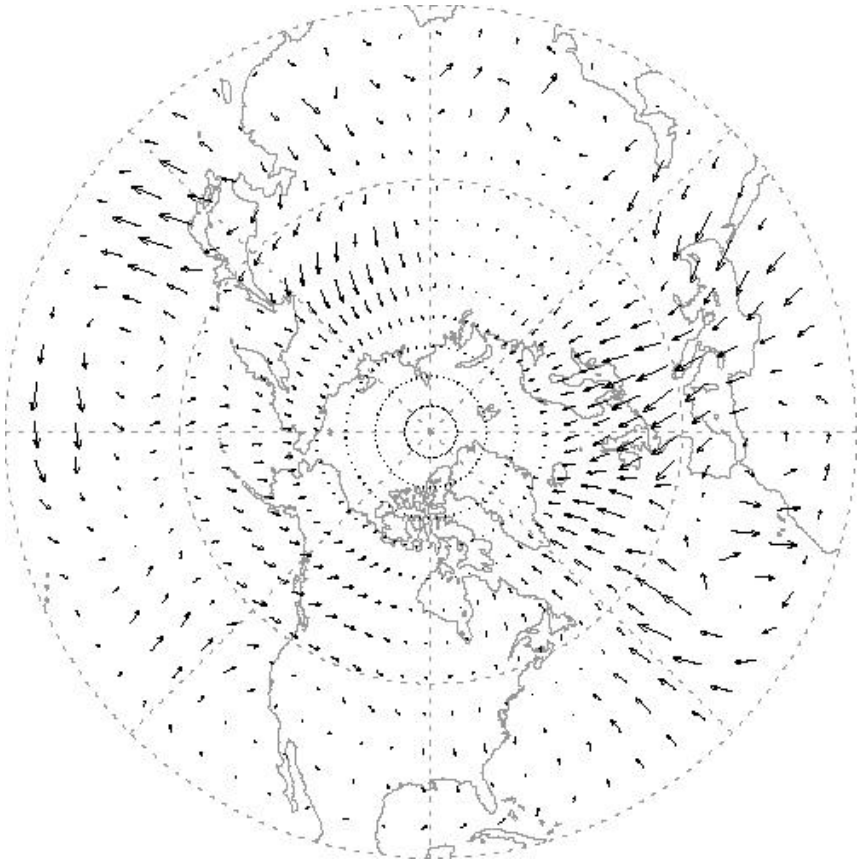

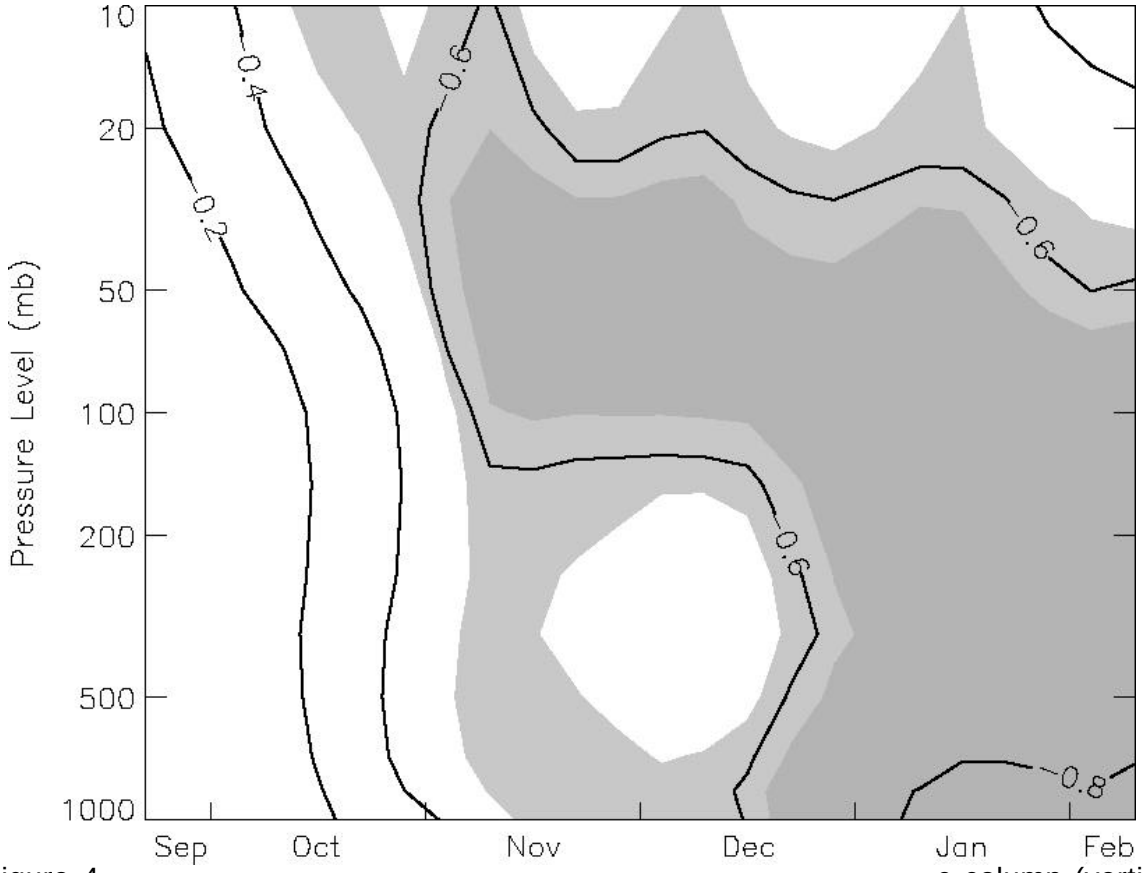

Figure 4- c column (vertical axis) of normalized 42 day rolling average hemispheric AO index response to positive Siberian snow forcing. Contours drawn at 2, - -6, 8 standard deviations. Light (dark) shading indicates 90% (95%) statistical significance.

lly- -Palm (EP) flux is computed, to evaluate the relative

Figure 4 17a shows the snow-
October. Also presented are the stationary and transient components that comprise the

response to forcing by Siberian snow, and the figure shows that stationary waves dominate the total wave flux response. Figure 4 17b similarly shows meridional EP flux
-
latitudes, representing the poleward refraction of wave activity that occurs in response to
s dominate where there is a peak in
the total wave flux response. For two key tropospheric facets of the snow forced vertical wave mean flow teleconnection pathway, the climatic response of transient waves is shown to be relatively small compared to that
conclude that the stationary WAF diagnostic is an appropriate metric for diagnosing the

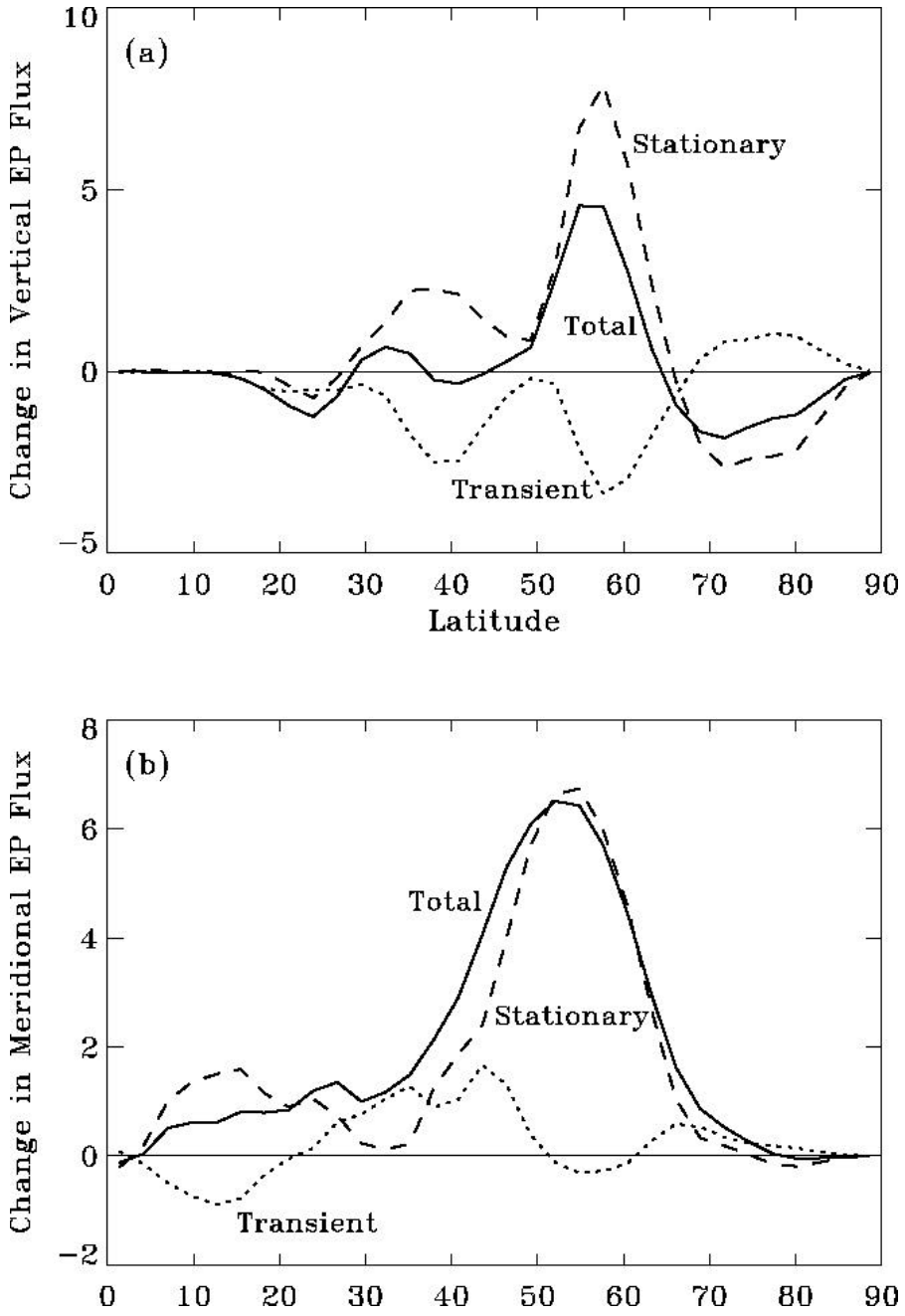

Figure 4-17: Eliassen-Palm flux response (solid line) to positive Siberian snow forcing, at 500 hPa elevation over Northern Hemisphere latitudes, including stationary (dashed line) and transient (dotted line) components. a) Vertical flux response for October (10^{16} hPa-m^3). b) Meridional flux response for January (10^{13} m^3). Zero flux response line also included for reference.

planetary wave and overall atmospheric teleconnection response to Siberian snow

Discussion

Drawing on established wave mean flow interaction theory and recent studies involving stratospheric tropospheric coupling, a detailed atmospheric teleconnection pathway has -scale -scale AO mode modulations. This with the aid of pictorial illustrations shown in Figure -18, panels 1 6. A positive Siberian snow forcing decreases the local surface co- -scale train strengthens the upward component of this wave train, producing an increase in upward stationary WAF which propagates up through the troposphere (panel 2). Upon ese WAF anomalies weaken the stratospheric polar vortex (panel 3). Stationary waves throughout the Northern Hemisphere are drawn towards the -tropospheric this poleward wave refraction draws the vortex- negative zonal wind anomalies downward at high latitudes, and also produces positive zonal wind anomalies at lower latitudes, resulting in dipole zonal wind anomalies (panel 5). Note that corresponding geopotential height anomalies are associated with the zonal wind anomalies (not shown). This upper tropospheric dipole anomaly in turn causes hemispheric- to occur at lower elevations, and a positive feedback develops whereby the coupled

6). This pathway occurs over the course of a few weeks, and several distinct pulses are apparent from mid autumn through winter, maintained in part by strong naturally occurring upward wave activity during the winter (Fig. 4- downward propagation of a negative AO anomaly during the winter season from the stratosphere to the surface, as shown -16.

It is important to emphasize that this atmospheric teleconnection pathway that results from the SIB experiments is consistent with: 1) established atmospheric wave mean flow interaction theory, originally developed in the 1960's; 2) much, though not all, -troposphere coupling as it relates to the AO – winter AO been documented in the literature, so the pathway is not novel with respect to atmospheric

various pathway components are coherently linked to yield a negative winter AO mode

such, this physically- Siberian snow – nal- surface snow anomalies can indeed be a viable modulator of hemispheric- climate.

1) Co-location of local surface temp anomaly with strong stationary wave activity

2) Upward WAF increases over Siberia, and propagates up through troposphere

Figure 4 18: The atmospheric teleconnection pathway relating a positive Siberian snow forc
positive (negative) anomaly. Panels 1 and 2.

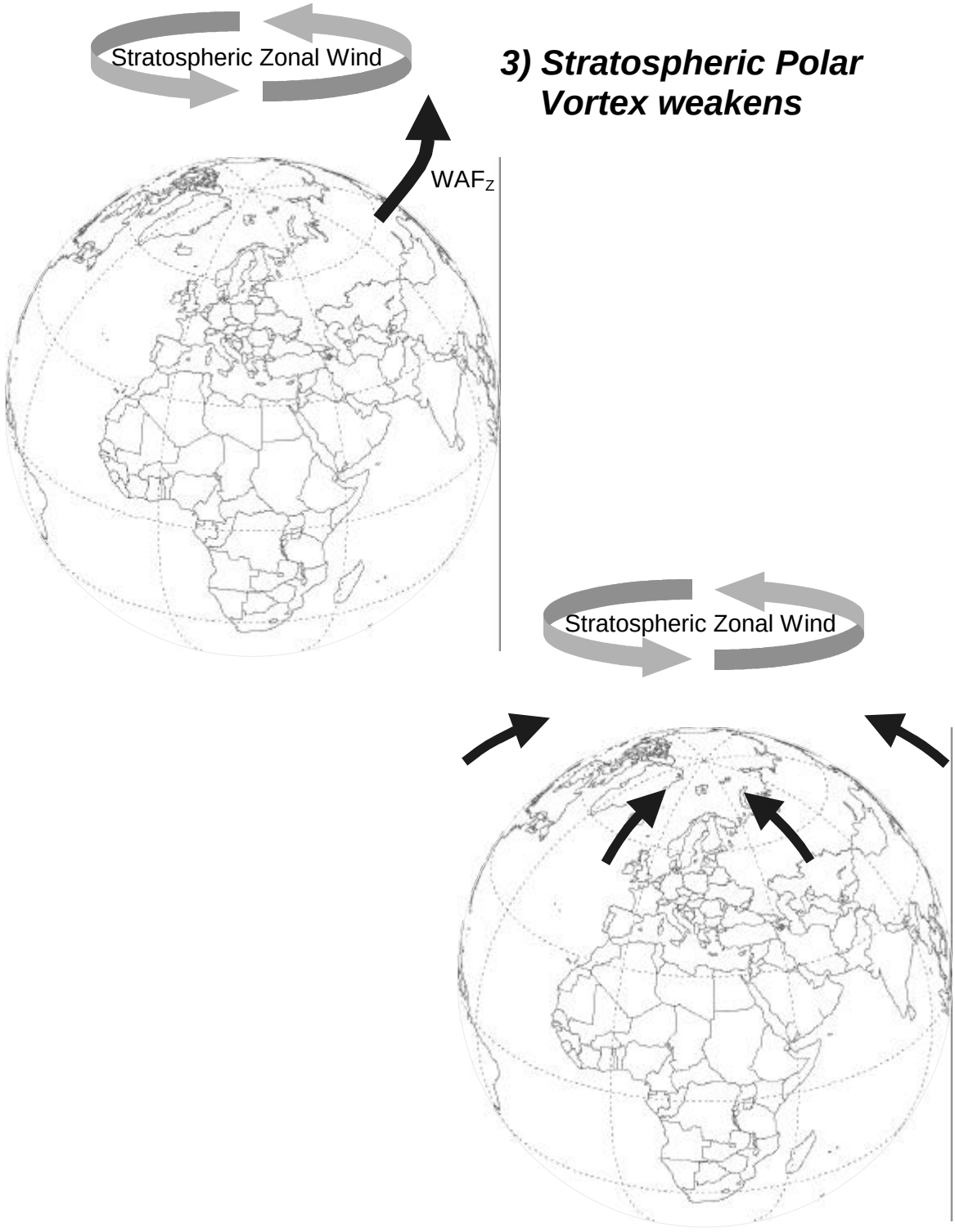

Figure 4-18, continued: Panels 3 and 4.

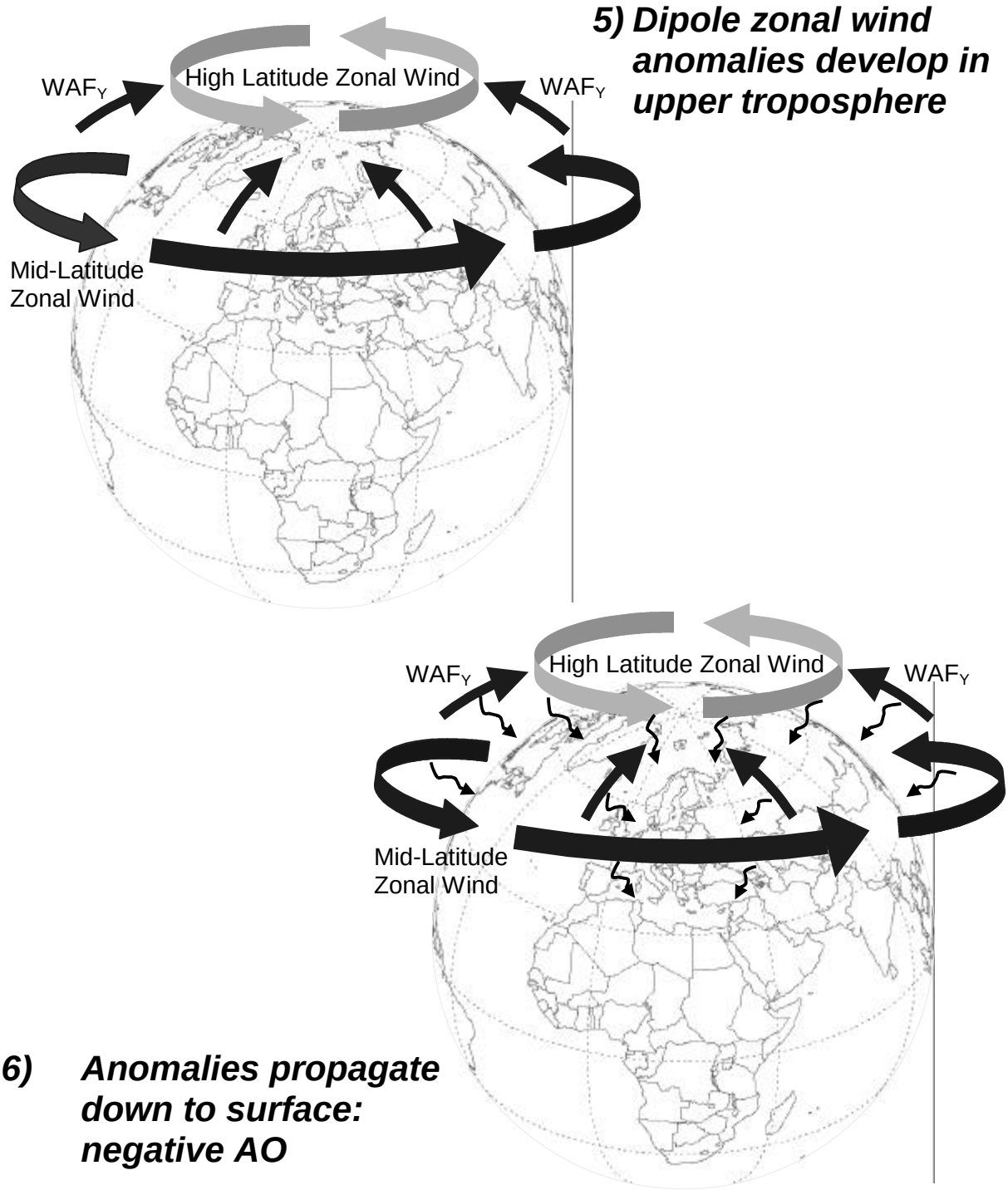

Figure 4-18, continued: Panels 5 and 6.

Chapter 5

Orographic Constraints on Siberian Snow Forcing

5.1 Description of Experiments

5.1.1 Background

Previous studies of climate modulation by land surface snow consistently point to Eurasia, and specifically Siberia, as a critical region. The results presented earlier in Chapter 4 support this assertion by identifying a detailed atmospheric teleconnection pathway which describes the physical mechanisms by which realistic continental-scale snow anomalies over Siberia result in hemispheric-scale AO mode modulations. Therefore it is of interest to understand the specific physical and dynamical reasons why land surface snow anomalies in this region can influence winter climate on a hemispheric scale.

One hypothesized factor is the presence of large mountain ranges adjacent to Siberia. Cohen et al. (2001) describes an apparent poleward migration of observed autumn Siberian High pressure anomalies which eventually forms the winter AO pattern, and suggests that the expected eastward downgradient migration is impeded by high orographic barriers. More importantly, the stationary wave activity flux used as a diagnostic measure in Saito et al. (2001) and Chapter 4 of this thesis originates in part from orographic obstructions (Plumb, 1985; Ringler and Cook, 1999). Other GCM studies highlight the sensitivity of planetary waves and stratospheric-tropospheric coupling to surface orographic amplitude (Taguchi et al., 2001; Taguchi and Yoden, 2002; Walker and Magnusdottir, 2003).

In addition to comprising a large, contiguous region subject to seasonal snow cover, Siberia is bordered to the south and east by some of the tallest mountain ranges in the world. The Altay, Sayanski, Yablonovoi and Cherski mountains all consistently exceed 1000 meters in elevation, with a peak elevation of roughly 4500 meters at Mt. Belukha. Together with the Tibetan Plateau, they form a continuous southwest-northeast ridge between Nepal and the Arctic Ocean, as illustrated in Figure 5-1a using NOAA 5-minute gridded elevation data (NOAA, 1988). These high orographic barriers are largely responsible for the major upward, eastward and primarily equatorward transmission of

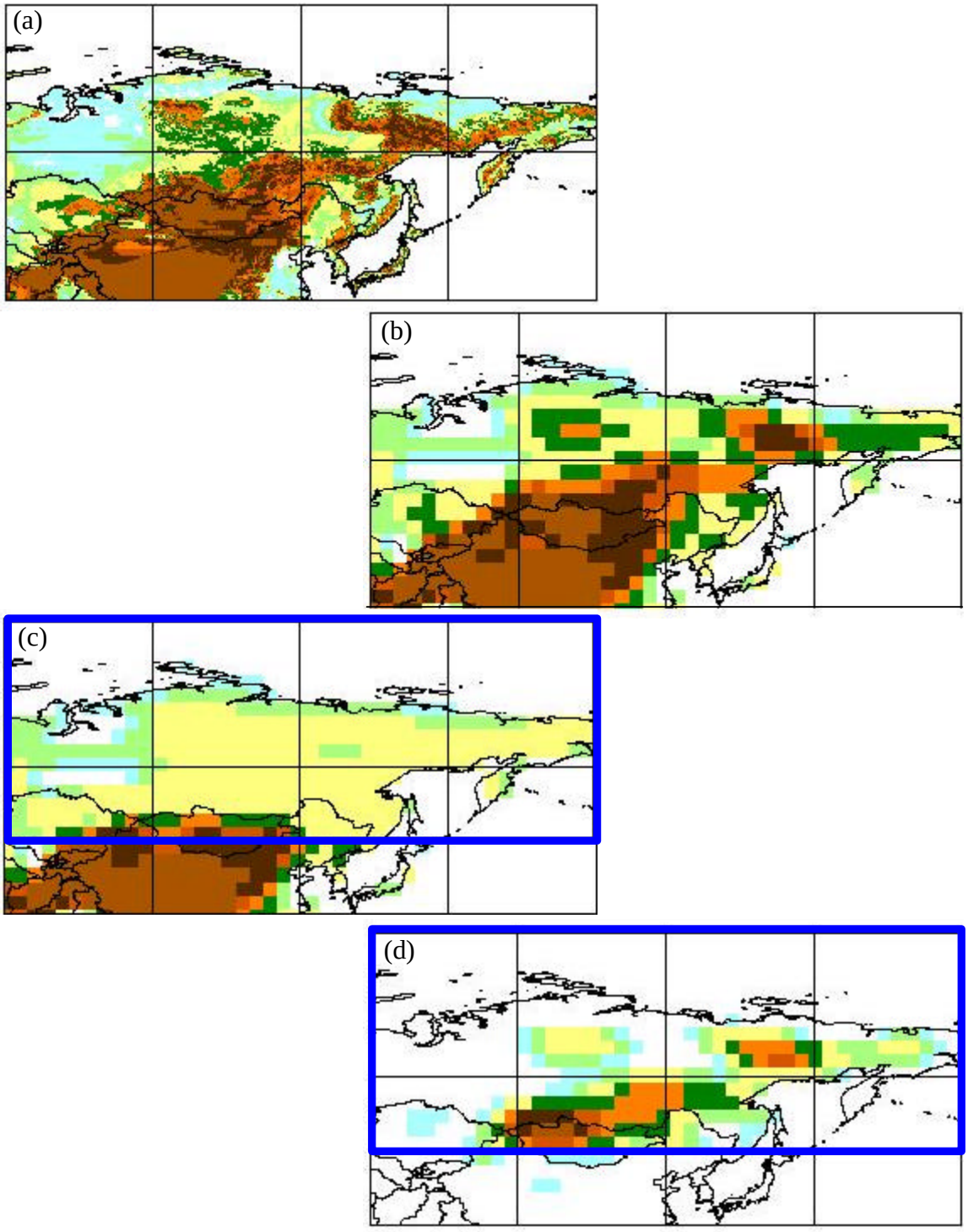

Figure 5-1: Land surface orography over Siberia. Shading represents 50-200 m (lightest), 200-400 m, 400-1000 m, 1000+ m (darkest). a) NOAA 5-minute gridded data. b) ECHAM3 GCM at T42 resolution (SIB). c) Adjusted orography for "No Mountains" experiments (ORO). d) Difference SIB – ORO. Box indicates region in which model orography was adjusted.

stationary wave energy that originates over Siberia (Plumb, 1985). This Siberia wave train is mechanically forced by the low-level physical obstructions, and also thermally forced by related diabatic heating anomalies (Ringler and Cook, 1999).

The teleconnection pathway relating Siberian snow anomalies to the winter AO mode, described in Chapter 4, is initiated by additional forcing of the Siberian wave train. A positive Siberian snow perturbation produces a local negative diabatic heating anomaly, which acts as an added surface thermal forcing on the orographically-generated overlying stationary wave train. An upwards vertical wave activity flux anomaly is produced at the surface, and propagates through the troposphere and into the stratosphere. Therefore it is reasonable to expect that the snow-AO pathway is a direct consequence of the high orographic barriers that border Siberia to the south and east.

5.1.2 Approach

In this chapter, the role of orography in enabling a Siberian snow-forced winter AO response is investigated. The U.S. Navy ten-minute global elevation dataset (Cuming and Hawkins, 1981) was used to develop gridcell-average surface elevations for the ECHAM3 model; T42 resolution elevations over Asia are shown in Figure 5-1b. A comparison of Figures 5-1a and 5-1b demonstrates that the orography over Asia is reasonably well represented by the model, and that the high-elevation mountains adjacent to Siberia are sufficiently resolved. The orographically-generated region of stationary wave activity originating in Siberia is similarly well represented by the model, as described in Chapter 4. Overall, the ECHAM3 model serves as an appropriate platform for evaluating the role of orography in the Siberian snow-AO teleconnection pathway.

A pair of snow-forced ensemble experiments is performed, analogous to the SIB experiments described in Chapter 4. The principal difference is that the model's orographic boundary condition in central and eastern Siberia is limited to a maximum elevation of roughly 400 meters. For these "no mountains" experiments, an initial maximum elevation of 400 meters is prescribed for all gridcells within 45ºN-90ºN and 60ºE-180ºE, outlined in Figure 5-1c. This region includes the mountains to the south and east of Siberia, but does not include the Tibetan Plateau. The height and areal extent of the Tibetan Plateau makes it influential to basic atmospheric dynamics, and its modification could result in large alterations to the general circulation of the modeled atmosphere.

Gridcell elevations near the southern (45ºN) border of the altered elevation region are adjusted to maintain a smooth gradient with the Tibetan Plateau to the south. Other numerical adjustments were performed to ensure the stability and robustness of the model. The revised orography was spectrally fitted to the T42 resolution that was used, to filter out noise associated with spectral resolution inconsistencies. Also, the global mean surface pressure (specified as a model boundary condition) was modified to maintain a global mean sea level pressure of roughly 1013 hPa. This surface pressure boundary condition must increase to account for the additional air mass that results from lowering surface elevations.

The final Siberian surface elevations applied in the "no mountains" experiments are shown in Figure 5-1c. Aside from the southern border, elevations throughout the

adjusted Siberia region are less than 400 meters, with most of the region below 300 meters. The 1000 meter ridge that formerly extended northeast from Nepal to the Arctic Ocean now terminates in Mongolia. Figure 5-1d presents the difference between the base GCM orography and the "no mountains" orography (i.e., Fig. 5-1b – Fig. 5-1c). The orography changes primarily consist of reduced elevations along the Siberian ridge, and also a slight lowering of the plateau located south of the Taimyr Peninsula. Due to the spectral fitting that was applied, non-mountainous regions in northern and western Siberia were slightly modified, though the magnitude of these elevation changes were generally within ± 50 meters.

This adjusted orographic boundary condition is applied to both the high snow and low snow GCM experiments performed in this chapter. The identical Siberian snow forcings used for the SIB experiments are applied for these "no mountains" experiments, and the ensemble mean climate response to this positive Siberian snow forcing (i.e., high snow – low snow) in the absence of Siberian mountains is denoted as ORO. The negative winter AO mode response to snow and associated teleconnection pathway that occur for SIB will be re-evaluated in the following sections for ORO. The similarities and/or differences between them will be studied to assess the extent to which the orographic barriers south and east of Siberia constrain the modeled snow-AO relationship.

5.2 AO Mode Response to Snow without Siberian Mountains

As described in Chapter 4, SIB generates a clear local surface climatic response in autumn to a positive snow perturbation over Siberia, in the form of higher albedo, lower temperature, and higher sea level pressure (SLP). The snow forcing and corresponding local thermodynamic response are both maintained during the winter, while responses beyond the Siberia forcing region are also produced, culminating in a hemispheric scale SLP dynamical response that is indicative of a negative AO mode. The SIB seasonal mean surface temperature and SLP response is summarized in Figure 5-2, which is repeated from Figure 4-7b,c,e,f. The negative winter AO response is clearly indicated in Figure 5-2d by a large positive SLP anomaly over the arctic and broad negative SLP anomalies at mid-latitudes, centered about the North Pacific and North Atlantic oceans.

The corresponding fields for ORO are presented in Figure 5-3. The local autumn surface thermodynamic response to snow is once again simulated, as indicated by lower temperatures in Figure 5-3a and higher SLP in Figure 5-3b. This is not surprising, since the snow forcing is identical for SIB and ORO. In winter however (Fig. 5-3c,d), the surface temperature anomaly is much more localized, and the SLP anomaly field no longer produces a negative AO mode response. Rather than the fully-formed positive (negative) SLP anomalies at high (mid) latitudes seen for SIB, ORO produces isolated negative responses over the far North Atlantic and North Pacific, and similarly disconnected positive responses over western North America, central and eastern Asia, and the western North Atlantic. If anything, in the absence of Siberian mountains the winter SLP response to Siberian snow resembles a weakly positive AO mode.

In Chapter 4, an unstandardized AO index metric was developed to facilitate a quantitative comparison between the extensive and limited snow experiments. It is computed by subtracting the average SLP north of 61.5N from the average SLP within

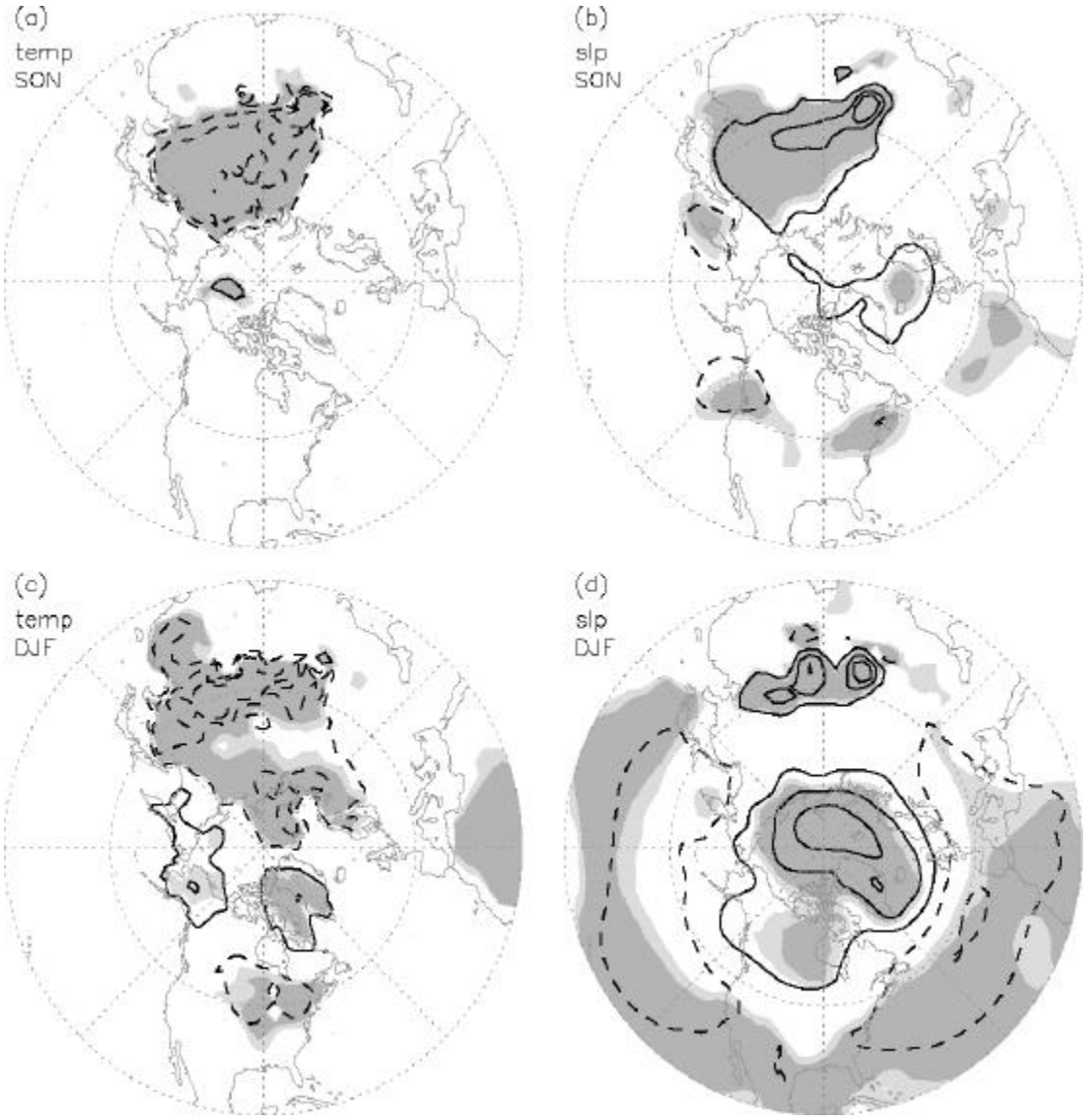

Figure 5-2: Surface climatic response to positive Siberian snow forcing, over the extratropical Northern Hemisphere, for SIB, during autumn (a,b) and winter (c,d) seasons. Surface temperature (a,c) contours drawn at ± 1, 3, 5 °C. Sea level pressure (b,d) contours drawn at ± 1, 3, 5 hPa. Dashed line denotes negative contour value. Light (dark) shading indicates 90% (95%) statistical significance.

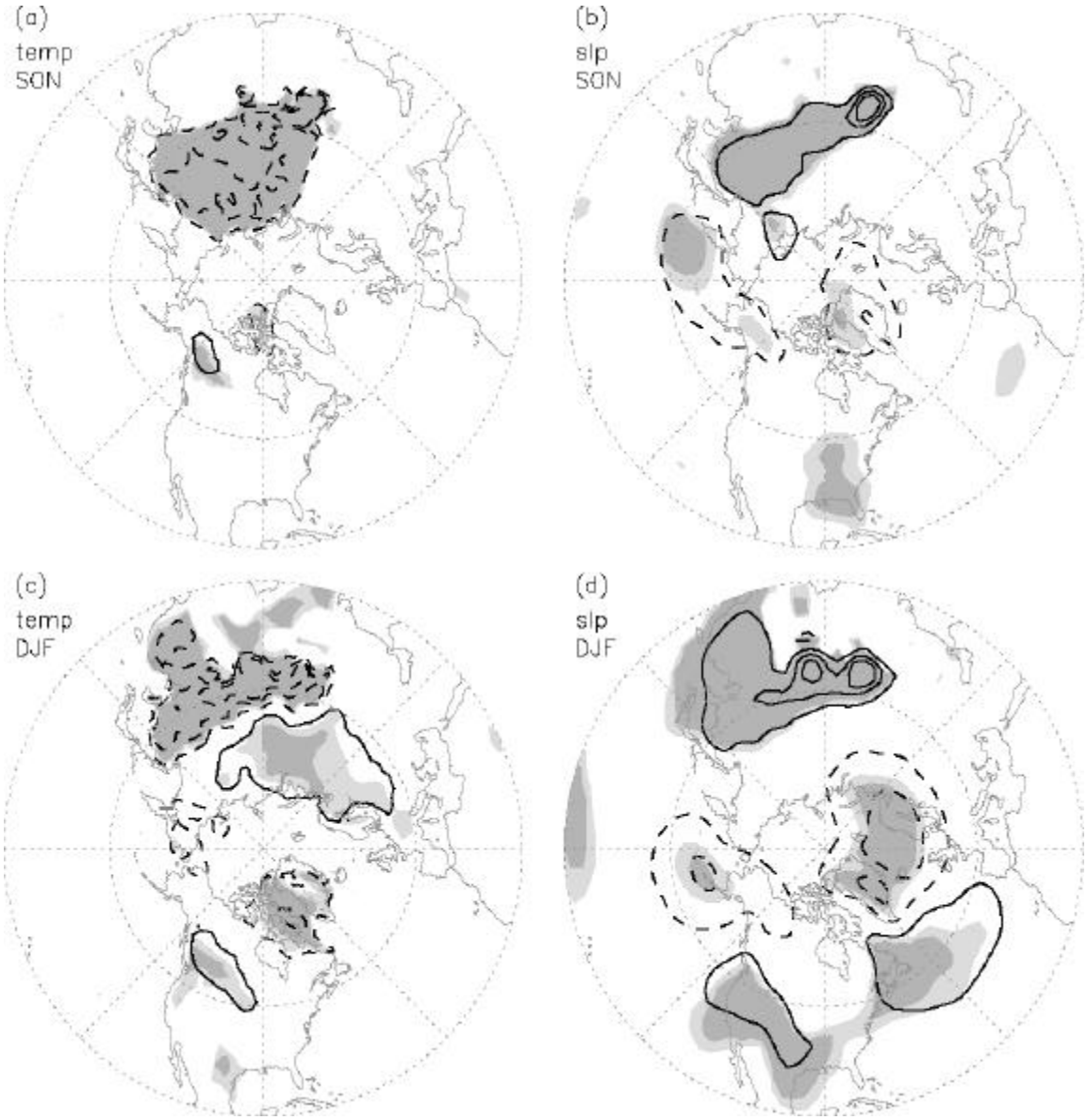

Figure 5-3: Same as Figure 5-2, but for ORO.

the zonal band from 28N to 50N; these two regions capture the centers of action in the SLP EOF1 field. This metric is used once again to evaluate the AO mode response to snow throughout the atmospheric column, as it evolves over the autumn-winter season. In Figure 5-4 we present the weekly evolution of a 42-day moving average AO index response, computed and normalized over twelve atmospheric levels from 1000 hPa to 10 hPa. SIB is shown in Figure 5-4a (repeated from Fig. 4-16), and ORO is shown in Figure 5-4b. A major feature of the snow-forced negative AO signal is its characteristic downward propagation from the stratosphere to the surface from late autumn through winter, which is indicated in Figure 5-4a. This propagation pattern is not evident in Figure 5-4b; furthermore the initial late-autumn stratospheric AO signal (i.e., weakened polar vortex), from which the downward propagation originates, also fails to materialize. Thus rather than just suppressing the ultimate surface negative winter AO response to Siberian snow as indicated in Figure 5-3d, the absence of Siberian mountains inhibits the entire snow-forced AO signal, throughout the atmospheric column and over the entire autumn-winter season.

Instead of producing a downward propagating negative AO signal, Figure 5-4b indicates that ORO produces a moderately significant positive AO signal during the late winter, extending throughout the troposphere and into the lower stratosphere. For the three-month winter (DJF) seasonal mean, the normalized AO index at the surface, 500 hPa and 50 hPa exhibit statistically significant (at least 94%) increases of 0.64, 0.60 and 0.62 standard deviations, respectively. These quantitative AO index results over the atmospheric column are consistent with the weakly positive snow-forced surface AO pattern produced for ORO in Figure 5-3d. In contrast to Figure 5-4a (SIB), no clear temporal propagation pathway is evident in Figure 5-4b (ORO) which leads to the positive late-winter AO signal.

Clearly, the mountains to the south and east of Siberia are critical to the modeled negative winter AO mode response to a positive Siberian snow perturbation. When these orographic barriers are reduced as model boundary conditions in ORO, the downward propagating AO signal from the stratosphere to the surface from late autumn through winter is no longer produced. This suggests that the vertical atmospheric teleconnection pathway described in Chapter 4, involving upward propagating stationary wave anomalies followed by a weakened stratospheric polar vortex and downward propagating wave and mean flow anomalies, breaks down at an early stage in the absence of Siberian mountains. Thus these mountains represent an orographic constraint on the aforementioned snow – AO teleconnection pathway.

Furthermore, ORO produces the unexpected result of a moderately positive late winter AO response to a positive Siberian snow perturbation. This response is opposite that of the expected and physically justified negative AO response for SIB. Two questions therefore arise: 1) at what stage does the absence of Siberian mountains disrupt the snow – AO teleconnection pathway; and 2) can the positive AO signal without Siberian mountains be explained via physical mechanisms? These questions will be addressed in the next section by analyzing stationary wave activity and its response to snow, for the ORO experiments.

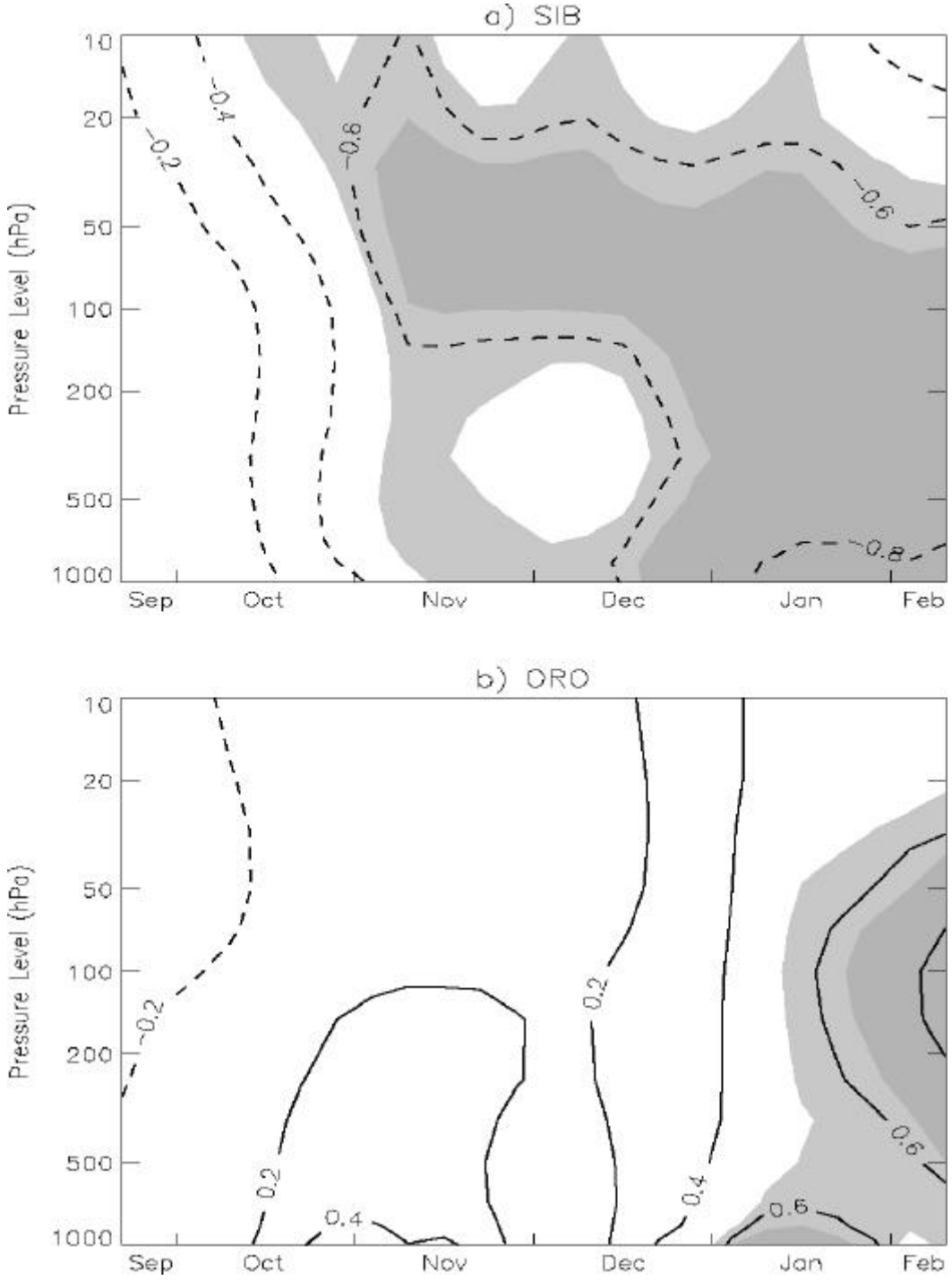

Figure 5-4: Weekly evolution (horizontal axis) over the atmospheric column (vertical axis) of normalized 42-day moving average hemispheric AO index (difference between the average SLP north of 61.5N and the average SLP within the zonal band from 28N to 50N) response to positive Siberian snow forcing. Contours drawn at ± 2, 4, 6, 8 standard deviations. Dashed line denotes negative contour value. Light (dark) shading indicates 90% (95%) statistical significance. a) SIB. b) ORO.

5.3 Stationary Wave Activity Without Siberian Mountains

5.3.1 Disruption of Snow – AO Teleconnection Pathway

It was demonstrated in Chapter 4 that the control ECHAM3 GCM does a credible job of reproducing the stationary wave activity throughout the Northern Hemisphere, including the orographically-generated Siberia wave train. The effect of removing Siberian mountains on this prevailing stationary wave energy transmission will now be investigated. Figure 5-5 shows the seasonal average vertical WAF at 500 hPa over the extratropical Northern Hemisphere for SIB, averaged over all 40 realizations that comprise both the extensive and limited snow experiments. Note that these fields are nearly identical to the corresponding WAF fields produced by the CTRL simulation shown in Figure 4-10a,c, which indicates that this average over both snow perturbation conditions acts as a valid proxy for climatological average snow conditions. The two centers of stationary wave activity over eastern Siberia and the North Atlantic are clearly evident in winter (Fig. 5-5a). In autumn (Fig. 5-5b), these wave trains are already apparent, but have not yet fully developed, especially over the North Atlantic.

Figure 5-6 shows the corresponding vertical WAF climatology at 500 hPa for ORO. The two centers of stationary wave activity are still evident, but the magnitude of the upward Siberia wave train is notably reduced in both autumn and winter. Figure 5-7 shows the difference (SIB-ORO) for each season. At the heart of this wave train over far-east Asia, the vertical WAF decreases by as much as 50% in the absence of Siberian mountains, for both autumn and winter. The center of this wave train is also shifted slightly eastward, into the far-western North Pacific, especially in winter. Stationary wave activity over Siberia is in all likelihood sustained in ORO by the dominant extratropical orographic barriers represented by the Tibetan Plateau, but removing the mid to high latitude mountains in Siberia has a clear disruptive effect. Similarly, the eastward and equatorward components of the Siberia wave train (not shown) are substantially reduced but not altogether removed when Siberian mountains are removed. Note in Figures 5-5 through 5-7 that the North Atlantic wave train is more or less unchanged between SIB and ORO, indicating that the impact on stationary wave activity is regional in scale, not global.

In the SIB experiments, Siberian snow variability is co-located within a region of major stationary activity. The large diabatic heating anomaly associated with the autumn snow perturbation generates an additional thermal forcing of this wave train, resulting in a large local upward WAF anomaly over Siberia during autumn, as shown in Figure 5-8a (repeated from Fig. 4-12). For ORO the same snow perturbation occurs within a substantially weakened stationary wave train. As a result, the autumn snow perturbation produces a more modest local upward WAF anomaly, in both magnitude and spatial extent, as shown in Figure 5-8b. Consistent with the eastward shift of this wave train for ORO, the upward WAF response is centered around the far-western North Pacific instead of Siberia.

The combination of a weaker vertical wave train and a diminished snow-forced upward WAF anomaly is insufficient to propel this thermally forced additional wave

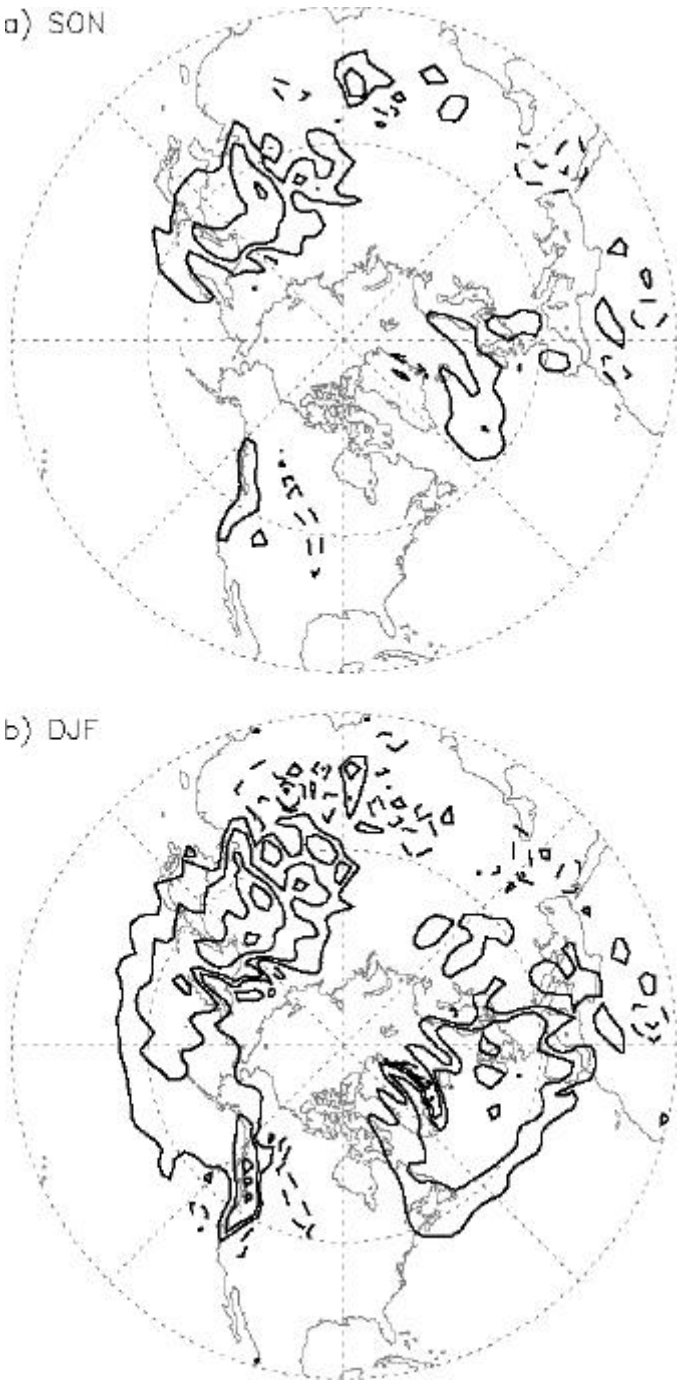

Figure 5-5: Seasonal average vertical wave activity flux climatology at 500 hPa elevation over the extratropical Northern Hemisphere for SIB, averaged over 40 ensemble realizations that comprise both extensive and limited snow experiments. Contour intervals drawn at ± .03, .07, .15, .25 m^2s^{-2}. Dashed line denotes negative contour value.

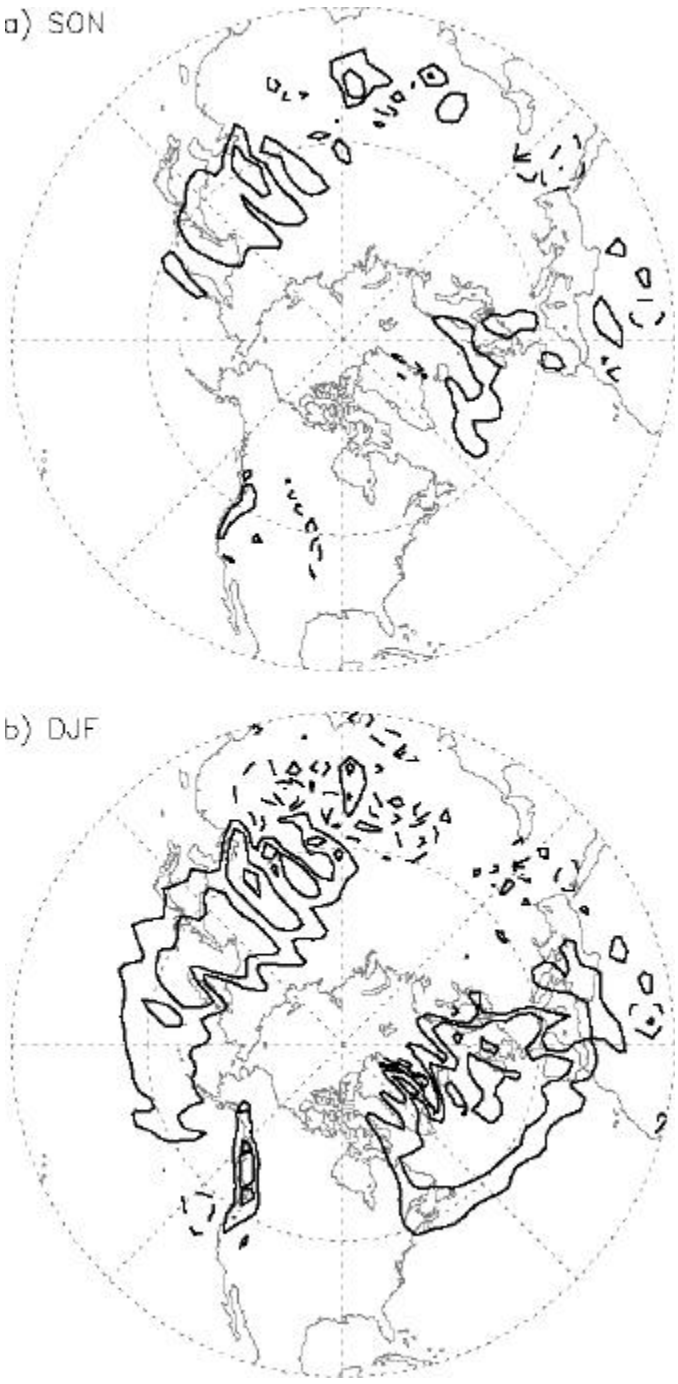

Figure 5-6: Same as Figure 5-5, except for ORO.

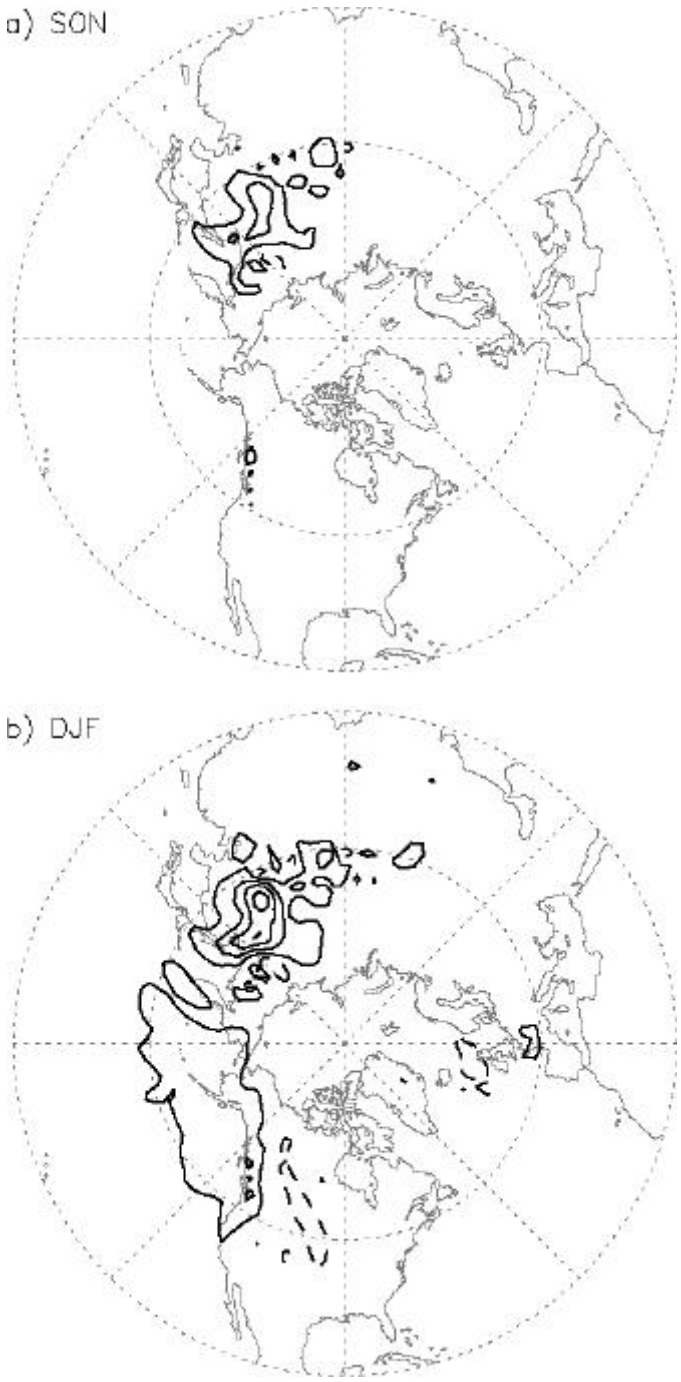

Figure 5-7: Same as Figure 5-5, except for the difference SIB-ORO. Contour intervals drawn at ± .02, .06, .10, .16 m^2s^{-2}. Dashed line denotes negative contour value.

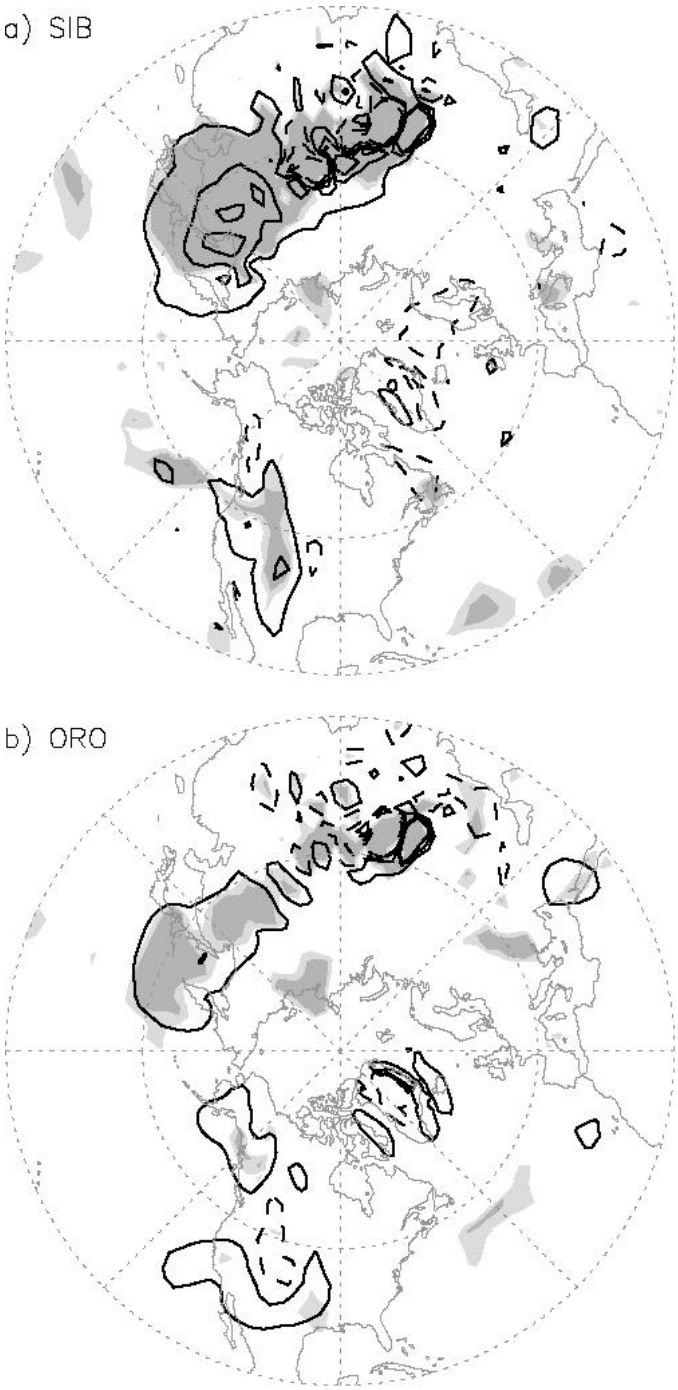

Figure 5-8: Vertical wave activity flux response to positive Siberian snow forcing, at 850 hPa elevation over the extratropical Northern Hemisphere, for autumn. Contours drawn at ± 0.01, 0.04, 0.08 m^2s^{-2}. Dashed line denotes negative contour value. Light (dark) shading indicates 90% (95%) statistical significance. a) SIB. b) ORO.

energy up through the troposphere and weaken the stratospheric polar vortex, as is the case for SIB and as reported in observations (Kuroda and Kodera, 1999; Limpasuvan and Hartmann, 2000). Figure 5-9 shows the latitude vs. pressure profile of WAF response during mid-November, averaged over 107E-180E to capture the shifted Siberia wave train for ORO. For 42-day averages (Fig. 5-9a), the modest snow-forced upward WAF anomaly is evident at the surface over Siberia wave train latitudes, but diminishes rapidly with elevation. Weekly averages (Fig. 5-9b) exhibit larger low-level upward WAF anomalies, consistent with the notion expressed in Chapter 4 that these snow-forced anomalies occur in transient pulses throughout the autumn-winter season. This upward anomaly pulse does propagate up through the troposphere, but fails to break through to the stratosphere.

Figure 5-9 represents typical WAF response patterns over the course of the autumn-winter simulation period. Thus without Siberian mountains, the initial upward tropospheric wave anomaly propagation component of the snow – AO teleconnection pathway does occur, but is weakened considerably. The anomaly fails to extend into the polar vortex, thereby disrupting the teleconnection. Since the local surface WAF response to the Siberian snow perturbation (Fig. 5-8) is dependent on the orographic barriers adjacent to Siberia, removal of these barriers suppresses this local response and prevents the subsequent remote teleconnection response from fully developing.

5.3.2 Possible Interpretation of Positive AO Mode Response to Snow

Although the snow-forced upward WAF anomaly is notably diminished for ORO, some additional thermally forced wave energy is nevertheless introduced into the atmosphere by the Siberian snow perturbation. Instead of the downward propagating poleward wave refraction seen for SIB, the primary horizontal stationary wave response for ORO appears to be a modest global-scale equatorward refraction throughout the troposphere, beginning in October and continuing through February. This equatorward refraction is evident for the Siberia wave train in Figure 5-9. Furthermore, Figure 5-10 shows time vs. pressure profile evolutions of 42-day average meridional WAF response for ORO, averaged over the shifted Siberia wave train, North Atlantic wave train, and extratropical Northern Hemisphere. All three regions exhibit a reasonably consistent pattern of equatorward stationary wave refraction (negative contours), beginning in October. Anomalies are restricted to the troposphere, and have two main periods, the first occurring in November during the primary autumn snow forcing, and the second occurring during the winter when stationary wave activity is generally stronger.

Meridional WAF anomalies are largest around 250 hPa, but are distributed throughout the troposphere, and no clear vertical propagation of the signal is indicated. Thus this refraction does not appear to evolve gradually from either above or below, which is consistent with the AO index response shown in Figure 5-4b. The similarity between the three regions shown in Figure 5-10 implies that the equatorward refraction is hemispheric in scale, as opposed to the initial snow-forced upward WAF anomaly which is restricted to the Siberia wave train (see Fig. 5-8b). During the November period the Siberia wave train exhibits a somewhat larger equatorward refraction, but by winter the North Atlantic wave train shows greater refraction. In general, only a few weeks after the

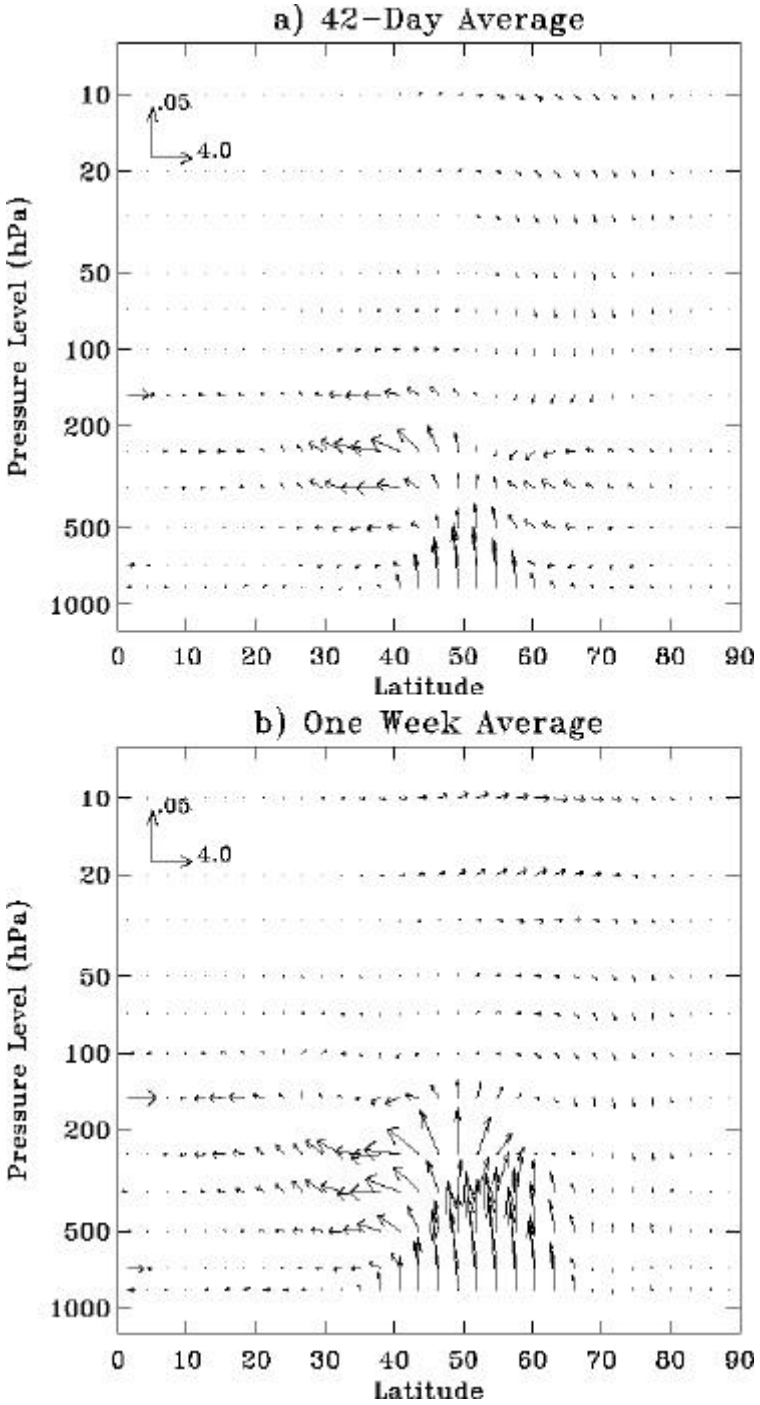

Figure 5-9: Latitude (0N-90N) vs. pressure level (850hPa-10hPa) profiles of wave activity flux response to positive Siberian snow forcing, for ORO. Vectors represent meridional and vertical fluxes averaged over the Siberia wave train; scale in m^2s^{-2} is indicated on figure. a) 42-day average period in mid-November. b) One-week average period in mid-November.

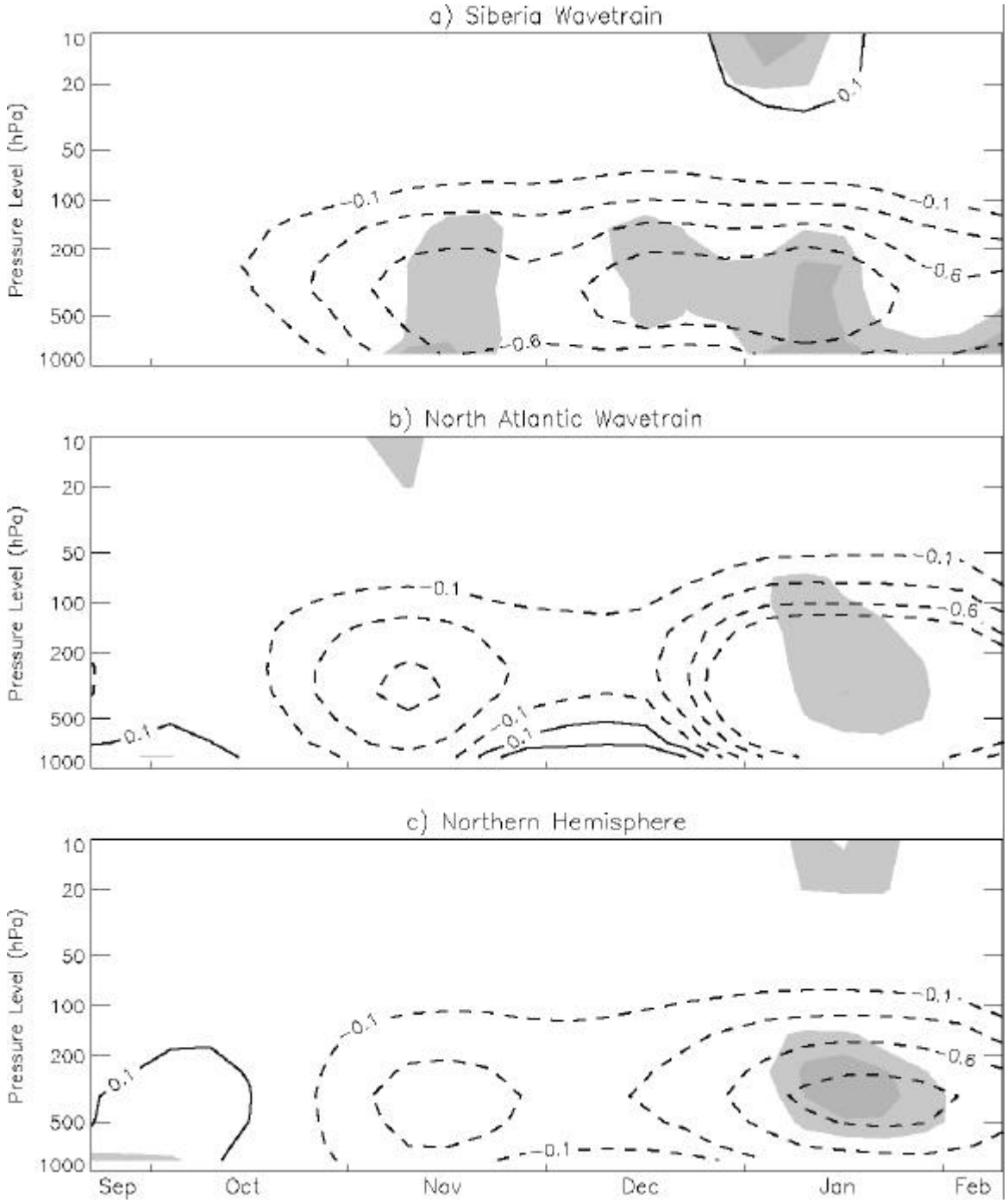

Figure 5-10: Weekly evolution (horizontal axis) over the atmospheric column (vertical axis) of meridional wave activity flux response to positive Siberian snow forcing, for ORO. Contours represent 42-day moving average over extratropical (36.5N-81N) regions, drawn at ± .1, .3, .6, .9 m^2s^{-2}. Dashed line denotes negative (equatorward) contour value. Light (dark) shading indicates 90% (95%) statistical significance. a) Siberia wave train. b) North Atlantic wave train. c) Northern Hemisphere.

Siberian snow anomaly begins in early October, an equatorward WAF anomaly begins throughout the troposphere and spans the entire Northern Hemisphere.

One possible interpretation of these results is that the additional thermally forced wave energy excites the prevailing equatorward component of the planetary Rossby waves. Without Siberian mountains, the snow-forced upward WAF anomaly does not propagate up through the entire troposphere to weaken the stratospheric polar vortex. This anomalous energy therefore remains in the troposphere, where it simply acts to enhance the dominant tropospheric wave activity centers over Siberia and the North Atlantic. Since the wave energy spreads upward and equatorward, the added wave energy is manifested as an equatorward anomaly that spreads quickly throughout the troposphere. The eastward component of the wave trains allows the added energy to be distributed throughout the Northern Hemisphere, although eastward anomalies are negligible compared to equatorward ones.

The hemispheric-scale equatorward WAF anomalies are indicative of poleward momentum flux anomalies, which result in dipole mean flow anomalies (Zhou et al., 2001). For ORO, this is indicated by positive (negative) zonal-mean zonal wind anomalies at higher (lower) latitudes (not shown). In conjunction with the equatorward WAF anomalies, these mean flow anomalies also occur in pulses, but accrue over time and eventually culminate in a moderately positive AO mode anomaly in late winter, as indicated in Figure 5-4b. Unlike for SIB, each anomaly pulse appears throughout the troposphere, and does not propagate down from an initial stratospheric vortex anomaly.

Hence the moderately positive AO mode response that occurs for ORO may result from a simple enhancement of the prevailing equatorward stationary wave activity. This positive AO anomaly is considerably weaker than the negative AO mode response in SIB, for two likely reasons. First, the initial upward WAF anomaly is weaker for ORO (Fig. 5-8), so that there is less energy input to perturb the atmospheric circulation. Second, a positive feedback mechanism was identified for SIB in Chapter 4 between downward propagating mean-flow anomalies and poleward wave refraction, such that there was a perpetual forcing of the poleward WAF anomalies. For ORO, no such feedback mechanism is apparent; equatorward wave refraction is driven only by snow-forced pulses of added wave energy.

This physical interpretation for the positive AO mode response for ORO is not as clear as the vertical teleconnection pathway and negative AO mode response identified for SIB. For example, why does the added wave energy enhance the meridional component of the prevailing wave activity, but not the zonal component? Also, how does the regional wave energy input over Siberia translate so rapidly into a hemispheric-scale equatorward refraction, without the aid of the stratosphere as seen for SIB? A detailed analysis of the Rossby wave dynamics simulated by the model is required to answer these questions, which is outside the scope of this thesis. Due to the limited extent of the positive AO index response shown in Figure 5-4b, and the lack of a clear AO mode response in mean flow parameters such as SLP in Figure 5-3d, it is quite possible that this positive AO response for ORO is simply due to random interannual fluctuations in the internal AO mode. Another possibility is that snow-forced hemispheric equatorward wave anomalies are exaggerated by the ECHAM3 model, due to the fact that the

equatorward component of the modeled climatological wave activity is overpredicted compared to observations, as acknowledged in Chapter 4.

5.4 Discussion

Siberia has previously been identified as a critical region for producing snow-forced winter AO anomalies. In addition to being a large, contiguous land surface area subject to substantial seasonal snow cover variations, Siberia is bordered to the south and east by mountain ranges that consistently exceed 1000 meters in elevation. The high orographic barriers in this region are largely responsible for the large region of stationary wave energy transmission that originates over Siberia. Chapter 4 has identified a clear atmospheric teleconnection pathway linking interannual early season snow variations over Siberia to interannual modulations of the winter AO mode. A primary component of this teleconnection is the enhanced upward propagation of energy along this Siberian wave train, driven by snow-forced diabatic heating anomalies at the surface.

In this chapter, the role of the orographic barriers adjacent to Siberia in producing this snow – AO teleconnection pathway has been investigated. The ECHAM3 GCM's orographic boundary condition is modified such that the downstream Siberian mountains are reduced, and the ensemble mean response to a realistic Siberian snow forcing is evaluated as in Chapter 4. Model results indicate that without the Siberian mountains, the negative winter AO response to a positive Siberian snow forcing is no longer produced. Furthermore, the snow – AO teleconnection pathway fails to develop beyond the initial upward propagation of local snow-forced stationary wave energy into the troposphere. The propagation of stationary wave energy into the stratosphere, the subsequent weakening of the polar vortex, and the ultimate downward stratosphere-to-surface propagation of coupled wave-mean flow anomalies and associated AO signals, do not occur in the absence of Siberian mountains.

These results indicate that the Siberian snow – winter AO relationship arises due to the specific and unique orographic conditions in the Siberia region. The mountains to the south and east of Siberia contribute substantially to the major center of stationary wave activity that is dominant over Siberia, especially in its upward propagating component. The modeled snow perturbations are regionally co-located within this strong Siberian wave train, so that the associated thermal wave forcing is constrained to a large upward wave activity flux anomaly that extends through the tropopause, thereby resulting in the snow – AO teleconnection pathway. Therefore the mountains adjacent to Siberia represent an orographic constraint on this modeled teleconnection pathway.

Without Siberian mountains, both the prevailing Siberian wave train and the snow-forced upward wave anomaly are considerably weaker, and the added wave energy is not forced to propagate all the way up to the stratosphere. Instead, this modest wave energy input remains in the troposphere, where it appears to enhance the prevailing centers of stationary wave activity over Siberia and North America. This seems to produce a hemispheric-scale equatorward wave flux anomaly, and corresponding poleward momentum flux and dipole mean flow anomalies, which eventually yield the unexpected result of a moderate positive AO mode response in late winter. The physical mechanisms

behind this apparent snow-forced positive winter AO anomaly in the absence of Siberian mountains are still unclear. The relatively mild positive AO response may in fact be physically unrelated to the snow forcing, and simply arise from either random fluctuations in the fundamental, internal AO mode of atmospheric variability, or biases in the ECHAM3 GCM.

What is clear however is that the orographic conditions around Siberia are key to instigating the previously established positive Siberian snow – negative winter AO teleconnection pathway, which is physically justifiable (Chapter 4) and supported by other observational and modeling studies found in the literature (Baldwin and Dunkerton, 1999; Kuroda and Kodera, 1999; Limpasuvan and Hartmann, 2000; Zhou et al., 2002). The results presented in this chapter indicate that snow anomalies over Siberia are capable of modulating the winter AO mode, due to its unique orographic features. Thus a physical argument is provided here to support previous studies which identify Eurasia and Siberia as the critical region for snow-forced winter AO anomalies. Additional modeling experiments are presented in the next chapter to further confirm this assertion, in which a region other than Siberia is forced with realistic snow perturbations. Identification of specific, influential snow-forcing regions for winter AO mode modulation will be advantageous to the prospective incorporation of land surface snow anomalies into future climate prediction efforts.

Chapter 6

Relative Impacts of Siberian and North American Snow Anomalies

6.1 Description of Experiments

Chapter 4 describes a clear, physically-based teleconnection pathway linking realistic, observation-based early season Siberian snow perturbations to a modulation of the winter AO mode of climate variability. This pathway draws on established wave-mean flow interaction theory, and is consistent with recent literature on stratospheric-tropospheric coupling of the AO signal. The co-location of the Siberian snow forcing within a region of strong stationary wave activity is identified as key to the initiation of the teleconnection pathway. Chapter 5 describes the influential role of regional orographic barriers in southern and eastern Siberia in producing this major stationary wave train over Siberia, which consequently enables the snow-forced pathway to occur. These results support the snow-AO linkages described in previous studies, and provide a physical basis by which Siberia acts as a critical region for snow-forced winter AO variability on interannual timescales.

This chapter continues the investigation of Siberia as a key snow-forcing region by comparing the climatic response between modeled snow perturbations in Siberia and North America. North America also represents a sizable land mass with extensive and variable snow conditions, and thus has the potential to modulate remote climatic phenomena such as the AO. However, this region does not feature a major stationary wave train, so the precise teleconnection pathway identified in response to the Siberia forcing may not be produced for the North America forcing. This explicit comparison of snow forcing over the two major land masses in the extratropical Northern Hemisphere will provide additional insight to the physical mechanisms behind the snow – AO relationship.

A pair of snow-forced ensemble experiments is performed, analogous to the SIB experiments in Chapter 4 and the ORO experiments in Chapter 5. The principal difference is that rather than prescribing land surface snow depths over a region in Siberia, a comparable region in North America is subjected to similarly realistic,

observation-based snow forcings. Figure 6-1 shows the snow forcing regions over Siberia and North America. Both regions span 36.5N – 90.0N latitude, and have equivalent longitudinal extents (67.5E – 140.5E for Siberia, 219.5E – 292.5E for North America). Note however that the North America region contains somewhat less land surface area than the Siberia region.

The same methodology detailed in Chapter 4 for specifying Siberian snow cover and snow depth forcings is used here for North American forcings. The only difference is that an alternate pair of time periods from the NOAA visible satellite observation dataset is used, to capture the highest and lowest recorded autumn snow cover specifically over North America. The period September 1996 – February 1997 is used for the high snow experiment, and the period September 1987 – February 1988 is used for the low snow experiment. Ensemble mean differences between the two experiments are computed (high snow – low snow) and denoted as NA, to evaluate the climatic response to this extreme but realistic positive snow perturbation over North America. In the following section, the teleconnection pathway that occurs for the SIB experiments will be evaluated for the NA experiments.

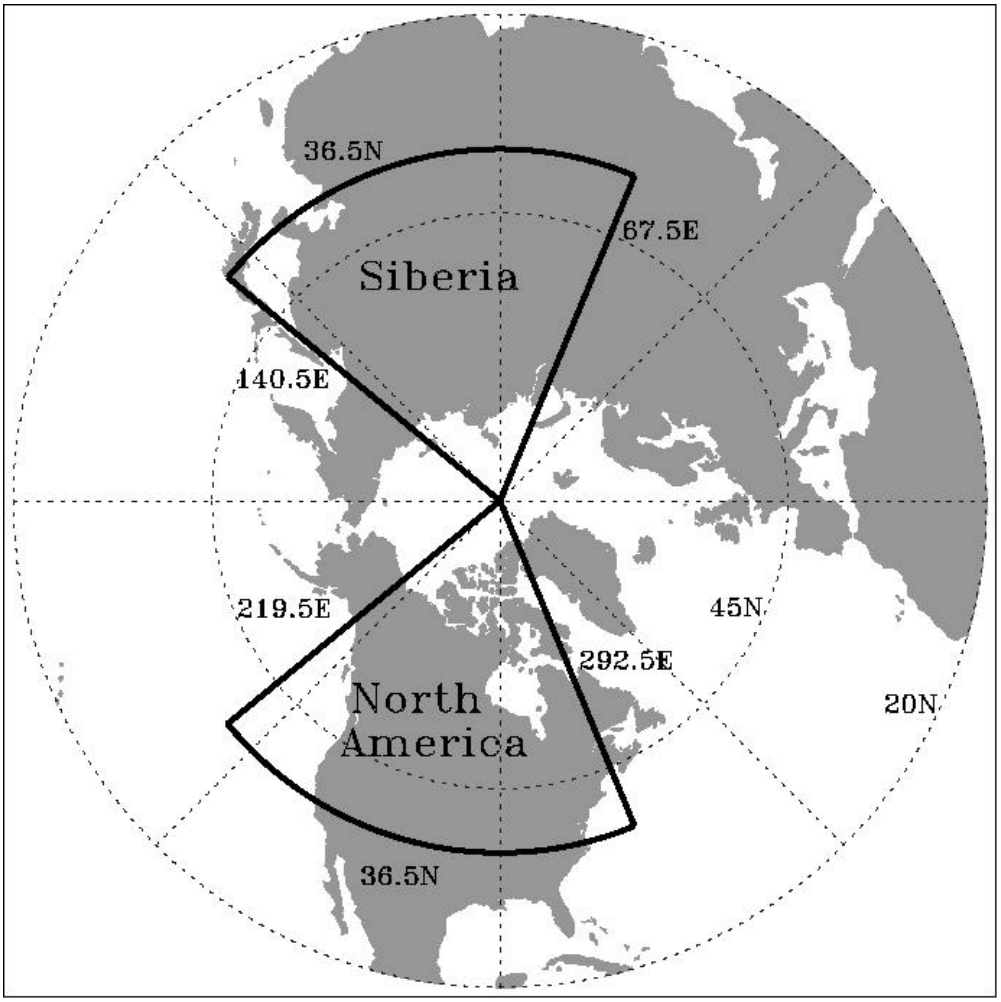

Figure 6-1: Snow forcing regions applied for over Siberia (SIB, ORO) and North America (NA).

6.2 Results

The teleconnection pathway documented in Chapter 4 is initiated by a strong local upward stationary wave anomaly over the Siberia snow forcing region. The regional co-location of the snow-forced negative surface temperature anomalies and a major stationary wave train centered over far-east Asia (hereafter referred to in this chapter as the Siberia wave train) is responsible for this strong upward WAF anomaly. The autumn season (SON) surface temperature response to a positive snow forcing is shown for SIB in Figure 6-2a (repeated from Fig. 4-7b), and for NA in Figure 6-2b. For both experiments, a clear negative surface temperature anomaly is evident directly over both forcing regions, which is the expected local response. Note that the magnitude of the response for SIB is relatively larger, because the two years of snow cover data used for SIB constitute a larger forcing than the years used for NA (see Robinson et al. 1993; Robinson 2000).

Figure 6-3 shows the seasonal average WAF climatology over the extratropical Northern Hemisphere for the base ECHAM3 model, repeated from Figure 4-10. The Siberia forcing region occurs well within the Siberia stationary wave train, whereas the North America forcing region occurs outside of both the Siberia and North Atlantic wave trains. Thus the snow-forcing region for NA exhibits a negative surface temperature anomaly, but this anomaly is not co-located within a region of stationary wave activity.

Consequently, the local upward WAF anomaly seen for SIB is not produced by NA, as indicated by Figure 6-4 which shows the vertical wave activity flux (WAF; Plumb 1985) response to snow at 850 hPa elevation during autumn (SON). For SIB (Fig. 6-4a, repeated from Fig. 4-12), the snow-forced temperature anomaly serves to strengthen the pre-existing Siberian stationary wave train. For NA (Fig. 6-4b), there is essentially no wave train for the local temperature anomaly to strengthen, so no upwards WAF anomaly is produced. In other words, the local stationary wave response to a snow perturbation is strongly dependent on the prevailing stationary wave activity over the perturbation region.

Note in Figure 6-4b that weak areas of upward WAF anomalies do occur over western Europe and Siberia, well removed from the North America snow forcing region. These regions roughly coincide with the two major stationary wave trains that exist in the Northern Hemisphere, centered over far-east Asia and the North Atlantic. Thus rather than producing a strong localized upward wave anomaly that propagates into the stratosphere, the snow forcing over North America appears to modestly enhance the prevailing tropospheric stationary wave trains throughout the Northern Hemisphere. Possible reasons for this unexpected response will be hypothesized below.

However, this slight upward enhancement of the stationary wave trains for NA is not sufficient to initiate the teleconnection pathway by propagating up through the tropopause and weakening the stratospheric polar vortex, as is the case for SIB. Figure 6-5 shows the zonal wind response to snow at 50 hPa elevation during winter (DJF). For SIB (Fig.6-5a), weakening of the polar vortex is clearly indicated by an annular band of negative zonal wind anomalies centered around 60N, and an associated band of weak positive anomalies in lower latitudes (Holton 1972). For NA (Fig. 6-5b), there is no

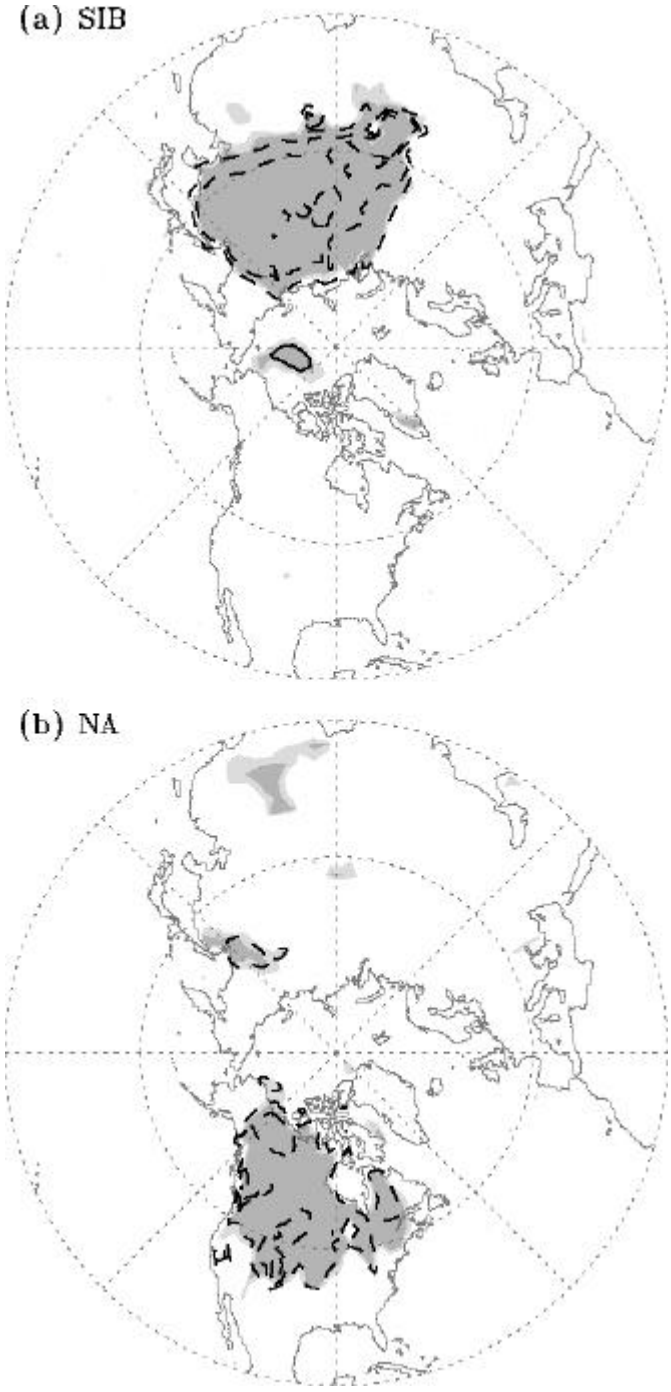

Figure 6-2: Surface temperature response to positive snow forcing, over the extratropical Northern Hemisphere, during autumn (SON). Contours drawn at ± 1, 3, 5 °C. Dashed line denotes negative contour value. Light (dark) shading indicates 90% (95%) statistical significance. a) SIB. b) NA.

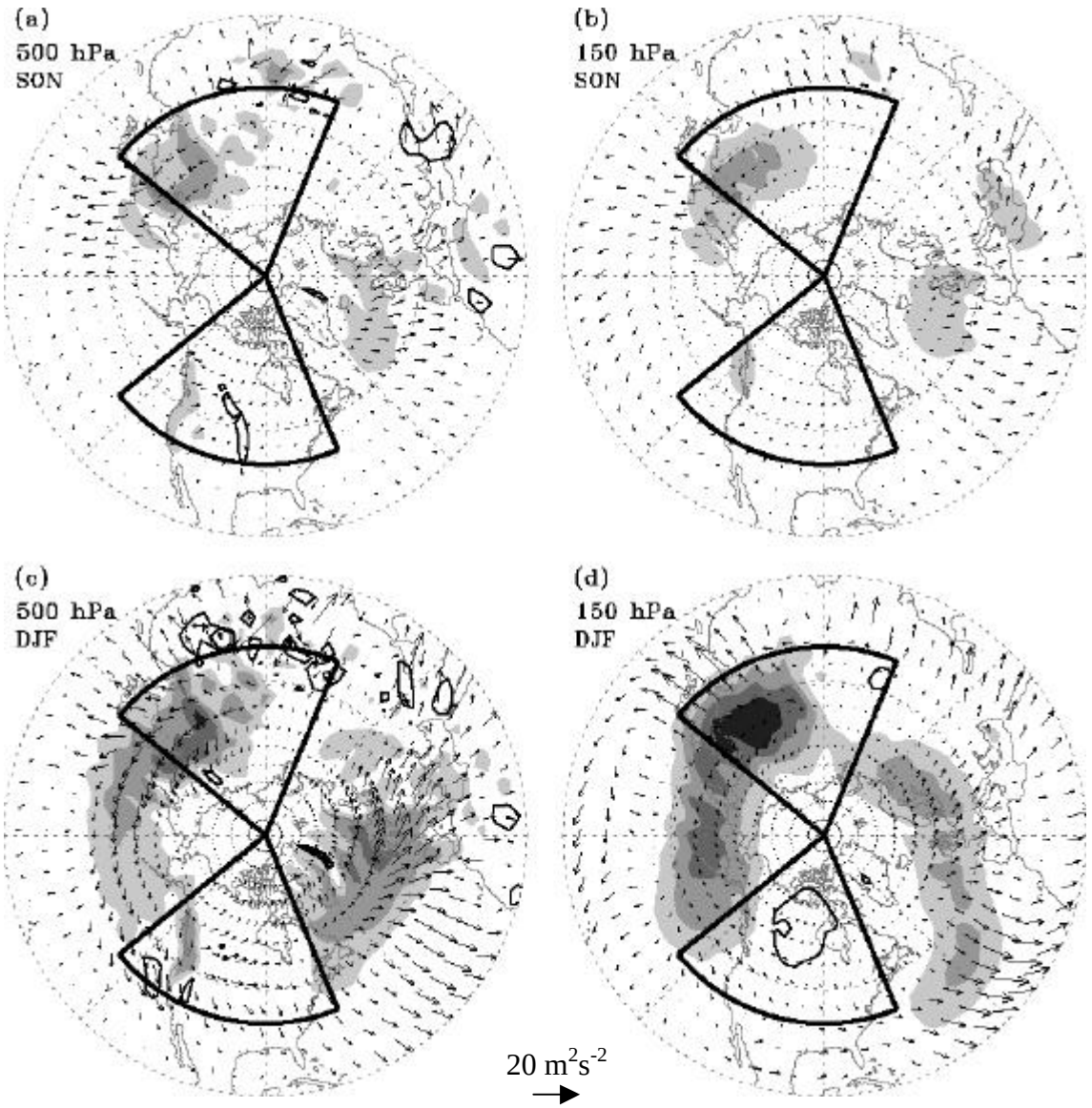

Figure 6-3: Three-dimensional wave activity flux (WAF) climatology over the extratropical Northern Hemisphere, for the CTRL simulation (repeated from Fig. 4-10). Vectors denote horizontal fluxes (scale indicated on figure), and filled (open) contours denote upward (downward) vertical fluxes. Also shown are the Siberia and North America forcing regions. a) 500 hPa elevation, autumn. b) 150 hPa elevation, autumn. c) 500 hPa elevation, winter. d) 150 hPa elevation, winter. Contours for 500 hPa (a,c) drawn at ± .03, .07, .15, .25 m^2s^{-2}. Contours for 150 hPa (b,d) drawn at ± .01, .02, .03, .04 m^2s^{-2}.

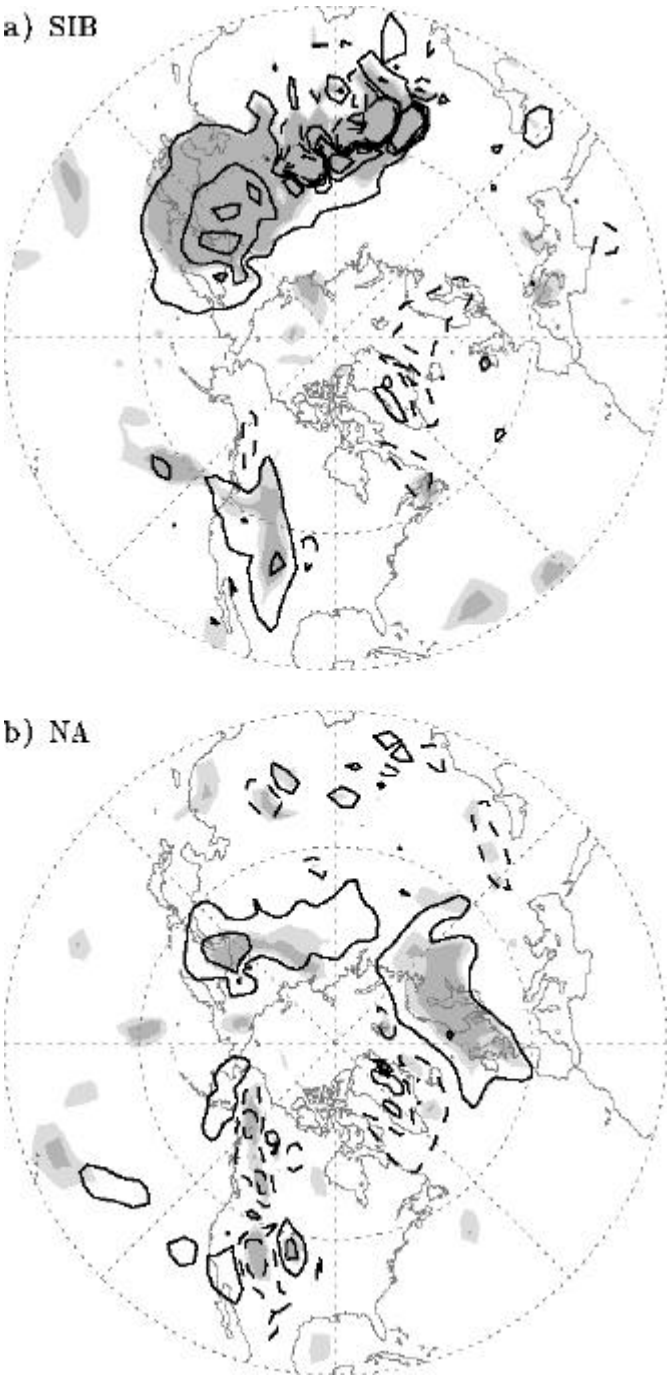

Figure 6-4: Vertical wave activity flux response to positive snow forcing, at 850 hPa over the extratropical Northern Hemisphere, for autumn (SON). Contours drawn at ± 0.01, 0.04, 0.08 m^2s^{-2}. Dashed line denotes negative contour value. Light (dark) shading indicates 90% (95%) statistical significance. a) SIB. b) NA.

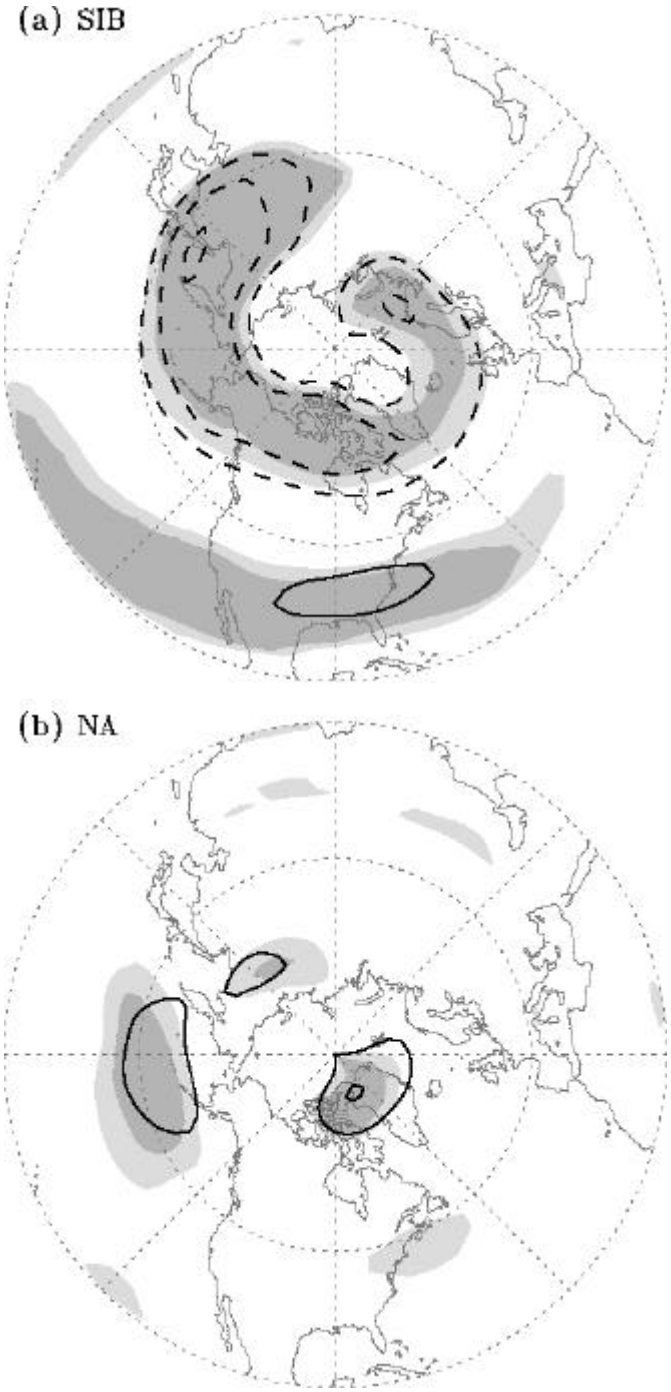

Figure 6-5: Winter (DJF) zonal wind response to positive snow forcing, at 50 hPa over the extratropical Northern Hemisphere. Contours drawn at ± 2, 3, 4 ms^{-1}. Dashed line denotes negative contour value. Light (dark) shading indicates 90% (95%) statistical significance. a) SIB. b) NA.

coherent hemispheric-scale change to the stratospheric zonal wind field, which indicates that the polar vortex is minimally affected by North American snow forcing.

For SIB, the subsequent downward component of the pathway involves the propagation of mean-flow anomalies associated with the weakened vortex, from the stratosphere down to the surface. This downward propagation can be summarized by evaluating the snow-forced change in an unstandardized AO index metric, computed as the difference in geopotential height between mid and high latitude zonal bands (see Chapter 4). The weekly evolution over the atmospheric column of this AO index response to snow is presented for SIB in Figure 6-6a (repeated from Fig. 4-16). A negative AO index anomaly first appears in the late autumn stratosphere, indicative of the weakened polar vortex response to the upward WAF anomaly over Siberia. The anomaly then gradually propagates downward, culminating in a strong negative AO index response at the surface by mid-winter.

The corresponding AO index evolution for NA is presented in Figure 6-6b. In the absence of a strong upward WAF anomaly (Fig. 6-4b), the polar vortex exhibits no apparent weakening (Fig. 6-5b). Since this upward component of the pathway does not occur for NA, the subsequent downward propagation of negative AO index anomalies also fails to materialize in Figure 6-6b. Thus the atmospheric teleconnection pathway and ultimate negative AO mode modulation that occurs in response to a Siberian snow forcing is not produced for a comparable North American snow forcing. This modeling result provides additional confirmation that Siberia is a critical region for producing the snow – winter AO mode statistical relationship found in the observational record.

Figure 6-6b instead shows a weak positive AO index anomaly appearing in the late autumn troposphere and gradually intensifying over time, which suggests that a North American snow forcing may actually result in a slight positive AO mode response. This unexpected result for NA is counter to both the observed snow – AO mode relationship and the physically-based pathway described for SIB. Figure 6-7 shows the winter sea level pressure (SLP) field response to snow for SIB and NA. The response to Siberian snow (Fig. 6-7a, repeated from Fig. 4-7f) clearly resembles a negative AO pattern. The response to North American snow (Fig. 6-7b) is somewhat reminiscent of a positive AO pattern, though it is weaker and not as well formed. The high-latitude anomaly is much weaker in Figure 6-7b, and the mid-latitude anomalies are not as broad. Note that the positive SLP anomaly over North America in Figure 6-7b is a direct local response to the snow forcing, which generally occurs later in the season for NA than for SIB.

These results for NA are analogous to the results for the ORO experiments presented in Chapter 5, in which the Siberian snow forcing is applied to a modified GCM in which mountains adjacent to Siberia are removed as model boundary conditions. Since the Siberia stationary wave train is generated in part by these orographic barriers (Plumb 1985), their removal results in a substantially diminished wave train. Consequently the snow-forced upward WAF anomalies are weaker, and unable to propagate to the stratosphere and weaken the polar vortex. The diminished Siberia wave train in ORO results in a weakened local upward WAF anomaly, while the lack of a co-located wave train in NA results in no local upward WAF anomaly. In either case, the polar vortex does not weaken, the teleconnection pathway is interrupted, and a negative winter AO mode anomaly does not form.

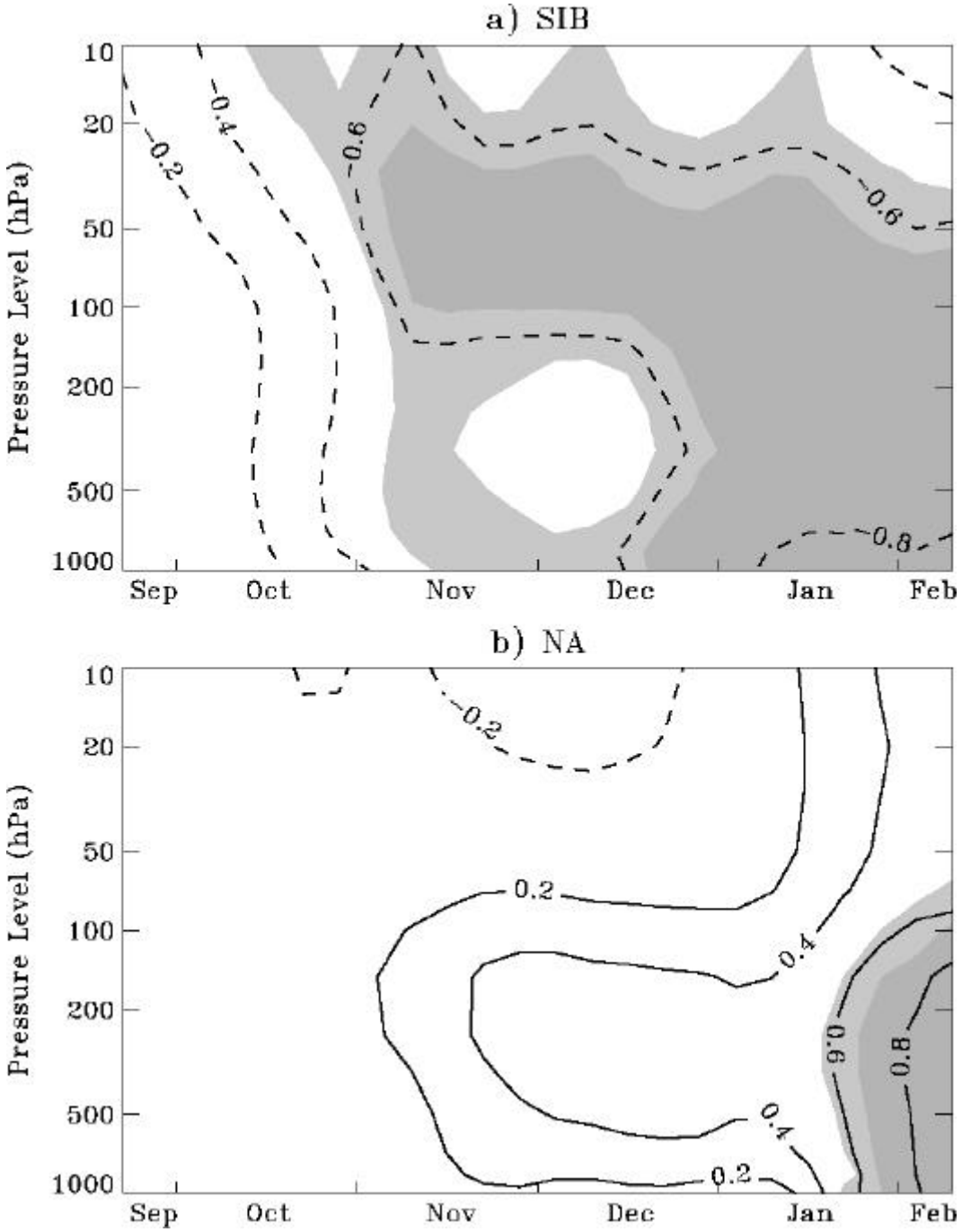

Figure 6-6: Weekly evolution (horizontal axis) over the atmospheric column (vertical axis) of normalized 42-day moving average hemispheric AO index response to positive snow forcing. Contours drawn at ± 2, 4, 6, 8 standard deviations. Dashed line denotes negative contour value. Light (dark) shading indicates 90% (95%) statistical significance. a) SIB. b) NA.

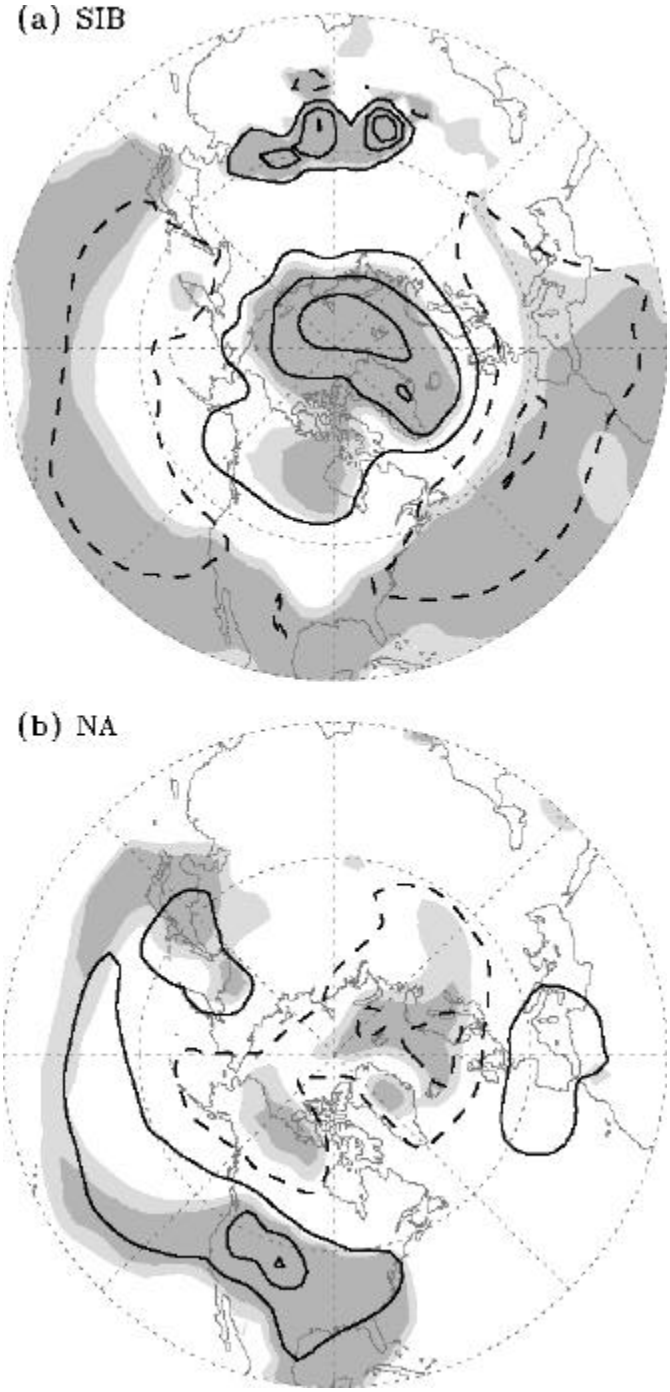

Figure 6-7: Winter (DJF) sea level pressure response to positive snow forcing, over the extratropical Northern Hemisphere. Contours drawn at ± 1, 3, 5 hPa. Dashed line denotes negative contour value. Light (dark) shading indicates 90% (95%) statistical significance. a) SIB. b) NA.

Chapter 5 also describes a weak positive AO response for ORO, whereupon it was suggested that the modest snow-forced input of stationary wave activity over Siberia simply results in a hemispheric-scale enhancement of the prevailing equatorward wave activity throughout the troposphere. The equatorward wave flux produces a poleward momentum flux, which results in dipole mean flow anomalies indicative of a positive AO mode response.

A similar interpretation can be made for NA, whereby the snow-forced diabatic heating anomaly over North America translates into a modest enhancement of the two stationary wave trains, in particular their prevailing upward and equatorward components. The upward enhancement is indicated in Figure 6-4b by weak upward WAF anomalies in the vicinity of these wave trains. The equatorward component is indicated in Figure 6-8, which shows the zonally averaged, time vs. pressure level profile evolution of 42-day average meridional WAF response, for NA. As for ORO, the enhanced wave trains are manifested as a hemispheric-scale equatorward anomaly that begins in mid-autumn and continues through the winter season. This enhancement of the prevailing equatorward tropospheric stationary wave activity, and the associated poleward momentum flux, is likely responsible for the positive AO mode response produced by NA.

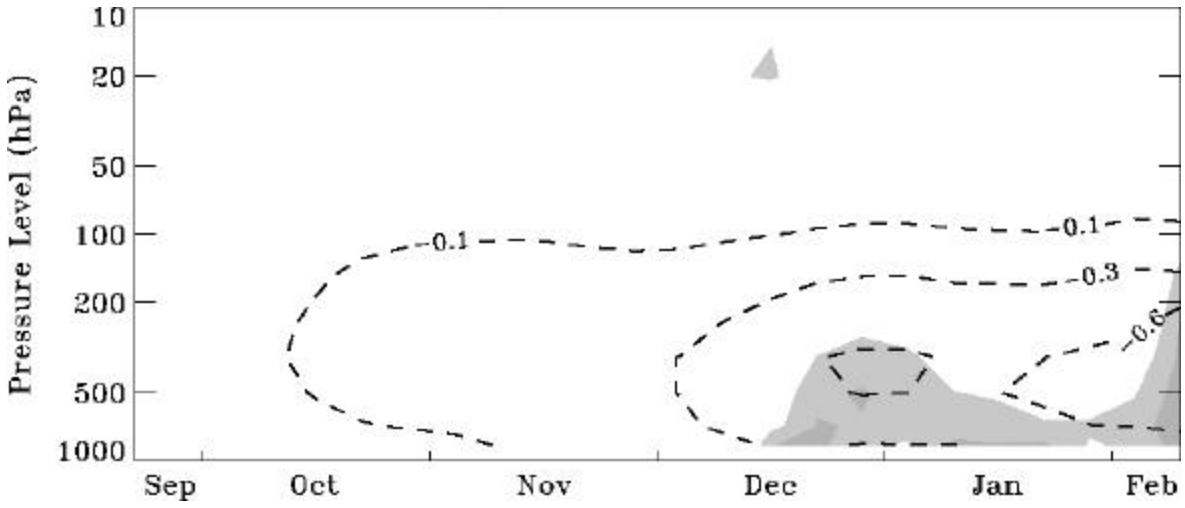

Figure 6-8: Weekly evolution (horizontal axis) over the atmospheric column (vertical axis) of meridional wave activity flux response to positive North American snow forcing (NA). Contours represent 42-day moving average, over the extratropical (36.5N-81N) Northern Hemisphere, drawn at ± .1, .3, .6, .9 m^2s^{-2}. Dashed line denotes negative (equatorward) contour value. Light (dark) shading indicates 90% (95%) statistical significance.

6.3 Discussion

The modeled relationship between early season land surface snow anomalies and modulation of the winter AO mode is facilitated by the co-location of the local snow anomaly within a region of strong prevailing stationary wave activity. The two dominant stationary wave trains in the Northern Hemisphere are centered over far-east Asia and the North Atlantic. For SIB, the snow-forcing region is co-located with the Siberia stationary wave train, so that the local diabatic heating anomalies associated with the snow forcing strengthen this wave train, producing upward WAF anomalies that initiate a physically-based teleconnection pathway. For NA, the snow-forcing region is not co-located with a stationary wave train, so there is no mechanism by which local WAF anomalies can develop and propagate upwards. Consequently, a negative AO mode response to snow is not produced for NA.

Instead, a modest upward and equatorward enhancement of the two tropospheric wave trains occurs for NA, which appears to result in a slight positive AO mode response to North American snow forcing. As for ORO, the physical mechanisms behind this apparent and unexpected response are not clear, such as the means by which the diabatic heating anomaly over North America enhances the wave trains located outside of the snow-forcing region. As mentioned in Chapter 5, it is quite possible that the positive AO response for NA is due to model biases, stemming from the model's overestimation of the equatorward component of climatological stationary wave activity flux. Another possibility is that the response has nothing to do with the snow-forcing, and simply arises from random fluctuations in the internal AO mode. However, the equatorward WAF anomalies first form in mid-autumn, just prior to the positive AO mode formation, for both NA (Fig. 6-8) and ORO (Fig. 5-10). This result argues against a random fluctuation. Additional research efforts involving Rossby wave dynamics are required to confirm or refute this apparent and unexpected positive winter AO mode response to North American snow forcing.

Chapter 7

Relative Impacts of Surface Thermodynamic Processes

7.1 Motivation

Most of the literature on climate modulation by land surface snow focuses on the dramatically higher albedo of snow-covered vs. snow-free land as the principal thermodynamic forcing mechanism. The decreased absorption of incoming solar radiation in the presence of snow is understood to result in lower surface temperatures. However, other thermodynamic mechanisms can also contribute to the surface temperature decrease, such as increased thermal emissivity, decreased thermal conductivity, and increased latent heat flux via snowmelt (Cohen 1994). These additional surface processes relate to the insulating properties of snow, and are affected by the depth as well as the presence of the snowpack. It is reasonable to assume that continental-scale interannual snow anomalies are characterized by varying snow depths as well as snow cover extents. Therefore the assertion that surface albedo is the dominant snow-forced thermodynamic mechanism may not be justified.

The experimental design developed in Chapter 2, and the snow forcing methodology developed in Chapter 4, allows for an explicit comparison of snow cover/albedo vs. snow depth/insulation with respect to winter climate. It was acknowledged in Chapter 4 that the snow cover forcing applied in the SIB experiments occurs primarily during autumn months (Fig. 4-4), whereas the snow depth forcing occurs throughout the autumn-winter model integration period (Fig. 4-6). In this chapter additional GCM experiments will be presented, in which only the snow cover or snow depth forcing is applied over Siberia, to evaluate the relative effect of these partial snow forcings and their related surface thermodynamic processes on the winter AO mode.

7.2 Snow Cover / Surface Albedo

7.2.1 Description of Experiments

A pair of snow-forced ensemble experiments is performed, analogous to the SIB experiments in Chapter 4. The principal difference is that the snow cover forcing is applied, but not the snow depth forcing is not. In this way the albedo change associated with snow cover is incorporated into the experiment, but the insulation changes associated with snow depth are minimized. The climate response to a positive Siberian snow forcing for this snow cover only, albedo dominated experiment is denoted as ALB.

Figure 7-1b shows the snow depth timeseries for a gridcell in central Siberia, for ALB. For comparison, the corresponding timeseries for SIB is shown in Figure 7-1a (repeated from Fig. 4-5). For ALB, wherever snow cover exists as dictated by each experiment's respective time period from the NOAA visible satellite snow cover dataset, the snow depth is prescribed at the climatology values obtained from the CTRL simulation. In other words, the temporal shift of the gridcell snow depth climatology applied in SIB is omitted in ALB. In cases where the high snow experiment calls for snow cover, but the climatology indicates either no snow or shallow snow (i.e., less than 2.51 cm SWE), a depth of 2.51 cm SWE is prescribed. This value represents a minimum snow depth for the high snow experiment, and was selected to ensure a thermodynamically active snow layer based on the ECHAM3 snow parameterization scheme. SWE values used by the model are converted to snow depth in Figure 7-1 using a snow density of 300 kg/m^3 (see Chapter 2). In cases where the low snow experiment calls for no snow, but the climatology indicates snow cover, a depth of zero is assigned.

In this way, a snow forcing occurs only when the high snow experiment is snow covered (high albedo) while the low snow experiment is not (low albedo). Thus the partial snow forcing in ALB only occurs during the early stages of the snow season, as indicated in Figure 7-1b. Later in the season, when both the high snow and low snow experiments are snow-covered, snow depths are identical so the snow forcing ceases. This is in contrast to SIB, where earlier snow is consistently associated with deeper snow, so that a snow forcing occurs via insulation processes throughout the model integration, as indicated in Figure 7-1a.

7.2.2 Results

Figure 7-2 shows the autumn (SON) and winter (DJF) surface response to a positive Siberian snow cover only, albedo-dominated forcing (ALB), for albedo, temperature and SLP. This figure can be compared against the corresponding response fields for SIB shown in Figure 4-7. Despite the lack of snow depth forcing, the autumn season (Fig. 7-2a,b,c) exhibits the expected local surface response to a positive snow forcing. This confirms that the solar reflectivity associated with snow cover is an important contributor to the local climatic response to snow. The local albedo response for ALB and SIB are nearly identical, since ALB incorporates the snow cover/albedo forcing. For temperature and SLP however, the magnitude of the response for ALB is less than that for SIB. This

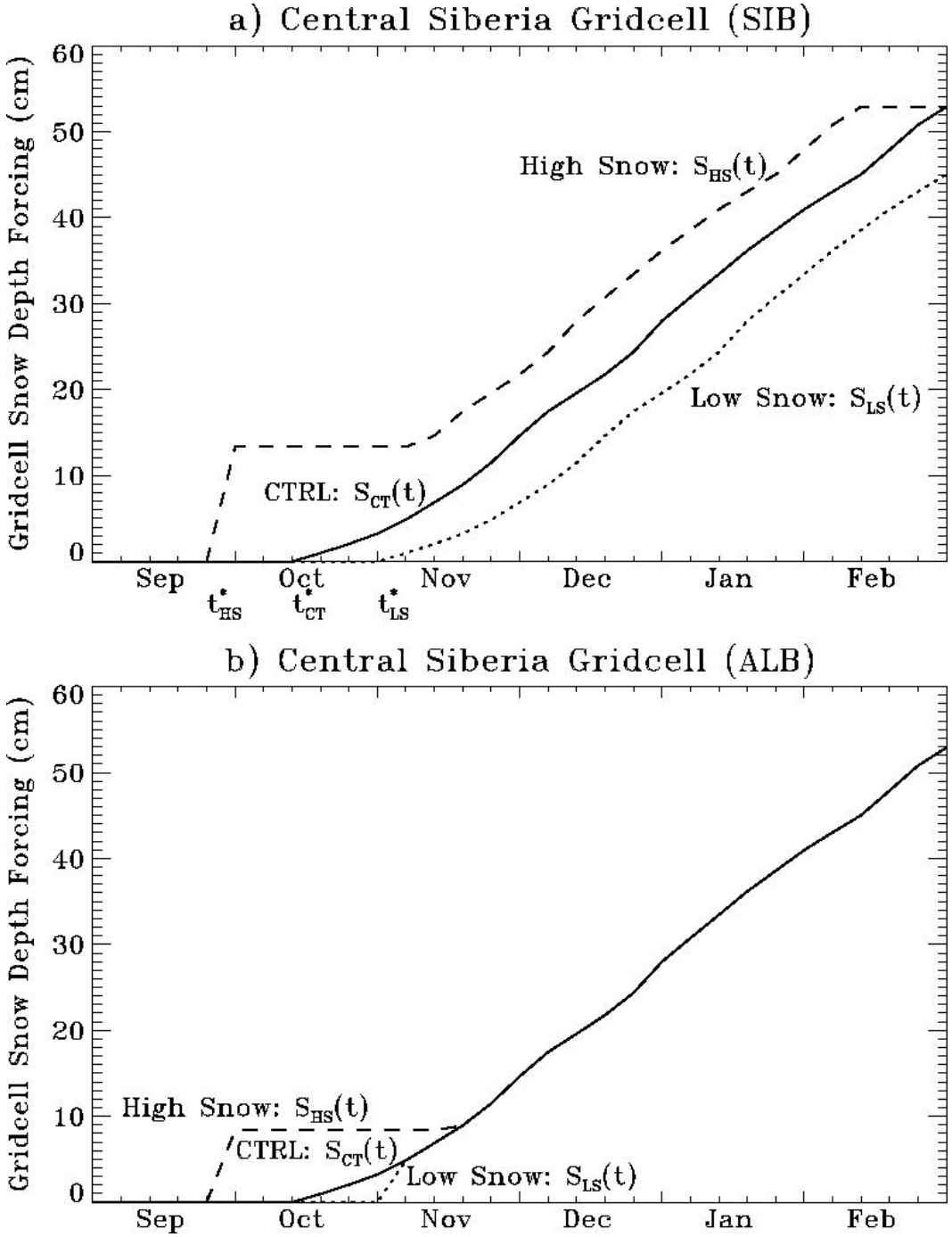

Figure 7-1: Snow forcing timeseries applied at a gridcell in central Siberia, for a) SIB and b) ALB. Dashed (dotted) line represents high (low) snow experiments. Also shown is the snow depth timeseries for the CTRL simulation (solid line).

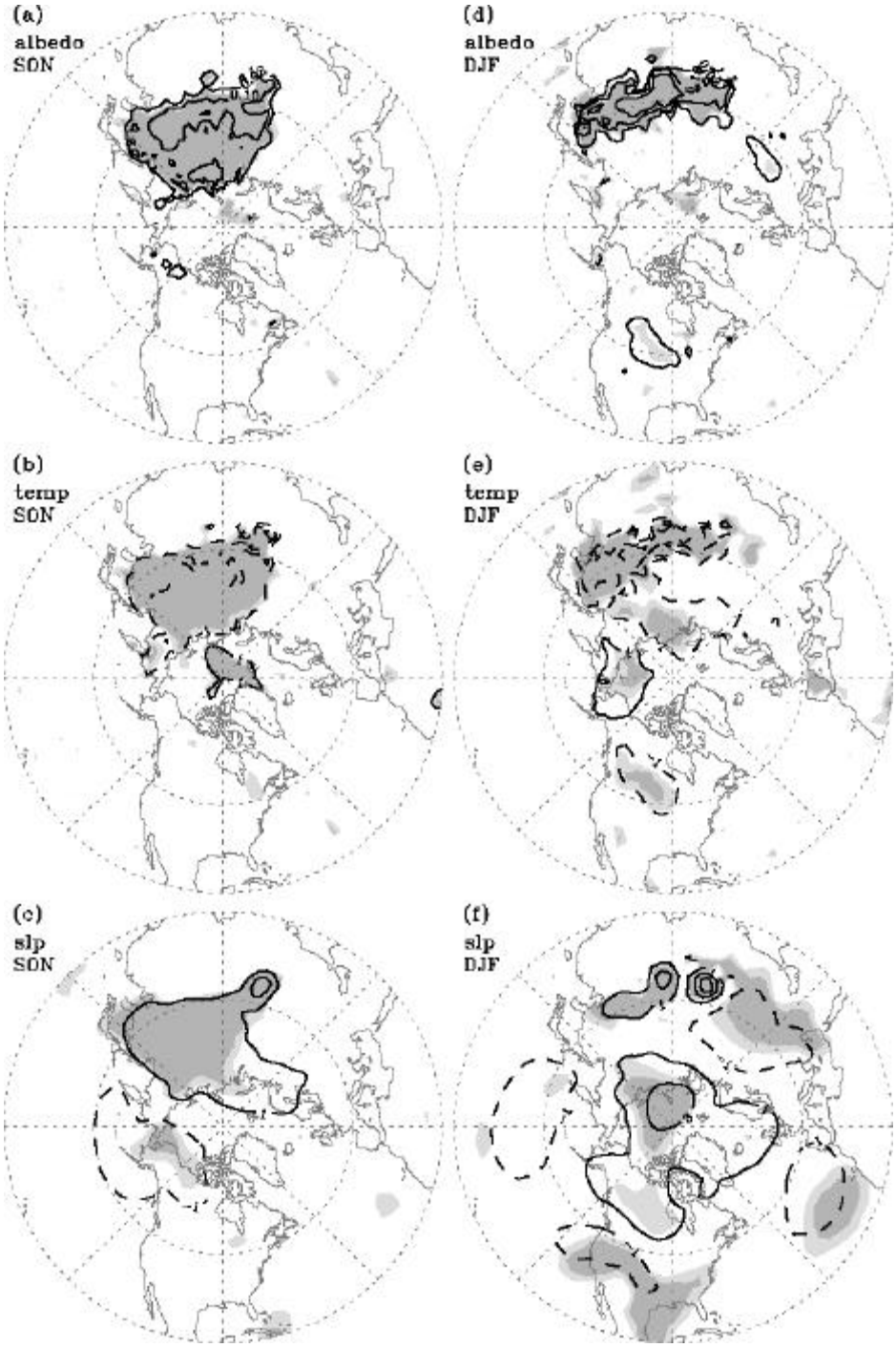

Figure 7-2: Surface climatic response to positive Siberian snow cover forcing (ALB), over the extratropical Northern Hemisphere, for autumn (a-c) and winter (d-f) seasons. Surface albedo (a,d) contours drawn at ± 0.02, 0.1, 0.25. Surface temperature (b,e) contours drawn at ± 1, 3, 5 °C. Dashed line denotes negative contour value. Sea level pressure (c,f) contours drawn at ± 1, 3, 5 hPa. Light (dark) shading indicates 90% (95%) statistical significance.

indicates that snow depth/insulation processes, excluded from ALB, are also important contributors.

During the winter season (Fig. 7-2d,e,f), the local albedo and temperature response for ALB is again consistent with expectations but weaker compared to SIB. The winter SLP response field somewhat resembles the negative AO mode as seen for SIB, but the centers of action are noticeably weaker, and the mid-latitude anomalies are also much less coherent. Thus when only snow cover forcings are applied over Siberia, the subsequent winter climate mode response is diminished considerably. Elements of the teleconnection pathway identified for SIB will now be evaluated for ALB to ascertain the precise cause of this diminished climate response.

Figure 7-3 shows the vertical wave activity flux (WAF) response to snow cover at 850 hPa elevation during autumn (SON), for SIB (repeated from Fig. 4-12) and ALB. Whereas a clear snow-forced strengthening of the Siberia stationary wave train occurs for SIB, this strengthening is mitigated for ALB, due to the diminished local temperature response seen in Figure 7-2b. Since the Siberia wave train extends throughout the troposphere (see Chapter 4), this modest upward WAF anomaly can nevertheless propagate up along this wave train and reach the stratosphere.

Figure 7-4 shows the temporal evolution of the AO index response to snow over the atmospheric column, using the same unstandardized AO index metric applied in previous chapters. For ALB (Fig. 7-4b), a slight AO index decrease in the stratosphere appears in mid-autumn, indicative of a weakened polar vortex response to the snow-cover forced upward WAF anomaly seen in Figure 7-3b. However, this vortex anomaly dissipates almost immediately. A slight AO index decrease occurs throughout the troposphere in late-winter, consistent with the slight negative AO mode response seen in the winter SLP field (Fig. 7-2f). These two anomalies appear uncoupled, i.e., the early-season vortex response does not propagate down to produce the late-season AO mode response. In contrast, SIB (Fig. 7-4a, repeated from Fig. 4-16) indicates a very clear downward propagation and strong winter AO mode response.

This apparent disruption of the teleconnection pathway and subsequent winter AO response for ALB can be explained in part by the characteristics of the partial snow forcing. The albedo increase associated with the snow cover forcing leads to a sharp and almost immediate temperature decrease, and a rapid initialization of the teleconnection pathway. This is evidenced by the relatively early initial weakening of the polar vortex during mid-autumn shown in Figure 7-4b. However, the snow cover forcing is an inherently transient phenomenon; a given location is subject to a forcing only during times when the high snow experiment is snow covered and the low snow experiment is snow free. Once the low snow experiment becomes snow covered as well, the forcing ceases. As a result, the forcing occurs as a southward-migrating latitudinal band, located between the snowlines of the two experiments. No single location maintains an appreciable snow forcing throughout the model integration period. This transient snow cover forcing is insufficient to sustain the initial mid-autumn vortex weakening into the winter. Consequently the stratospheric anomalies dissipate, rather than building in strength and propagating down to yield a negative AO response.

The phase of the ultimate winter AO mode response that results for ALB is consistent with the causal relationship to Siberian snow identified earlier, i.e., a positive

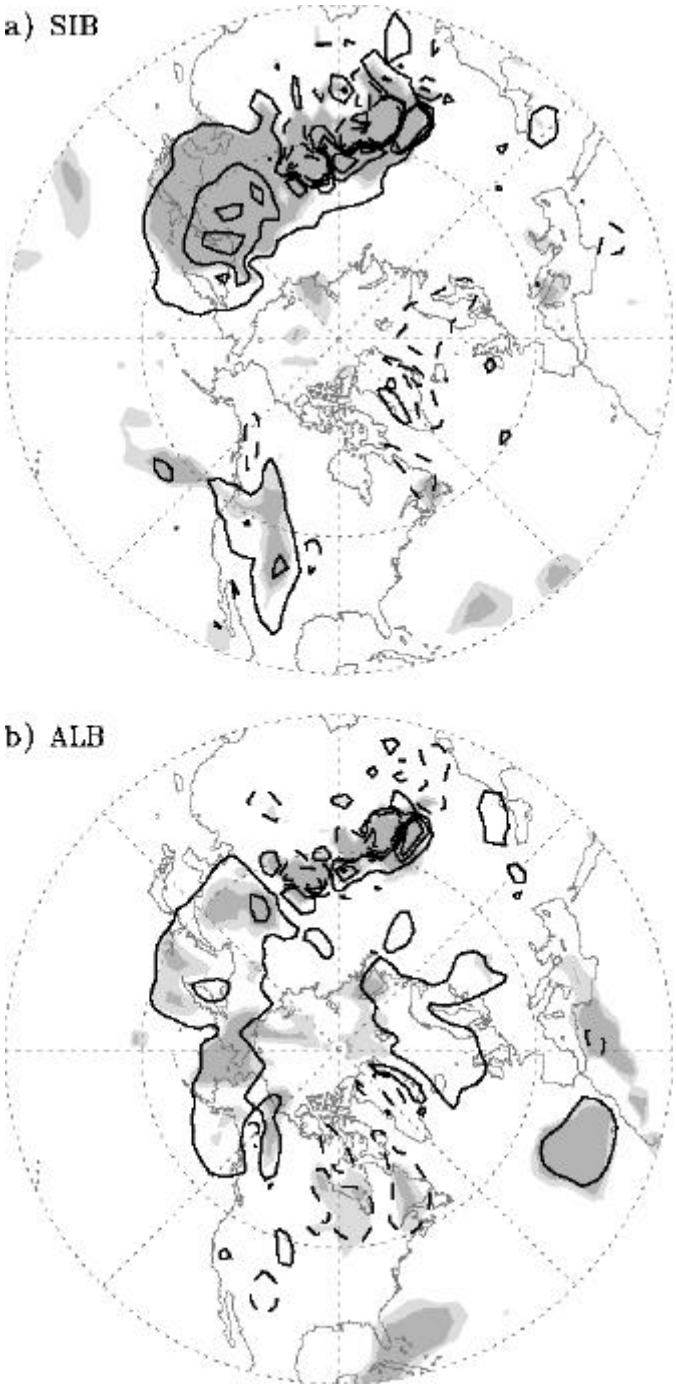

Figure 7-3: Vertical wave activity flux response to positive Siberian snow forcing, at 850 hPa elevation over the extratropical Northern Hemisphere, for autumn. Contours drawn at ± 0.01, 0.04, 0.08 m^2s^{-2}. Dashed line denotes negative contour value. Light (dark) shading indicates 90% (95%) statistical significance. a) SIB. b) ALB.

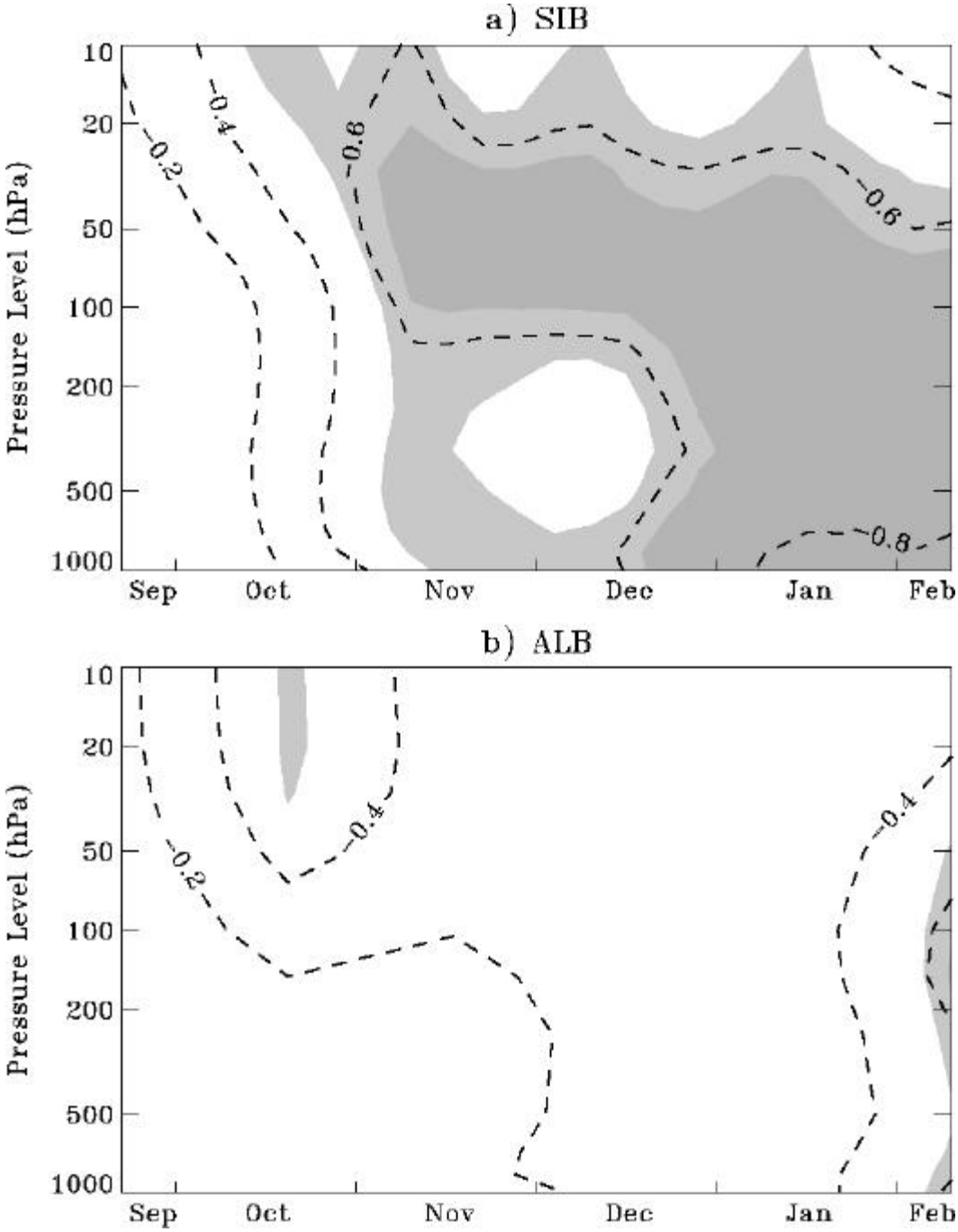

Figure 7-4: Weekly evolution (horizontal axis) over the atmospheric column (vertical axis) of normalized 42-day moving average hemispheric AO index (difference between the average SLP north of 61.5N and the average SLP within the zonal band from 28N to 50N) response to positive Siberian snow forcing. Contours drawn at ± 2, 4, 6, 8 standard deviations. Dashed line denotes negative contour value. Light (dark) shading indicates 90% (95%) statistical significance. a) SIB. b) ALB.

snow forcing leads to a negative AO mode response. However, the teleconnection pathway linking Siberian snow anomalies to the winter AO mode, rigorously established earlier, is apparently disrupted when snow depth anomalies and their associated insulation properties are neglected. Therefore the mild AO response for ALB shown in Figure 7-2f cannot be conclusively attributed to the Siberian snow cover forcing; in fact the disjointed nature of the SLP response field suggests that it may simply be due to random internal fluctuations. The results of the ALB experiments imply that the snow cover/albedo process is not the sole thermodynamic mechanism involved in hemispheric-scale, snow-forced climate modulation.

7.3 Snow Depth / Insulation

7.3.1 Description of Experiments

Once again a pair of snow-forced ensemble experiments is performed, analogous to the SIB experiments in Chapter 4. The principal difference this time is that the surface albedo is specified at the background (i.e., snow-free) value, for each gridcell in the Siberia forcing region and at every timestep. The snow cover and snow depth forcings themselves are unchanged from SIB. In this way, the large albedo difference associated with snow-covered vs. snow-free land is explicitly suppressed, leaving the insulating properties of the snowpack as the only thermodynamic mechanism associated with the snow forcing. At a given location, this forcing begins at the onset of snow for the high snow experiment, and the temporally shifted snow depth timeseries (Fig. 7-1a) ensure that a snow depth difference between the two experiments is maintained through the end of the simulation. The climate response to a positive Siberian snow forcing for this insulation only experiment is denoted as INS.

7.3.2 Results

Figure 7-5 shows the autumn (SON) and winter (DJF) surface response to a positive Siberian snow depth/insulation only forcing (INS), for albedo, temperature and SLP. Note that the albedo response fields (Fig. 7-5a,d) are negligible since albedo differences are explicitly suppressed for these experiments. Nevertheless, the autumn season exhibits the expected local surface temperature and SLP response to a positive snow forcing, although the magnitude is again less than for SIB. In fact, the response due to insulation properties shown in Figure 7-5b,c is roughly equivalent in magnitude to the response due to albedo properties shown in Figure 7-2b,c. This result demonstrates that insulation properties associated with snow depth, and albedo properties associated with snow cover, have a comparable effect on local climate. This result contradicts previous studies which asserted that albedo is the dominant thermodynamic mechanism.

During the winter season (Fig. 7-5e,f), the local surface response for INS is again consistent with expectations but weaker compared to SIB. The winter SLP response field for INS (Fig. 7-5f) resembles the negative AO mode, but the magnitude of the response is notably weaker than for SIB (Fig. 4-7f). When only snow insulation forcings are applied

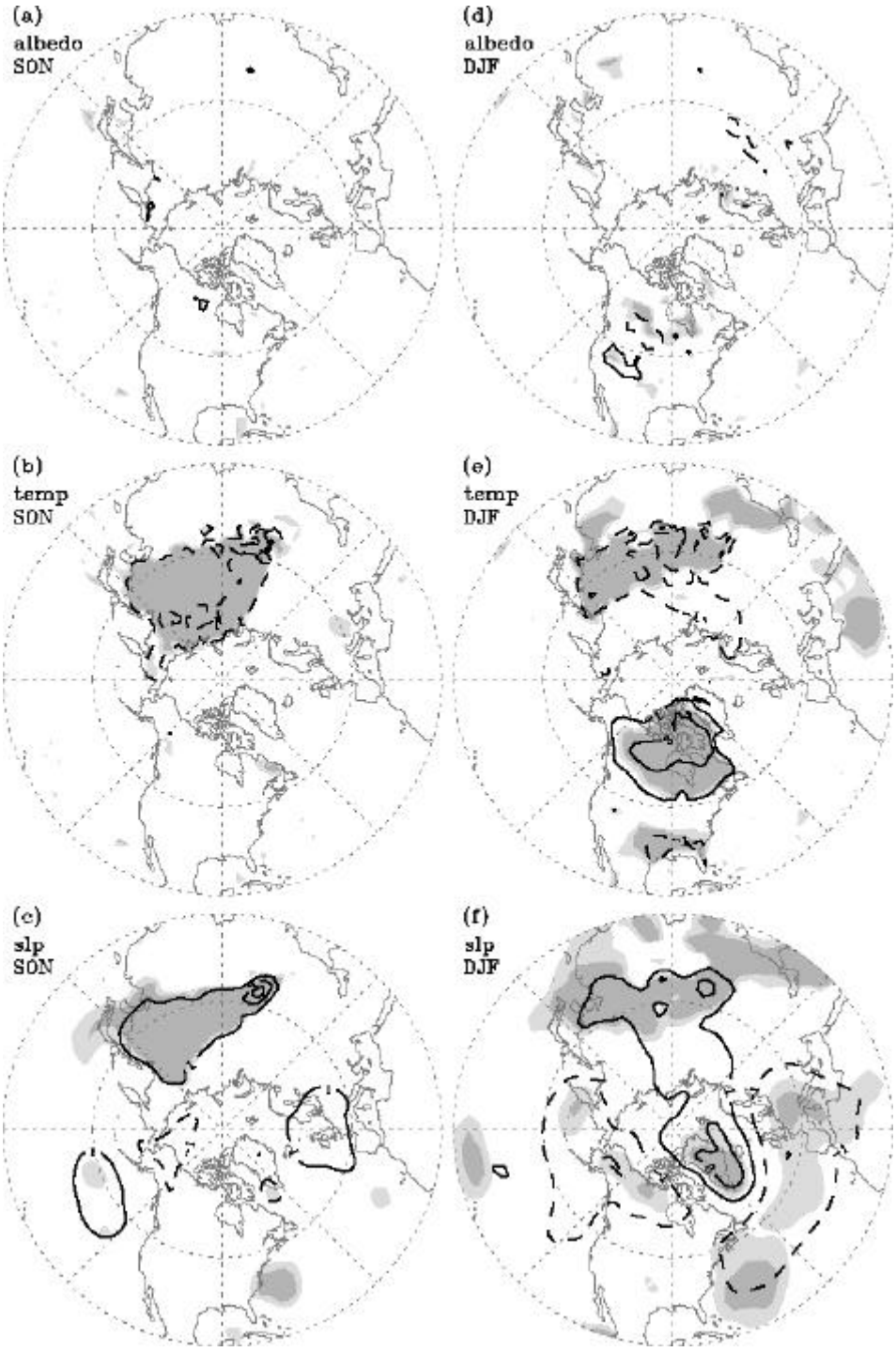

Figure 7-5: Surface climatic response to positive Siberian snow depth forcing (INS), over the extratropical Northern Hemisphere, for autumn (a-c) and winter (d-f) seasons. Surface albedo (a,d) contours drawn at ± 0.02, 0.1, 0.25. Surface temperature (b,e) contours drawn at ± 1, 3, 5 °C. Dashed line denotes negative contour value. Sea level pressure (c,f) contours drawn at ± 1, 3, 5 hPa. Light (dark) shading indicates 90% (95%) statistical significance.

over Siberia, the subsequent winter climate response is again diminished considerably. Thus neither the snow cover/albedo (ALB) nor the snow depth/insulation (INS) forcing acting alone is sufficient to produce the clear negative AO mode response seen when both processes act in conjunction (SIB).

Figure 7-6 shows the vertical wave activity flux (WAF) response to snow depth at 850 hPa elevation during autumn (SON), for SIB (repeated from Fig. 4-12) and INS. As is the case for ALB, the snow-forced strengthening of the Siberia stationary wave train is mitigated for INS, due to the diminished local temperature response seen in Figure 7-5b. These modest upward WAF anomalies can nevertheless propagate up to the stratosphere along the Siberia wave train. Figure 7-7 shows the temporal evolution of the AO index response to snow over the atmospheric column, using the same unstandardized AO index metric applied in previous chapters. For INS (Fig 7-7b), a clear AO index decrease develops in the early winter stratosphere (indicative of a weakened polar vortex), and begins to propagate down into the troposphere by late winter. This pattern is somewhat similar to the downward propagation seen for SIB (Fig. 7-7a, repeated from Fig. 4-16), although the initial vortex weakening occurs later in the season, and the downward propagation does not reach the surface. Overall, the downward component of the teleconnection pathway produced for INS is clearly weaker than that for SIB, although it is more prevalent than that for ALB.

In contrast to ALB, INS does not generate an abrupt initial temperature decrease, since the albedo response is artificially suppressed. The insulation processes associated with snow depth that are simulated generally do not influence surface temperatures as dramatically as the albedo process, therefore the teleconnection pathway is slower to initialize. This is evidenced by the relatively late initial weakening of the polar vortex during early winter shown in Figure 7-7b. However, the snow depth forcing is perpetual; at a given location the forcing begins when snow first arrives for the high snow experiment, and continues throughout the duration of the model simulation.

Although the magnitude of the initial forcing is weakened due to the suppression of the albedo process, the constant nature of the snow depth forcing over Siberia allows the weakened vortex to sustain itself during the winter months. Consequently, it begins to propagate down following the downward component of the teleconnection pathway, as indicated in Figure 7-7b. However, this propagation is unable to reach the surface and yield a fully formed negative AO mode response by the end of the model integration period, since the initial vortex weakening is delayed by the lack of a snow cover/albedo forcing. Thus when only snow depth/insulation processes are simulated, the teleconnection pathway appears to be partially disrupted, resulting in a weaker but reasonably coherent winter AO mode response to snow as seen in Figure 7-5f. The results of the INS experiments indicate that sustained thermodynamic forcings associated with snow depth/insulation processes are instrumental to hemispheric-scale, snow-forced climate modulation.

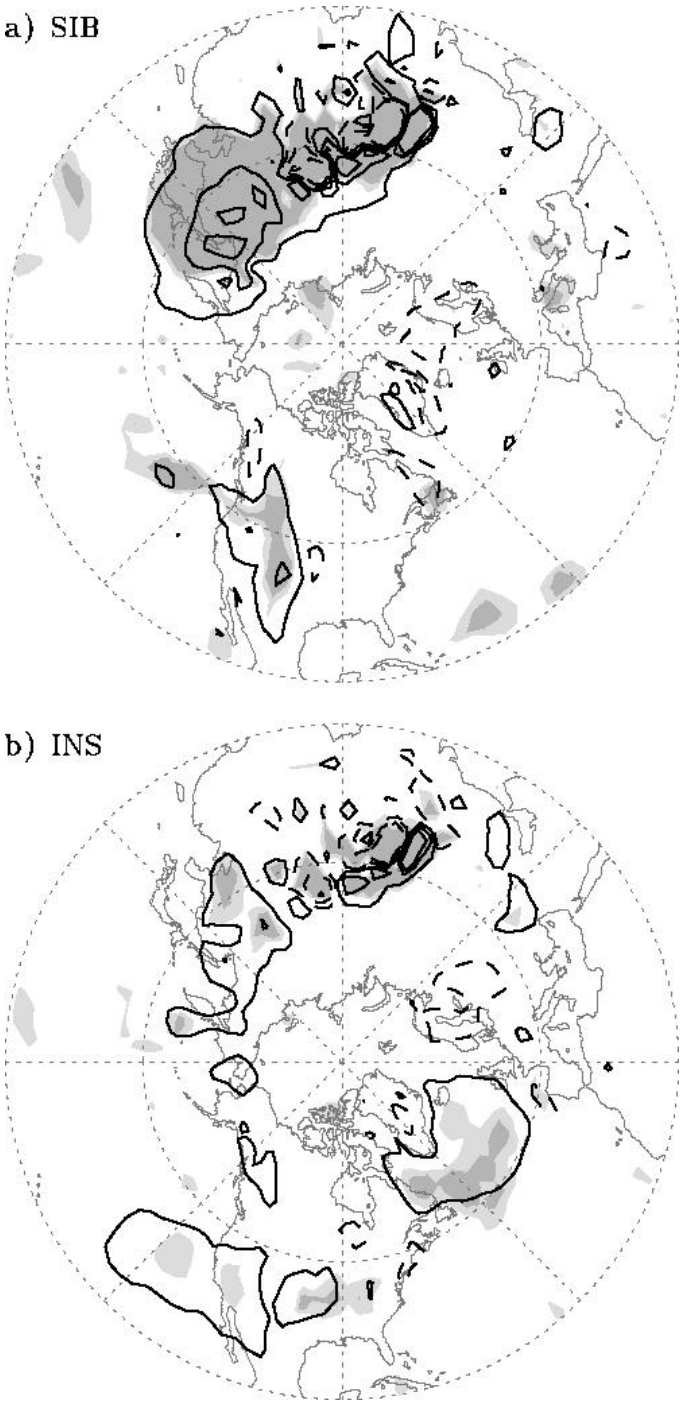

Figure 7-6: Vertical wave activity flux response to positive Siberian snow forcing, at 850 hPa elevation over the extratropical Northern Hemisphere, for autumn. Contours drawn at ± 0.01, 0.04, 0.08 m^2s^{-2}. Dashed line denotes negative contour value. Light (dark) shading indicates 90% (95%) statistical significance. a) SIB. b) INS.

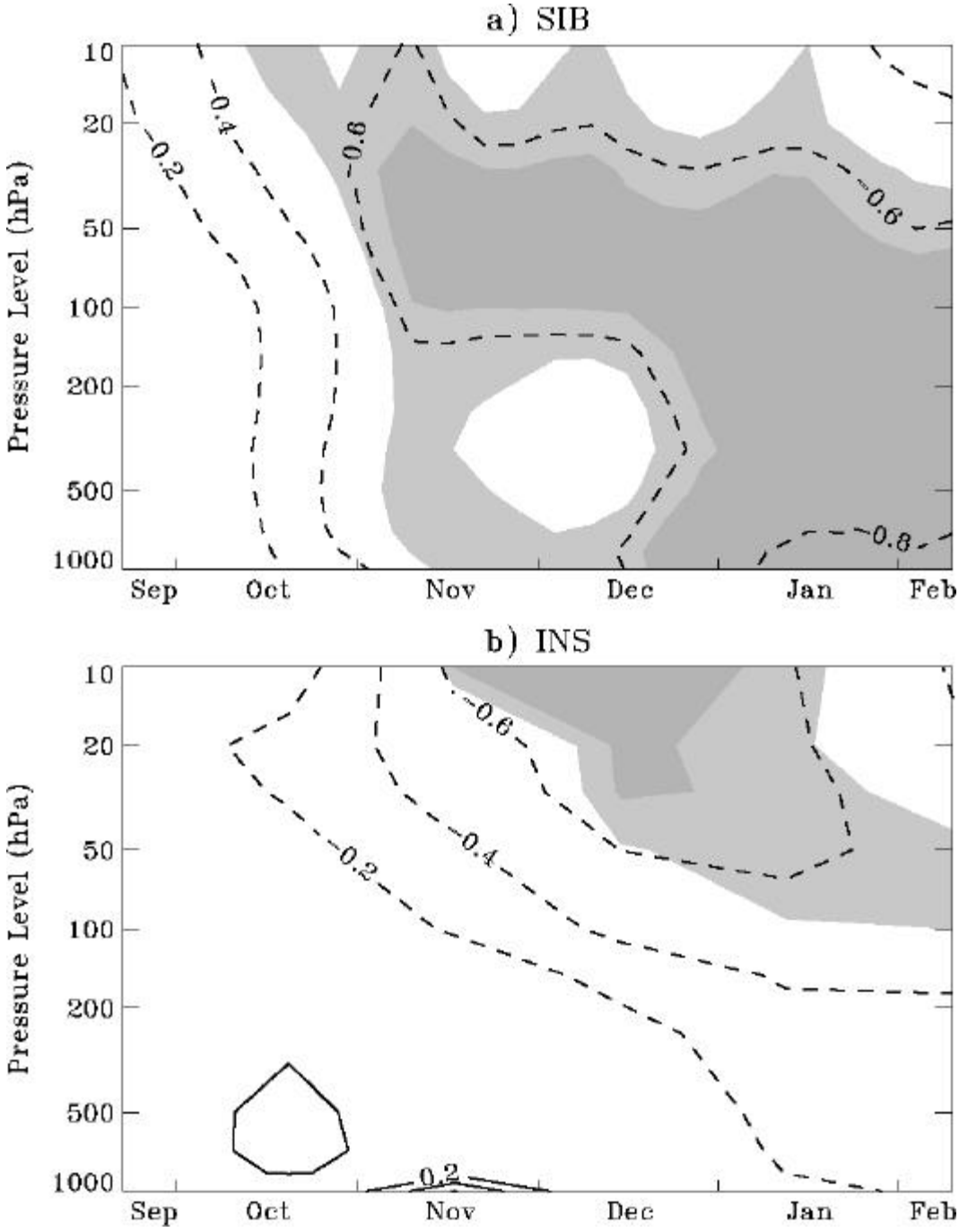

Figure 7-7: Weekly evolution (horizontal axis) over the atmospheric column (vertical axis) of normalized 42-day moving average hemispheric AO index (difference between the average SLP north of 61.5N and the average SLP within the zonal band from 28N to 50N) response to positive Siberian snow forcing. Contours drawn at ± 2, 4, 6, 8 standard deviations. Dashed line denotes negative contour value. Light (dark) shading indicates 90% (95%) statistical significance. a) SIB. b) INS.

7.4 Discussion

7.4.1 Local Climate Response to Partial Siberian Snow Forcings

The local surface climate response to various Siberian snow forcing conditions is summarized in Figure 7-8, which shows timeseries of anomalies due to a positive snow forcing (high snow – low snow), for model input snow depth, albedo and temperature, averaged over Siberia. In Figure 7-8a, the snow depth anomaly plotted for SIB and INS is simply the difference between the high snow and low snow curves presented earlier in Figure 4-6. A steady and rapid increase occurs in September and October, and a large snow depth anomaly is maintained for the duration of the simulation period. For ALB the magnitude of the snow depth anomaly is substantially reduced, due to the exclusion of snow depth forcings. Largest values occur in mid-autumn, when snow cover is most variable, then drop off as snow cover becomes more consistent and complete between the high snow and low snow experiments. Note that the residual anomaly during winter for ALB is due to the minimum snow depth of 2.51 cm SWE applied to the high snow experiment. Figure 7-8a clearly demonstrates the transient (perpetual) nature of the snow forcing for the ALB (SIB,INS) experiments.

The albedo response is shown in Figure 7-8b. INS exhibits no response, since the albedo processes are manually suppressed for this experiment. The albedo response is slightly larger for SIB than ALB, even though the additional forcings contained in SIB represent snow depth, which is typically associated with insulation processes and not albedo. This is due to the ECHAM3 GCM land surface parameterization, in which surface albedo is computed as an asymptotically increasing function of snow depth (see Chapter 2). Thus the ALB experiments capture most, but not all, of the albedo-related climate response to snow. Conversely, the INS experiments reflect primarily insulation processes, but also include albedo processes to a limited degree. Since the albedo varies very little for deep snow, the albedo process in INS is minimal during winter when the snowpack is deep.

The temperature response is shown in Figure 7-8c. The anomalies for ALB and INS are similar, and each represents roughly half of the total temperature decrease for SIB. Clearly, the local climate response to snow is not dominated by albedo processes as previously believed. Rather, albedo and insulation processes contribute equally to the overall snow-forced response. Thus snow depth and associated insulation processes, such as thermal emissivity, thermal conductivity and latent heat, should not be neglected when evaluating or predicting the local and remote surface climate response to snow.

It is important to recognize that the relative influence of snow cover/albedo and snow depth/insulation on surface temperature and hemispheric climate may vary with the GCM and land surface scheme used, and that these processes are still parameterized rather crudely in most models. This deficiency poses an ongoing challenge to the simulation of the local temperature response to snow in GCMs, which could in turn compromise the remote climate response. However, it is certainly reasonable to consider snow cover and snow depth perturbations together, since increased snow depth is generally associated with increased snow cover. Furthermore, the albedo and insulation

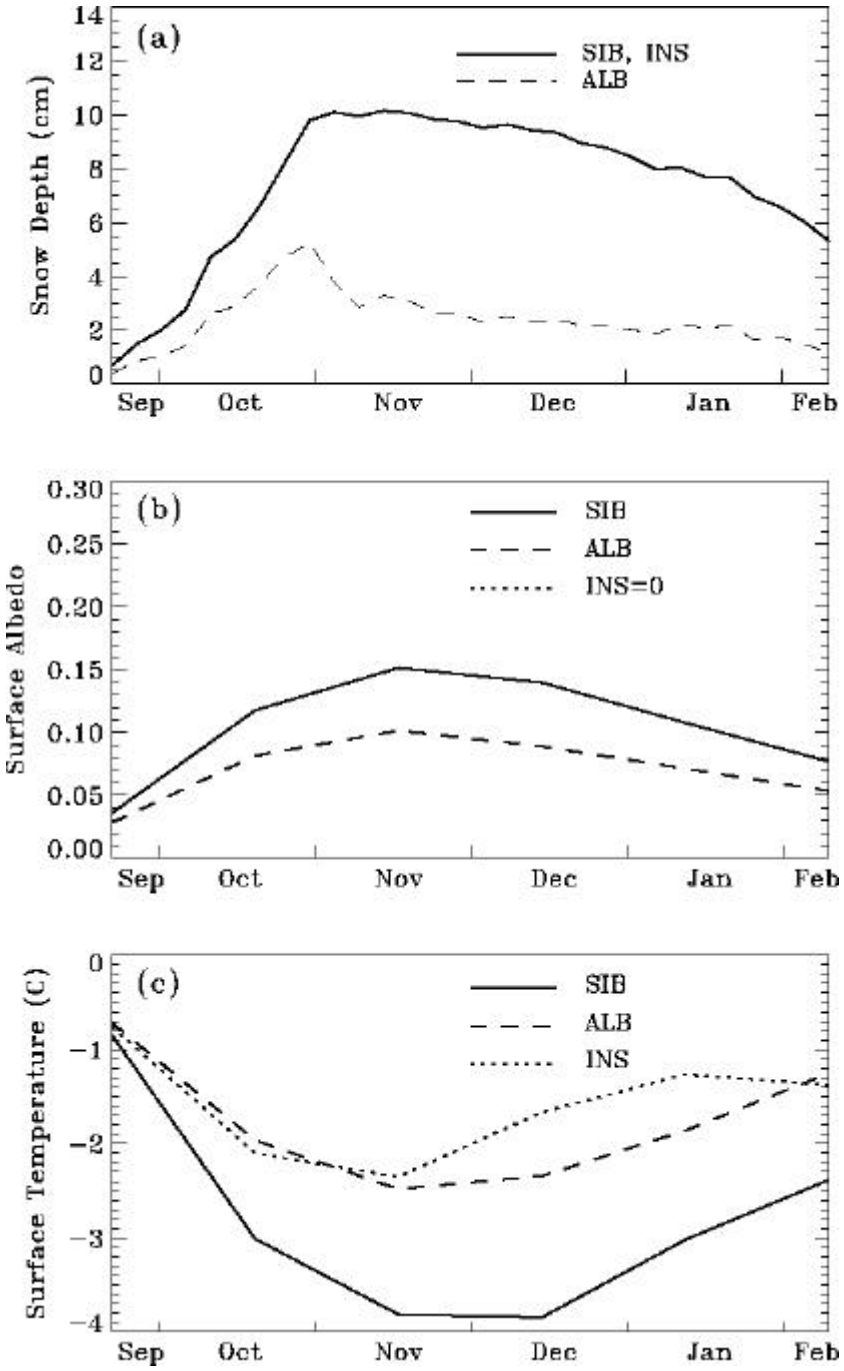

Figure 7-8: Timeseries of Siberia average anomalies for land surface parameters, due to a positive snow forcing (high snow – low snow), for SIB, ALB and INS. a) Model input snow depth. b) Surface albedo. c) Surface temperature.

processes act in the same direction, i.e., both produce a negative local surface temperature anomaly in response to increased snow forcing. Therefore the modeled local temperature response to snow may be reasonable and robust even if the individual surface thermodynamic processes are not parameterized precisely.

7.4.2 AO Mode Response to Partial Siberian Snow Forcings

In Chapter 4, the co-location of a snow-forced surface temperature anomaly within a region of major stationary wave activity was recognized as the key to the casual relationship established between Siberian snow anomalies and the winter AO mode. In Chapters 5 and 6, the importance of this co-location was investigated, by conducting experiments in which the snow forcing and associated local temperature response occurred in a region with reduced or minimal stationary wave activity. The absence of a strong wave train prevented WAF anomalies (produced locally by the temperature anomalies) from propagating up to the stratosphere and weakening the polar vortex. This effectively disrupted the snow – AO teleconnection pathway, and prevented the positive snow forcings from producing a negative winter AO mode response.

This chapter also investigates the importance of the regional co-location, but by reducing the snow-forced local temperature anomaly rather than weakening the stationary wave train. The ALB and INS experiments accomplish this local temperature anomaly reduction in slightly different ways, resulting in somewhat different climatic responses, although both experiments inhibit the ultimate negative winter AO mode response. The ALB experiment produces a rapid initial weakening of the stratospheric polar vortex, but the transient nature of the snow cover/albedo forcing inhibits the sustained formation of this stratospheric anomaly, effectively disabling its subsequent downward propagation. For INS, the restriction to snow depth/insulation processes essentially delays the weakened vortex response and subsequent downward propagation. For both experiments, the end result is a disruption of the teleconnection pathway, so that a negative AO anomaly does not fully form in response to these partial Siberian snow forcings and their diminished local temperature anomalies.

Both the snow cover and snow depth forcings need to act in concert to produce the required temperature anomaly and subsequent pathway response. The abrupt albedo change associated with the initial snow cover forcing is needed for the pathway to begin early enough to run its full course by the end of winter. The insulation processes associated with the sustained snow depth forcing is needed to maintain the pathway over the autumn-winter season. For SIB, the two partial snow forcings complement each other, producing a negative vortex anomaly that is sustained into the winter months, and which begins early enough for the subsequent downward propagation to develop into a fully formed negative AO mode response. Clearly, both the snow cover/albedo and snow depth/insulation processes are necessary for the causal relationship between Siberian snow and the winter AO mode to fully materialize.

Chapter 8

Conclusions

8.1 Original Contributions

In this thesis, a causal relationship has been established between Siberian snow anomalies and modulation of the dominant pattern of climate variability in the extratropical Northern Hemisphere, as represented by the winter AO mode. A GCM modeling study has been performed which explicitly isolates the mean climatic response to a realistic, observation-based snow forcing over Siberia. A positive snow forcing during the autumn – winter season is found to produce a negative winter AO mode response that accounts for roughly 30% of the observed AO mode variability. Furthermore, a seasonal teleconnection pathway has been identified, which describes precisely how regional-scale anomalies in Siberian snow conditions lead to hemispheric-scale variations in the winter AO mode. This pathway involves wave-mean flow interaction processes throughout the troposphere and stratosphere, consistent with both established theory and recent literature. The identification of such a physically-based pathway is important for a complete understanding of the snow – winter climate relationship, and to confirm that the relationship is real and not a chance or modeling artifact.

This research builds upon previous investigations of large scale climate modulation by land surface snow. An original contribution to this research field is the design and implementation of a focused GCM modeling study, specifically geared towards identifying snow-forced modulations of the fundamental, internally-varying mode of atmospheric variability described by the winter AO. Previous modeling studies of snow-forced climate modulation have generally been exploratory in nature, employing idealized conditions and/or small ensemble sizes, which preclude definitive conclusions from being drawn. This thesis improves upon these previous idealized GCM studies in a number of ways. First, realistic, observation-based snow boundary conditions are developed and applied, based upon historical visible satellite data. This helps to ensure that the modeled climatic response to snow is reasonable and applicable to the observed climatic response. Second, a large-ensemble modeling approach consisting of twenty independent realizations is employed, to distinguish snow-forced modulations of the AO mode from the naturally-occurring interannual variability associated with the AO mode.

Third, the snow forcing is limited to Siberia, a region which holds the greatest potential for snow-forced winter climate modulation.

The focused modeling investigation described in this thesis provides an important contribution to the overall effort to define a Siberian snow – winter AO mode relationship. The modeling results are generally consistent with statistical analyses that have been performed using observed long-term datasets. Both types of analyses have drawbacks, therefore an agreement between observational analyses and numerical modeling experiments is critical to building a more complete case. This research represents the most explicit and detailed modeling study to date in this field. Model results complement the extensive set of observational analyses that have been conducted, and therefore strengthens the argument for a viable winter climate response to snow anomalies over Siberia.

As discussed in Chapter 4, it is important to note that the teleconnection pathway that has been identified does not reveal any new processes with respect to atmospheric dynamics. Each element of the pathway is either drawn from established atmospheric wave-mean flow interaction theory, or has previously been documented in recent literature on troposphere – stratosphere coupling. The original contribution associated with this pathway identification involves the recognition that all of the elements are coherently linked to produce a negative winter AO mode response, and that the entire pathway is initiated by a realistic positive snow forcing over Siberia. As such, the pathway and ultimate AO mode response serves as a rare demonstration of hemispheric-scale climate dynamics being influenced by regional-scale land surface conditions.

Therefore, this thesis also contributes to the field of land surface – atmosphere interaction. This field of research typically investigates interactions at local or regional spatial scales, and during the warm season when soil moisture is the most crucial land surface parameter. The Siberian snow – winter AO relationship established here demonstrates land surface – atmosphere interaction at much broader continental and hemispheric scales. Furthermore, the interaction takes place outside of the warm season, when snow depth rather than soil moisture is the relevant land surface parameter. These results serve to expand the scope of recognized land surface – atmosphere interaction processes.

A final original contribution is the explicit identification of Siberia as a critical region for facilitating the snow – winter climate relationship. The combined geographic and orographic characteristics of Siberia are unique to that region. Siberia is a broad, contiguous land surface region subject to extensive winter snow but highly variable autumn snow. Furthermore, the major mountain ranges that border Siberia to the south and east produce a dominant stationary wave train spanning from central Siberia to the central North Pacific. As a result, local surface temperature anomalies that directly result from Siberian snow anomalies are regionally co-located within the major Siberia wave train. This unique co-location produces strong local upward WAF anomalies, which are necessary to initiate the teleconnection pathway and ultimately result in a negative winter AO mode response to snow. The suite of modeling experiments conducted for this thesis demonstrate that these conditions are unique to Siberia, which confirm that it is a critical region for enabling the teleconnection pathway.

8.2 Research Limitations

Even though this thesis presents a rigorous modeling study of the Siberian snow – winter AO relationship, there are nevertheless limitations associated with the modeling approach and research results. As for any GCM modeling study, results may be model specific, since the mathematical simulation of the atmospheric system has yet to evolve to a point where model results are robust and consistent across all GCMs. Thus the teleconnection pathway and ultimate negative AO response using ECHAM3 GCM, which amounts to roughly 30% of the observed AO mode variability, may be exaggerated, suppressed, or otherwise imprecise compared to other models.

Some of the acknowledged weaknesses of ECHAM3 and the modeling approach described in Chapter 2 suggest that the model may in fact be underestimating the winter AO response to Siberian snow. For example, a critical component of the vertical teleconnection pathway involves the propagation of stationary wave activity into the stratosphere, and subsequent weakening of the polar vortex. However, the stratosphere is poorly resolved in ECHAM3, with only four of its nineteen vertical layers centered above 100 hPa, and only seven layers above 200 hPa. The poor stratospheric resolution may dampen the polar vortex anomalies that occur in response to Siberian snow forcings, which subsequently may inhibit the downward propagating hemispheric mean-flow anomalies that make up AO mode response. A GCM with a fully-resolved stratosphere may result in a more responsive polar vortex, and produce larger snow-forced AO mode anomalies which are closer in magnitude to observations.

Similarly, the cartesian gridcell resolution of roughly 2.8º latitude by 2.8º longitude is adequate for resolving hemispheric-scale atmospheric patterns, but it necessarily results in a dampening of the land surface orography. As an example, the peak ECHAM3 surface elevation within the region of Siberian mountain removal for the ORO experiments (Fig. 5-1b) is 1176 m. For the NOAA 5-minute gridded elevation data (Fig. 5-1a), the corresponding peak elevation is 2377 m, about twice as high. The stationary wave train over Siberia, critical to the upward propagation of snow-forced WAF anomalies into the stratosphere, is forced to a large extent by the regional orography. Using a finer gridcell resolution would have a more accurate model orographic boundary, which would likely strengthen the Siberia wave train, produce larger snow-forced WAF anomalies, and result in a stronger ultimate AO mode response.

Another limitation of this research work is the utilization of only the highest and lowest snow conditions from the observational record for model forcings. A substantial AO mode response is produced for this realistic but extreme forcing condition; however no insight has been gained regarding the linearity or robustness of the response over a range of observed snow anomaly conditions. Such an extreme forcing analysis was conducted with the specific aim of establishing the viability of the Siberian snow – winter AO relationship, and identifying the physical mechanisms and pathways involved. As discussed in the following section, a logical next step is to conduct a more comprehensive long-term modeling experiment, forced by the entire available Siberian snow record.

Finally, some specific details regarding stationary wave energy propagation still need to be clarified. In particular, it is unclear how the moderate regional influx of snow-forced upward wave energy, produced by the ORO and NA experiments, translate into a

hemispheric-scale enhancement of prevailing wave activity in the troposphere, without the aid of the stratosphere as seen for SIB. Furthermore, the specific relationship between the vertical extent of WAF anomaly propagation and the strength of the prevailing stationary wave train is still uncertain, i.e., it is unclear exactly how a weakened wave train precludes snow-forced upward WAF anomalies from reaching the stratosphere (Plumb 2003). A detailed analysis of the Rossby wave dynamics simulated by the model is required to address this limitation.

8.3 Recommendations for Future Research

8.3.1 Seasonal Climate Prediction

As discussed in Chapter 1, the motivation behind this research is an improved understanding of the causes of wintertime interannual climate variability in the extratropical Northern Hemisphere, and its application towards improved seasonal climate predictions. Incorporation of the Siberian snow – winter AO causal relationship described in this thesis may prove useful to current and future generations of climate prediction algorithms. The viability of using snow as a winter climate predictor was first demonstrated in Cohen and Entekhabi (1999), which found a statistically significant interannual correlation of 0.71 between observations of autumn snow cover over Eurasia and the winter AO mode. This thesis has specified Siberia as the critical region for producing this correlation, by identifying physical mechanisms and demonstrating a lack of response for snow anomalies in other regions. This new information can be incorporated to develop new and improved indices derived from regional autumn snow conditions, to yield a stronger statistical relationship with the winter AO mode. Updated indices may rely specifically on Siberian snow conditions, the difference between Siberian and North American snow conditions, and/or snow depth as well as snow cover anomalies. Future research efforts could fully explore these possibilities to evaluate whether an improved index can be developed for predicting the winter AO mode.

8.3.2 AO Response to Greenhouse Gas Forcing

In addition to improving seasonal climate prediction, the results of this research can potentially contribute to current research on recent AO trends and their association with anthropogenic climate change. An upward trend in the winter AO index has been observed over the past 25 years; it has been suggested that this trend is due at least in part to increasing greenhouse gas concentrations over this same period (Corti et al. 1999; Thompson et al. 2000). A number of GCM simulations report an increasing AO index trend in response to increased CO_2 forcings, though the modeled trend is generally less than the observed trend (Shindell et al. 1999; Gillett et al. 2002). These models also report a stronger polar vortex and equatorward tropospheric wave refraction as part of the greenhouse gas-forced response.

It is possible that the snow – AO relationship plays a role in the apparent greenhouse gas – AO trend. Increased CO_2 is understood to lead to warmer surface

temperatures, from which a decrease in snowfall and snow cover can reasonably (though not irrefutably) be expected. Such a negative snow anomaly over Siberia would likely initiate the pathway described in this thesis, but with the signs reversed. Namely, a stronger vortex, equatorward stationary wave refraction, and an increased winter AO would result, which is consistent with the climate response produced by the greenhouse gas-forced experiments.

Furthermore, an acknowledged weakness of GCMs is an underestimation of the interannual variability of continental-scale snow. If Siberian snow is indeed an integral component of the greenhouse gas – AO relationship, then incorporation of observed snow conditions in place of internal model-generated snow conditions should enhance this relationship (Baldwin 2002). As a result, the aforementioned model studies on greenhouse gas-forced AO trends may lead to an improved simulation of the observed trend. Future research efforts could re-interpret the results of these studies with respect to snow anomalies over Siberia, and if warranted repeat the experiments with the addition of observed Siberian snow conditions.

8.3.3 Long-Term Simulation Experiment

The focused modeling study performed for this thesis has successfully demonstrated a clear, physically-based winter climate response to extreme high vs. low Siberian snow anomalies, using a well-regarded atmospheric GCM. To verify the robustness of this result, future research efforts could investigate the climatic response to a range of Siberian snow anomalies, using a different GCM. This can best be achieved by performing a long-term (multi-year) simulation, large-ensemble experiment, in which a history of Siberian snow depths over all seasons, based on the entire observational record, is prescribed throughout the simulation period. The positive results presented here using an efficient and flexible modeling approach suggest that a comprehensive but more computationally expensive long-term simulation would be worthwhile.

Such an experiment would discern the linearity of the response to positive vs. negative snow anomalies, and the robustness of the response to anomalies of varying magnitude. In addition, an explicit predictability analysis could be performed to distinguish internally generated vs. externally forced variability in the winter AO signal, and assess the potential for improving seasonal climate forecasts. Finally, the inclusion of spring and summer seasons in the simulation would facilitate the investigation of two-way snow-climate coupling over all seasons, which is an emerging area of research (Saito and Cohen 2003). The GCM that is employed should improve upon the acknowledged weaknesses of ECHAM3 as used in this thesis, namely the stratosphere should be better resolved and a finer Cartesian grid resolution should be employed.

8.3.4 Atmospheric Wave Dynamics

Troposphere – stratosphere coupling and the role of both stationary and transient waves in their interaction is a rapidly evolving research area. A consensus characterization of coupled troposphere – stratosphere winter circulation as it relates to the AO mode has yet

to be reached by the atmospheric science community. The teleconnection pathway described in Chapter 4 is consistent with much, though certainly not all, of the current literature. As stated above, some of the features associated with the snow-forced stationary wave propagation are still ambiguous. Future research efforts could investigate these pathway features within the context of atmospheric dynamics, utilizing metrics and analyses specifically developed to study Rossby wave mechanics. It is hoped that the identification of surface snow anomalies as an initiator of previously recognized atmospheric pathway components will shed light on the precise dynamical processes involved in the coupled variability of the troposphere-stratosphere system.

8.3.5 GCM Snow Parameterization

It is commonly believed that the increase in surface albedo due to snow cover is the principal mechanism for snow-forced local climate variability. Chapter 7 demonstrates that in fact snow depth and associated insulation characteristics of the snowpack exert a comparable influence on local surface temperatures. Furthermore, the difference between snow cover and snow depth has been shown to affect the magnitude, timing and persistence of the snow-forced teleconnection pathway and ultimate AO mode response. The emerging influence of snow anomalies on both local and remote climate variability necessitates a re-evaluation of GCM snow parameterizations schemes, especially given that current GCMs generally parameterize land surface snow in a fairly simplistic manner (see Chapter 2). Future research efforts could be geared towards a more precise and detailed validation of the modeled local temperature response to particular snow characteristics. Also, the snow budget and surface energy processes simulated by GCM snow parameterization schemes could be improved. Such efforts would lead to an improved understanding of both the local climatic response to land surface snow anomalies, and the subsequent impact on winter Northern Hemisphere climate.

Appendix A

Empirical Orthogonal Function Analysis

The following is excerpted from a detailed description of empirical orthogonal function analysis presented in Peixoto and Oort (1992):

> The empirical orthogonal function (EOF) analysis, sometimes referred to as eigenvector or principal components analysis, provides a convenient method for studying the spatial and temporal variability of long time series of data over large areas. This method splits the temporal variance of the data into orthogonal spatial patterns called empirical eigenvectors.
>
> Since its introduction in the atmospheric sciences by Lorenz (1956) eigenvector analysis has been widely used to describe geophysical fields in hydrology, oceanography, and solid earth geophysics, besides meteorology and climatology. This approach enables one to identify a set of orthogonal spatial modes, such that, when ordered, each successive eigenvector explains the maximum amount possible of the remaining variance in the data. The eigenvectors are arranged in decreasing order according to the percentage of variance explained by them. Each eigenvector pattern is associated with a series of time coefficients that describes the time evolution of the particular spatial mode. The eigenvector patterns that account for a large fraction of the variance are, in general, considered to be physically meaningful and connected with important centers of action. Recently the use of EOF's has become widespread in identifying patterns of large-scale climate fluctuations. Since the modes are orthogonal in nature, any two modes are spatially uncorrelated and their time variations are also uncorrelated. Thus, in this sense, no one mode carries within itself any relationship to any other mode.
>
> The principal advantages of the eigenfunctions are that they provide the most efficient way of compressing geophysical data in both space and time and they may be regarded as uncorrelated (independent) modes of variability of the fields. The EOF's are the eigenvectors of the data covariance matrix whose elements are formed from the difference of the observations from their long-term means. Thus, the EOF's depend on the coherence of the departures from their normal values. In general, a large portion of the total variance can usually be represented by a small

number of modes, with the remainder representing minor features, smaller-scale fluctuations, and noise.

Let us consider a real-valued geophysical field *f(x,t)* defined simultaneously at *M* positions denoted as *x* with *N* observations at times *t*. In other words, we are dealing with an ensemble of *N* instantaneous samples (maps) of a scalar field *f(x,t)* defined at *M* stations.

Alternatively we can assume that each sample *n* constitutes a map with *M* elements that can be organized in an *M*x1 array of data represented by a column vector $\mathbf{f}_n$. When we consider all *N* maps together, we obtain an array of *N* column vectors forming an *M*x*N* rectangular matrix, **F**, with *M* rows (or *M* time series at each station) and *N* columns (maps). The matrix element f_{mn} represents the observation made at station *m* at time *n*. Instead of the data matrix, we will use another matrix whose elements are functions of deviations from their mean values, namely the covariance matrix **R**, as we will see next.

The set of the *N* vectors can be represented in an *M*-dimensional linear vector space spanned by an arbitrary unit basis $\{\mathbf{u}_1, \mathbf{u}_2,\ldots,\mathbf{u}_m\}$. The *N* data vectors are directed from the origin to a point in the *M* space. If there is some correlation between the *N* vectors we expect that the distribution of their extremities will be organized in clusters or along some preferred directions.

The problem that we want to solve is to find an orthogonal basis in the vector space $\{\mathbf{e}_1, \mathbf{e}_2,\ldots,\mathbf{e}_m\}$ instead of the original basis such that each vector $\mathbf{e}_m$ best represents the cluster of the original data vectors $\mathbf{f}_n$ with $n = 1,\ldots,N$. This is equivalent to finding a set of *M* vectors $\mathbf{e}_m$, whose orientation is such that the sum of square of the projections of all the *N* observation vectors $\mathbf{f}_n$ onto each $\mathbf{e}_m$ is maximized sequentially. We assume that the vectors of the set {**e**} are mutually orthonormal so that by definition of the inner product:

$$(\mathbf{e}_m \cdot \mathbf{e}_j) = \mathbf{e}_m^T \mathbf{e}_j = \begin{cases} 1 & for \quad m = j \\ 1 & for \quad m \neq j \end{cases} \tag{A.1}$$

where $\mathbf{e}_m^T$ is the transpose vector of $\mathbf{e}_m$. The set of vectors {**e**} are called the empirical orthogonal functions (EOF's).

Appendix B

Effect of Ensemble Size on Simulation Results

Twenty-member ensembles are utilized in this thesis, to obtain a reliable mean climate state by capturing the range and distribution of naturally-occurring internal model variability. This relatively large ensemble also enables an explicit evaluation of ensemble size with respect to the reliability and variability of climate statistics. For a given ensemble, confidence limits can be developed to describe the range within which some statistic computed from the ensemble members can be expected to reside. Confidence limits generally become narrower (i.e., the statistic becomes more precise) with increasing ensemble size. Furthermore, for small, finite ensembles selected from an infinite population (approximated here by the twenty realizations performed for each experiment), different ensembles of the same size may yield markedly different confidence limits. As ensemble size increases to the point where the population distribution is well sampled by the ensemble members, confidence limits become more consistent over different ensembles of that size. The adequacy of an ensemble size can be assessed by the behavior of its confidence limits.

Figure B-1 presents confidence limits for the winter season (DJF) SLP at a gridcell located within the Icelandic Low pressure system, for the CTRL simulation, as a function of ensemble size. Figure B-1a represents the ensemble mean statistic, and Figure B-1b represents the ensemble standard deviation. For an ensemble size of three, confidence limits are derived as follows. Fifty sets of three realizations are selected at random from the full set of twenty, and upper and lower confidence limits are computed (see below) for each three-member ensemble set. The maximum (minimum) upper (lower) confidence limit from among the set of fifty is retained and plotted in Figure B-1, which therefore represents the widest range of confidence limits over the fifty ensemble sets. The same procedure is repeated for ensemble sizes three through eighteen. For an ensemble size of nineteen, twenty ensemble sets are used instead of fifty, since that is the maximum number of nineteen member combinations from a twenty member total, i.e., $\binom{20}{19} = \frac{20!}{19!1!} = 20$. For the total ensemble size of twenty, one set of confidence limits is directly computed from all twenty realizations.

For the mean (Fig. B-1a), confidence limits are computed for a given ensemble set of size *n* as

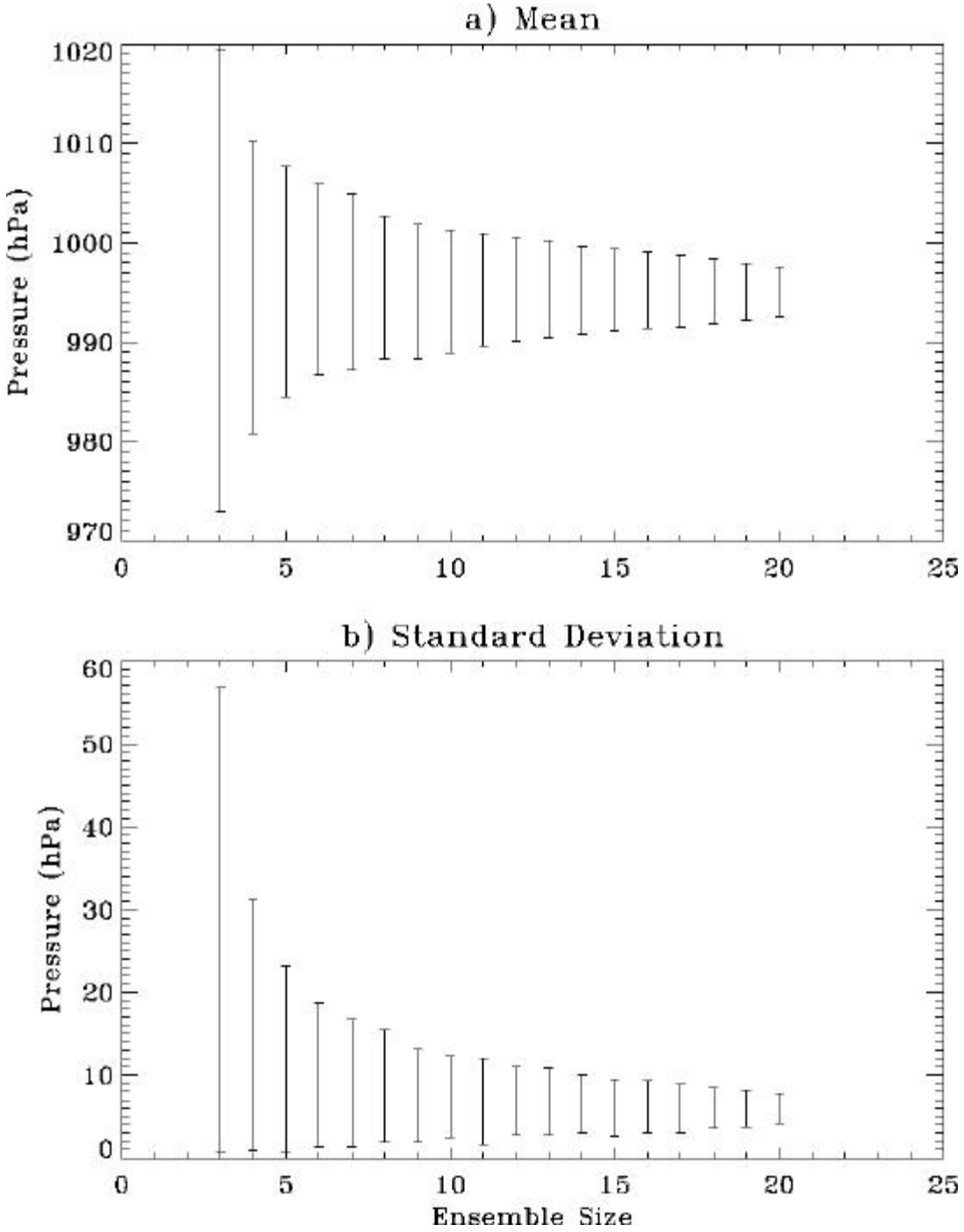

Figure B-1: Confidence limits plotted over a range of ensemble sizes, for winter (DJF) sea level pressure statistics at a gridcell located within the Icelandic Low, for the CTRL simulation. a) Ensemble mean. b) Ensemble standard deviation.

$$\bar{x} \pm t_{.975,n-1} \frac{s}{\sqrt{n}} \tag{B.1}$$

where $\bar{x}$ is the ensemble set mean, ó is the ensemble set standard deviation, and $t_{.975,n-1}$ is taken from the *t* distribution at 0.975 level of significance and *n-1* degrees of freedom. For the standard deviation (Fig. B-1b) confidence limits are computed for a given ensemble set of size *n* as

$$\frac{(n-1)s^{2}}{c^{2}_{.975,n-1}} \tag{B.2}$$

where $c^{2}_{.975,n-1}$ is taken from the chi-squared distribution at 0.975 level of significance and *n-1* degrees of freedom.

For ensemble sizes less than about ten, resulting confidence limits exhibit a sharp reduction with increasing ensemble size. This clearly demonstrates the unreliability associated with small ensembles. Mean parameter values computed using small ensemble sizes can vary considerably for different ensemble sets of that size. For larger ensemble sizes, confidence limits continue to decrease steadily as the full twenty-member ensemble is approached. Thus means computed from all twenty realizations are substantially more reliable estimates of the actual mean climatic state of the model experiment.

Note that the confidence limits are somewhat underestimated for larger ensemble sizes, since the realizations are being drawn not from an infinite population, but from a finite set of twenty realizations. Thus each ensemble set will have many members in common. For example, each of the fifty sets of eighteen realizations will differ by only two realizations. Nevertheless, the benefit of using twenty member ensembles rather than the six or fewer ensembles in previous snow-forced exploratory studies is clear. Additional realizations will of course continue to increase the precision of the mean climatic state, but generally twenty realizations is considered sufficient to capture the range and distribution, so that larger ensembles will yield relatively minimal improvement. This ensemble size analysis was repeated for different climate parameters, time periods, and GCM experiments, yielding similar results.

Appendix C

Effect of Snow Forcings on Surface Energy Balance

Because snow is maintained within the ECHAM3 GCM as an internal state variable, prescribing snow depths as an external boundary condition necessarily encroaches on the model's surface energy balance. Other studies have followed a slightly different approach for prescribing snow, in which the amount of snowfall produced by the atmosphere is adjusted, rather than the depth of snow at the surface. In either case, snow mass is added or removed, which interferes with surface energetics. To minimize potential disruptions in this research, the prescribed snow is allowed to melt and evaporate as dictated by the model's snow parameterization scheme, before being prescribed again at the following timestep. This allows all relevant surface processes to respond to the prescribed snow, so that the overall climatic response is more comprehensive, and less prone to accrued errors.

Surface energy balance terms averaged over the Siberia forcing region and the month of October are listed in Table C-1, for all twelve experiments. October is presented since the most dramatic snow anomalies occur in this month. Note that the Numerical Heat Loss term arises due to the linearization of the total heat flux entering the soil, as computed by the model (Roeckner et al. 1996). It is essentially a ground heat flux correction required by the numerical representation of the land surface, and is a minor contributor to the overall surface energy balance. The FREE experiment represents the energy balance for the base model (i.e., the CTRL simulation). All other experiments involve some form of prescribed snow forcing.

As indicated in Table C-1, none of the terms are unduly affected in any of the experiments. Values for all experiments are well within reasonable ranges for each energy balance term. Some notable changes do occur, but they are expected based on the nature of the applied forcing. Incoming shortwave radiation generally decreases (increases) with positive (negative) snow forcing, due to the high albedo of snow. Notice that for a given snow forcing, shortwave radiation is larger for INS than for SIB, since the surface albedo was explicitly set at the snow-free (i.e., smaller) value in INS. Outgoing longwave radiation similarly decreases (increases) with positive (negative) snow forcing. As discussed in Cohen and Rind (1991), the decreased temperatures associated with a positive snow forcing act to reduce longwave radiation. This process overrides the direct longwave radiation increase due to the higher thermal emissivity of

Experiment	Shortwave Radiation	Longwave Radiation	Sensible Heat Flux	Latent Heat Flux	Snow Melt	Numerical Heat Loss
FREE (CTRL)	66.21	-57.80	-3.38	-15.32	-0.48	0.21
FIX	66.91	-57.88	-3.38	-15.20	-0.67	-0.14
SIB High Snow	61.09	-52.16	0.29	-12.98	-5.32	-2.05
SIB Low Snow	69.44	-62.29	-5.64	-12.81	-0.06	0.01
ORO High Snow	59.78	-49.23	1.05	-12.89	-7.21	-3.15
ORO Low Snow	66.86	-58.81	-4.92	-12.79	-0.15	-0.68
NA High Snow	66.85	-58.29	-3.27	-15.47	-0.48	-0.02
NA Low Snow	67.32	-58.41	-2.52	-15.30	-0.50	-0.77
ALB High Snow	62.01	-52.19	-1.19	-14.22	-4.69	-1.13
ALB Low Snow	69.43	-61.51	-5.72	-12.33	-0.06	-0.53
INS High Snow	66.97	-51.67	-1.29	-15.67	-7.11	-2.96
INS Low Snow	70.44	-62.24	-5.92	-12.68	-0.07	-0.57

Table C-1:Surface energy balance terms (Wm^{-2}) over Siberia forcing region during October, for all GCM experiments. Positive (negative) values represent downward (upward) energy fluxes.

snow, and demonstrates the complexities and feedbacks associated with the surface energy response to snow. The slight changes in the sensible and latent heat flux terms are also indicative of this complexity, as they are controlled by temperature and humidity gradients at the surface, which are in turn affected by snow.

Lastly, the snowmelt term is noticeably higher for positive snow forcing experiments. This arises due to the prescription of snow in early October when the surface is often too warm to support and maintain the snow forcing. Until the prevailing seasonal and/or snow-forced surface cooling is sufficient to support snow, the prescribed snow melts, which releases latent heat. Note that the latent heat flux term in Table C-1 refers to vaporization, not melting. During winter months (not shown) the surface is cold enough to support the prescribed snow, and the snowmelt term is not substantially affected. This surface energy balance evaluation was repeated for different regions and time periods, yielding similar results.

Appendix D

Wave Activity Flux Computation

The three-dimensional wave activity flux (WAF) vector portrays stationary wave energy transmission throughout the atmospheric system. It is denoted here by the three element vector $\mathbf{F}_s$, where the first, second and third elements represent the eastward, poleward and upward flux components, respectively. This diagnostic is calculated for specified time-averaged periods at each of 128x64 cartesian gridcells and 12 vertical pressure levels, or 98,304 discrete points within the model's atmospheric domain. It is computed following equations (7.1) and (7.2) from Plumb (1985), as follows:

$$\mathbf{F}_s = p^* \cdot \cos f \times \begin{pmatrix} v'^2 - \dfrac{1}{2\Omega a \sin 2f} \dfrac{\partial (v'\Phi')}{\partial l} \\ -u'v' + \dfrac{1}{2\Omega a \sin 2f} \dfrac{\partial (u'\Phi')}{\partial l} \\ \dfrac{2\Omega \sin f}{S} \left[v'T' - \dfrac{1}{2\Omega a \sin 2f} \dfrac{\partial (T'\Phi')}{\partial l} \right] \end{pmatrix} \tag{D.1}$$

where

Φ' = deviation from zonal mean geopotential [$m^2 s^{-2}$]
u' = deviation from zonal mean zonal wind [$m s^{-1}$]
v' = deviation from zonal mean meridional wind [$m s^{-1}$]
T' = deviation from zonal mean temperature [K]
l = longitude [rad]
f = latitude [rad]
p^* = pressure / 1000 hPa [-]
a = radius of the earth [m]
Ω = angular velocity of the earth [$rad s^{-1}$]
S = static stability for unsaturated air [$K m^{-1}$]

The static stability S is computed as

$$S = \frac{d\hat{T}}{dz} + \frac{R_d \hat{T}}{C_p H} \tag{D.2}$$

where

$\hat{T}$ = areal average temperature over the Northern Hemisphere [K]
z = elevation [m]
R_d = gas constant for dry air, 287 J kg^{-1} K^{-1}
C_p = specific heat of dry air at constant pressure, 1004 J kg^{-1} K^{-1}
H = constant scale height [m]

Following Peixoto and Oort (1992), hydrostatics and the ideal gas law can be used to compute static stability as

$$S = \frac{p}{H}\frac{d\hat{T}}{dp} + \frac{R_d \hat{T}}{C_p H} \tag{D.3}$$

where

p = pressure [hPa]

Finally, the constant scale height H can be approximated as

$$H = \frac{R^* T^*}{g} \tag{D.4}$$

where

g = gravity, 9.81 m s^{-2}
R^* = tropospheric average gas constant, 298.0 J kg^{-1} K^{-1}
T^* = tropospheric average temperature, 250.0 K

References

Baldwin, M.P., 2001: Annular modes in global daily surface pressure. *Geophys. Res. Lett.,* **28,** 4115-4118.

Baldwin, M.P., 2002: Personal communication.

Baldwin, M.P. and T.J. Dunkerton, 1999: Propagation of the Arctic Oscillation from the stratosphere to the troposphere. *J. Geophys. Res.*, **104 (D24),** 30937-30946.

Bamzai, A.S. and J. Shukla, 1999: Relation between Eurasian snow cover, snow depth, and the Indian summer monsoon: An observational study. *J. Climate*, **12,** 3117-3132.

Barnett, T.P., L. Dumenil, U. Schlese, E. Roeckner and M. Latif, 1989: The effect of Eurasian snow cover on regional and global climate variations. *J. Atmos. Sci.,* **46,** 661-685.

Charney, J.G. and P.G. Drazin, 1961: Propagation of planetary scale disturbances from the lower into the upper atmosphere. *J. Geophys. Res.*, **66,** 83-109.

Christiansen, B., 2000: A model study of the dynamical connection between the Arctic Oscillation and stratospheric vacillations. *J. Geophys. Res.,* **105 (D24),** 29461-29474.

Clark, M.P. and M.C. Serreze, 2000: Effects of variations in east Asian snow cover on modulating atmospheric circulation over the North Pacific ocean. *J. Climate,* **13,** 3700-3710.

Cohen, J., 1994: Snow cover and climate. *Weather,* **49,** 150-156.

Cohen, J. and D. Entekhabi, 1999: Eurasian snow cover variability and Northern Hemisphere climate predictability. *Geophys. Res. Let.*, **26,** 345-348.

Cohen, J. and D. Entekhabi, 2001: The influence of snow cover on Northern Hemisphere climate variability. *Atmos.-Ocean*, **39,** 35-53.

Cohen, J. and D. Rind, 1991: The effect of snow cover on climate. *J. Climate*, **4,** 689-706.

Cohen, J., K. Saito and D. Entekhabi, 2001: The role of the Siberian High in Northern Hemisphere climate variability. *Geophys. Res. Lett.*, **28,** 299-302.

Cohen, J., D. Salstein and K. Saito, 2002: A dynamical framework to understand and predict the major Northern Hemisphere climate mode. *Geophys. Res. Lett.*, **29,** 10.1029/2001GL014117.

Corti, S., F. Molteni and T.N. Palmer, 1999: Signature of recent climate change in frequencies of natural atmospheric circulation regimes. *Nature,* **398,** 799-802.

Cuming, Michael J. and Barbara A. Hawkins, 1981. TERDAT: The FNOC System for terrain data extraction and processing. Technical Report Mil Project M-254 (second edition). Prepared for USN/FNOC and published by Meteorology International Inc.

Dewey, K.F., 1977: Daily maximum and minimum temperature forecasts and the influence of snow cover. *Mon. Wea. Rev.*, **105,** 1594-1597.

DKRZ, 1994: The ECHAM3 Atmospheric General Circulation Model. Deutsches Klimarechenzentrum Technical Report No. 6, ISSN 0940-9327, 182 pp.

Dong, B.W., R.T. Sutton, S.P. Jewson, A. O'Neill and J.M. Slingo, 2000: Predictable winter climate in the North Atlantic Sector during the 1997-1999 ENSO Cycle. *Geophys. Res. Lett.,* **27,** 985-988.

Douville, H. and J.-F. Royer, 1996: Sensitivity of the Asian summer monsoon to anomalous Eurasian snow cover within the Meteo-France GCM. *Climate Dyn.*, **12,** 449-466.

Edmon, H.J., Jr., B.J. Hoskins and M.E. McIntyre, 1980: Eliassen-Palm cross-sections for the troposphere. *J. Atmos. Sci.*, **37,** 2600-2616.

Feldstein, 2000: The timescale, power spectra, and climate noise properties of teleconnection patterns. *J. Climate,* **13,** 4430-4440.

Feldstein, 2002: The recent trend and variance increase of the annular mode. *J. Climate,* **15,** 88-94.

Foster, D.J., Jr. and R.D. Davy, 1988: Global snow depth climatology. USAF Environmental Technical Applications Center USAFETAC/TN-88/006, 48 pp.

Foster, J. and coauthors, 1996: Snow cover and snow mass intercomparisons of general circulation models and remotely sensed datasets. *J. Climate,* **9,** 409-426.

Frei, A. and D.A. Robinson, 1998: Evaluation of snow extent and its variability in the atmospheric model intercomparison project. *J. Geophys. Res.*, **103(D8),** 8859-8871.

Fyfe, J.C., G.J. Boer and G.M. Flato, 1999: The Arctic and Antarctic Oscillations and their projected changes under global warming. *Geophys. Res. Lett.*, **26,** 1601-1604

Gates, W.L., 1992: AMIP, The atmospheric model intercomparison project. *Bull. Amer. Meteor. Soc.*, **73,** 1962-1970.

Gates, W.L., and co-authors, 1998: An Overview of the Results of the Atmospheric Model Intercomparison Project (AMIP). Program for Climate Model Diagnosis and Intercomparison (PCMDI) Report No. 45, 47 pp.

Gillett, N.P., M.R. Allen, R.E. McDonald, C.A. Senior, D.T. Shindell and G.A. Schmidt, 2002: How linear is the Arctic Oscillation response to greenhouse gases? *J. Geophys. Res.*, **107(D),** 10.1029/2001JD000589.

Gong, D. and S. Wang, 1999: Definition of Antarctic Oscillation index. *Geophys. Res. Lett.,* **26,** 459-462.

Graf, H.F., J. Perlwitz and I. Kirchner, 1994: Northern Hemisphere tropospheric midlatitude circulation after violent volcanic eruptions. *Contrib. Atmos. Phys.,* **67,** 3-13.

Gutzler, D.S. and R.D. Rosen, 1992: Interannual variability of winter-time snow cover across the Northern Hemisphere. *J. Climate,* **5,** 1441-1447.

Hahn, D.G. and J. Shukla, 1976: An apparent relationship between the Eurasian snow cover and Indian monsoon rainfall. *J. Atmos. Sci.,* **33,** 2461-2462.

Hoerling, M.P., J.W. Hurrell and T. Xu, 2001: Tropical origins for recent North Atlantic climate change. *Science,* **292,** 90-92.

Holton, J.R., 1972: An Introduction to Dynamic Meteorology. Academic Press, New York, 319 pp.

Hurrell, J.W., 1995: Decadal trends in the North Atlantic Oscillation, Regional temperatures and precipitation. *Science*, **269,** 676-679.

Kalnay, E. and Coauthors, 1996: The NCEP/NCAR 40-year reanalysis project. *Bull. Amer. Meteor. Soc.,* **77,** 437-471.

Kaurola, J., 1997: Some diagnostics of the northern wintertime climate simulated by the ECHAM3 model. *J. Climate,* **10,** 201-222.

Keller, C.F., 1999: Climate, modeling, and predictability. *Physica D,* **133,** 296-308.

Kodera, K. and K. Yamazaki, 1994: A possible influence of recent polar stratospheric coolings on the troposphere in the Northern Hemisphere winter. *Geophys. Res. Let.,* **21,** 809-812.

Kodera, K. and Y. Kuroda, 2000: Tropospheric and stratospheric aspects of the Arctic Oscillation. *Geophys. Res. Let.,* **27,** 3349-3352.

Kuroda, Y. and K. Kodera, 1999: Role pf planetary waves in stratosphere-troposphere coupled variability in the Northern Hemisphere winter. *Geophys. Res. Lett.,* **26,** 2375-2378.

Latif, M., K. Arpe and E. Roeckner, 2000: Oceanic control of decadal North Atlantic sea level pressure variability in winter. *Geophys. Res. Let.,* **27,** 727-730.

Leathers, D.J. and D.A. Robinson, 1993: The association between extremes in North American snow cover extent and United States temperature. *J. Climate,* **6,** 1345-1355.

Limpasuvan, V. and D.L. Hartmann, 2000: Wave-maintained annular modes of climate variability. *J. Climate,* **13,** 4414-4429.

Lorenz, E.N., 1956: Empirical orthogonal functions and statistical weather prediction. MIT Dept. of Meteorology, Science Report 1, 49 pp.

McFadden, J.D. and R.A. Ragotzkie, 1967: Climatological significance of albedo in central Canada. *J. Geophys. Res*., **72,** 1135-1143.

Mehta, V.M., M.J. Suarez, J. Manganello and T.L. Delworth, 2000: Predictability of multiyear to decadal variations in the North Atlantic Oscillation and associated Northern Hemisphere climate variations. *Geophys. Res. Lett*., **27,** 121-124.

Namias, J., 1985: Some empirical evidence for the influence of snow cover on temperature and precipitation. *Mon. Wea. Rev*., **113,** 1542-1553.

National Snow and Ice Data Center (NSIDC)/World Data Center – A for Glaciology. 1966-1990. Former Soviet Union Hydrological Snow Surveys. Digital data available from nsidc@kryos.colorado.edu. University of Colorado, Boulder, Colorado.

Nicholls, N., 2000: The insignificance of significance testing. *Bull. Amer. Meteor. Soc.*, **82,** 981-986.

NOAA, 1988: Data Announcement 88-MGG-02, Digital relief of the surface of the Earth. NOAA, National Geophysical Data Center, Boulder, Colorado, 1988.

NRC, 1998: Decade-to-Century-Scale Climate Variability and Change: A Science Strategy. National Academy Press, Washington, D.C., 140 pp.

NRC, 1999: Making Climate Forecasts Matter. P.C. Stern and W.E. Easterling (eds.). National Academy Press, Washington, D.C., 175 pp.

Perlwitz, J. and H.F. Graf and R. Voss, 2000: The leading variability mode of the coupled troposphere-stratosphere winter circulation in different climate regimes. *J. Geophys. Res.,* **105 (D5),** 6915-6926.

Peixoto, J.P. and A.H. Oort, 1992: *Physics of Climate*. American Institute of Physics, New York, 520 pp.

Plumb, R.A., 1985: On the three-dimensional propagation of stationary waves. *J. Atmos. Sci.,* **42,** 217-229.

Plumb, R.A., 2003: Personal communication.

Ringler, T.D. and K.H. Cook, 1999: Understanding the seasonality of orographically forced waves: Interaction between mechanical and thermal forcing. *J. Atmos. Sci.*, **56,** 1154-1174.

Robertson, A.W., 2001: Influence of ocean-atmosphere interaction on the Arctic Oscillation in two general circulation models. *J. Climate,* **14,** 3240-3254.

Robertson, A.W., C.R. Mecheso and Y.-J. Kim, 2000: The influence of Atlantic sea surface temperature anomalies on the North Atlantic Oscillation. *J. Climate,* **13,** 122-138.

Robinson, D.A., K.F. Dewey and R.R.. Heim, Jr., 1993: Global snow cover monitoring, An update. *Bull. Amer. Meteor. Soc.,* **74,** 1689-1696.

Robinson, D.A., 2000: Weekly Northern Hemisphere snow maps: 1966-1999. *Preprints 12th Conf. Appl. Climatology,* Asheville, NC, AMS, 12-15.

Rodwell, M.J., D.P. Rowell and C.K. Folland, 1999: Oceanic forcing of the wintertime North Atlantic Oscillation and European climate. *Nature*, **398,** 320-323.

Roeckner, E., and Coauthors, 1992: Simulation of the present-day climate with the ECHAM model: Impact of model physics and resolution. Max-Planck-Institute for Meteorology Report No. 93, 171 pp.

Roeckner, E. and Coauthors, 1996: The atmospheric general circulation model ECHAM-4: model description and simulation of present-day climate. Max-Planck-Institute for Meteorology, Report No. 218, 90 pp.

Saito, K. and J. Cohen, 2003: The potential role of snow cover in forcing the interannual variability of the major Northern Hemisphere mode. *Geophys. Res. Lett.,* **30,** 10.1029/2001GL016341.

Saito, K., J. Cohen and D. Entekhabi, 2001: Evolution of atmospheric response to early-season Eurasian snow cover anomalies. *Mon. Wea. Rev.,* **129,** 2746-2760.

Seager, R., Y. Kushnir, M. Visbeck, N. Naik, J. Miller, G. Krahmann and H. Cullen, 2000: Causes of Atlantic Ocean climate variability between 1958 and 1998. *J. Climate,* **13,** 2845-2862.

Sellers, P.J., Y. Mintz, Y.C. Sud and A. Dalcher, 1986: A simple biosphere model (Sib) for use within general circulation models. *J. Atmos. Sci.*, **43,** 505-531.

Serreze, M.C., F. Carse, R.G. Barry and J.C. Rogers, 1997: Icelandic Low cyclone activity, Climatological features, linkages with the NAO, and relationships with recent changes in the Northern Hemisphere circulation. *J. Climate*, **10,** 453-463.

Shindell, D.T., R.L. Miller, G. Schmidt and L. Pandolfo, 1999: Simulation of recent Northern Hemisphere climate trends by greenhouse gas forcing. *Nature,* **398,** 452-455.

Stone, D.A., A.J. Weaver and R.J. Stouffer, 2001: Projection on climate change onto modes of atmospheric variability. *J. Climate*, **14,** 3551-3565.

Taguchi, M., T. Yamaga and S. Yoden, 2001: Internal variability of the troposphere-stratosphere coupled system simulated in a simple global circulation model. *J. Atmos. Sci.,* **58,** 3184-3203.

Taguchi, M. and S. Yoden, 2002: Internal interannual variability of the troposphere-stratosphere coupled system in a simple global circulation model. Part I: parameter sweep experiment. *J. Atmos. Sci.,* **59,** 3021-3036.

Thompson, D.W.J. and J.M. Wallace, 1998: The Arctic Oscillation signature in wintertime geopotential height and temperature fields. *Geophys. Res. Lett,* **25,** 1297-1300.

Thompson, D.W.J. and J.M. Wallace, 2001: Regional climate impacts of the Northern Hemisphere Annular Mode. *Science,* **293,** 85-89.

Thompson, D.W.J., J.M. Wallace and G.C. Hegerl, 2000: Annular modes in the extratropical circulation, Part II, Trends. *J. Climate*, **13,** 1018-1036.

Wagner, A.J., 1973: The influence of average snow depth on monthly mean temperature anomaly. *Mon. Wea. Rev.*, **101,** 624-626.

Walker, C.C. and G. Magnusdottir, 2003: Nonlinear planetary wave reflection in an atmospheric GCM. *J. Atmos. Sci.,* **60,** 279-286.

Wallace, J.M. and D.S. Gutzler, 1981: Teleconnections in the geopotential height field during the Northern Hemisphere winter. *Mon. Wea. Rev.,* **109,** 784-812.

Walland, D.J. and I. Simmonds, 1996: Sub-grid scale topography and the simulation of Northern Hemisphere snow cover. *Int. J. Climatol.*, **16,** 961-982

Walland, D.J. and I. Simmonds, 1997: Modelled atmospheric response to changes in Northern Hemisphere snow cover. *Climate Dyn.,* **13,** 25-34.

Walsh, J.E. and B. Ross, 1988: Sensitivity of 30-day dynamical forecasts to continental snow cover. *J. Climate*, **1,** 739-754.

Watanabe, M. and T. Nitta, 1998: Relative impacts of snow and sea surface temperature anomalies on an extreme phase in the winter atmospheric circulation. *J. Climate*, **11,** 2837-2857.

Watanabe, M. and T. Nitta, 1999: Decadal changes in the atmospheric circulation and associated surface climate variations in the Northern Hemisphere winter. *J. Climate*, **12,** 494-509.

WCRP, 1995: CLIVAR Science Plan. World Climate Research Program. Geneva.

Weiss, H., H.-A. Courty, W. Wetterstrom, L. Senior, R. Meadow, F. Guichard and A. Curnow, 1993: The genesis and collapse of third millennium north Mesopotamian civilization. *Science,* **261,** 995-1004.

Zhou, S., A.J. Miller, J. Wang and J.K. Angell, 2001: Trends of NAO and AO and their associations with stratospheric processes. *Geophys. Res. Lett.*, **28,** 4107-4110.

Zhou, S., A.J. Miller, J. Wang and J.K. Angell, 2002: Downward-propagating temperature anomalies in the preconditioned polar stratosphere. *J. Climate*, **15,** 781-792.